

NACA TN 4369

Library
Sept 19
200

CASE FILE COPY

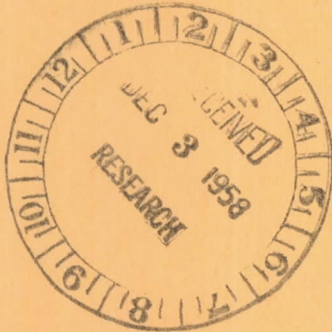
NATIONAL ADVISORY COMMITTEE FOR AERONAUTICS

TECHNICAL NOTE 4369

SLIP-FLOW HEAT TRANSFER FROM CYLINDERS
IN SUBSONIC AIRSTREAMS

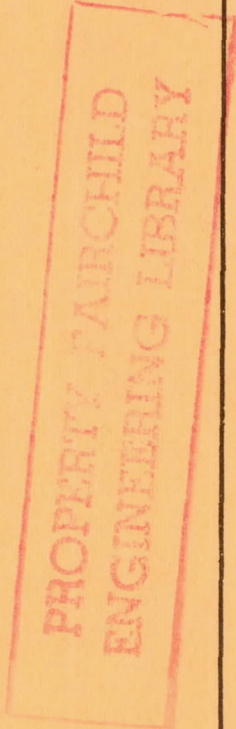
By Lionel V. Baldwin

Lewis Flight Propulsion Laboratory
Cleveland, Ohio



Washington
September 1958

DEC 1 - 1958



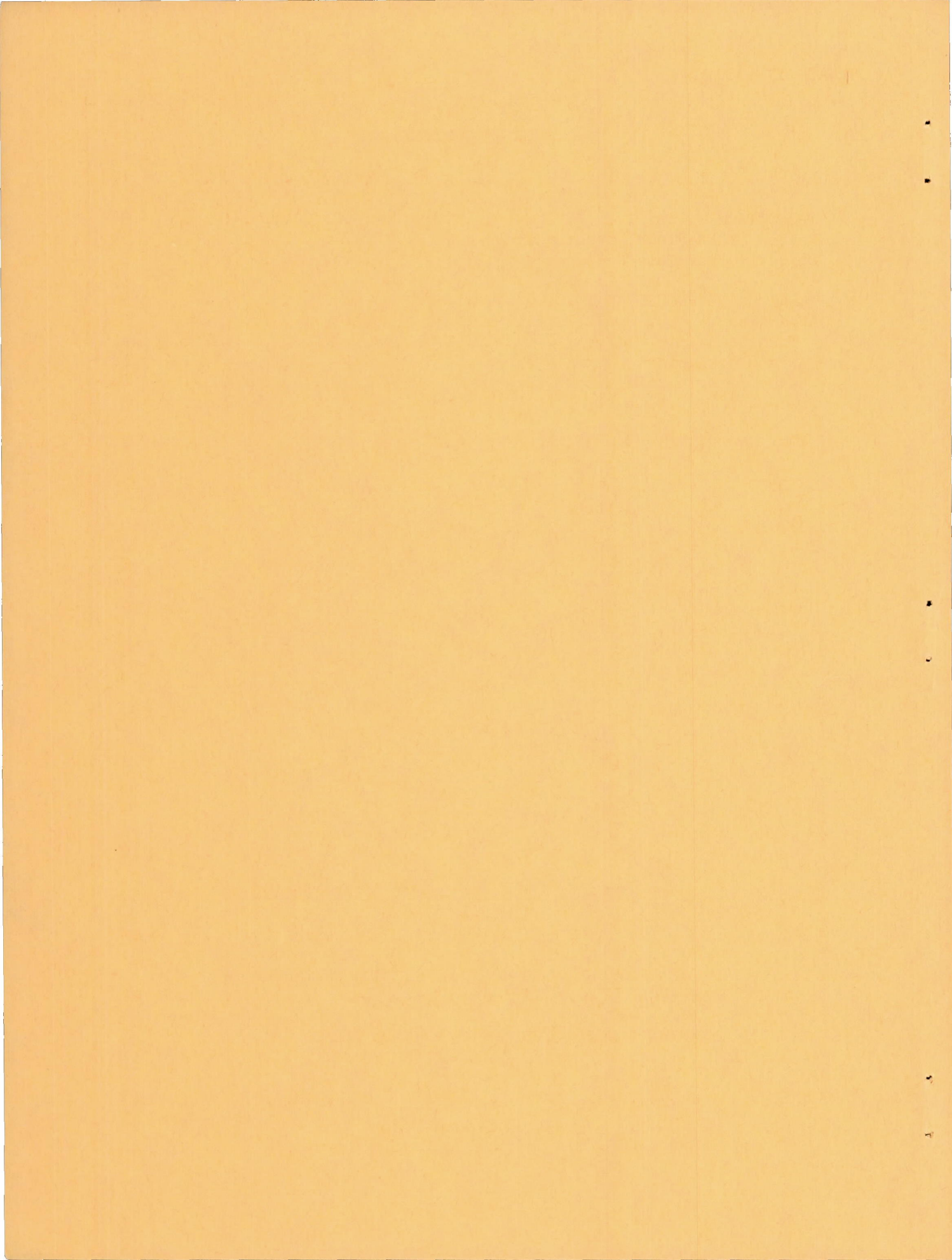


TABLE OF CONTENTS

	Page
SUMMARY	1
INTRODUCTION	2
Review of Previous Investigations	3
Objectives of This Research	5
APPARATUS AND PROCEDURE	5
Apparatus	5
Tunnel and air facility	5
Probe design and tungsten wire	6
Anemometer electrical equipment	8
Procedure	8
DIMENSIONLESS GROUPS OF CORRELATION	9
RESULTS	12
DISCUSSION	13
Preliminary Discussion of Results	13
Effect of Wire Temperature on Heat-Transfer Coefficient	14
Effect of Air Temperature on Heat-Transfer Coefficient	16
Correlation of Slip-Flow Heat-Transfer Data	17
Attempted General Correlation for Nusselt Number in Continuum, Slip, and Free-Molecule Flows	18
Hot-Wire-Anemometer Sensitivity	20
CONCLUDING REMARKS	22
APPENDIXES	
A - SYMBOLS	24
B - CORRECTIONS FOR CONDUCTION TO SUPPORTS	28
Linear Correction	28
Nonlinear Correction	33
C - DERIVATION OF HOT-WIRE-ANEMOMETER SENSITIVITY EQUATIONS	35
REFERENCES	37
TABLE I - RESULTS OF STUDY OF HEAT TRANSFER FROM CYLINDERS IN SUBSONIC SLIP FLOW	40
TABLE II - ORGANIZATION OF RESULTS FOR NOMINAL VALUES OF PARAMETERS	47
FIGURES	48

TABLE OF CONTENTS

Page

SUMMARY 1

INTRODUCTION 2

Review of Previous Investigations 3

Objectives of This Research 3

ALPHABETS AND PROCEDURES 4

Alphabets 4

Truncal and end 4

Truncal design 4

Parameter of 4

Procedure 4

PERMISSIONLESS GROUPS 5

EXHIBITS 6

DISCUSSION 7

Probability of 7

Effect of Wire 7

Effect of Air 7

Comparison of 7

Attended 7

Ship, and 7

Out-wire- 7

CONCLUDING REMARKS 8

REFERENCES 9

A - SYMBOLS 9

B - CORRECTIONS 9

Linear 9

Equivalent 9

C - DERIVATION 9

REFERENCES 9

TABLE I - RESULTS 10

TABLE II - RESULTS 10

TABLE III - RESULTS 10

TABLE IV - RESULTS 10

1-30

NATIONAL ADVISORY COMMITTEE FOR AERONAUTICS

TECHNICAL NOTE 4369

SLIP-FLOW HEAT TRANSFER FROM CYLINDERS IN SUBSONIC AIRSTREAMS

By Lionel V. Baldwin

SUMMARY

Over 1000 measured convective heat-transfer coefficients for normal cylinders in subsonic slip flow have been correlated by using Nusselt number as a function of Reynolds and Knudsen (or Mach) numbers. The experimental range corresponds to the following dimensionless groups: Mach number M , 0.05 to 0.80; Reynolds number Re , 1 to 75; Knudsen number Kn , 0.009 to 0.077. Air temperatures between 0° and 280° F and cylinder temperatures between 34° and 620° F were used. At $Kn = 0.009$, the Nusselt number (Nu) correlation extrapolated smoothly into continuum-flow empirical curves, which show Nu as a function of \sqrt{Re} with a small, regular variation in Nu from compressibility or Mach number effects. The data showed increasing sensitivity to Kn as it increased to 0.077. The experimental Nu curves at $Kn = 0.077$ qualitatively verified two characteristics predicted by free-molecular-flow theoretical analysis. These are a shift to first-power dependence on Re and large separation of constant Mach number parametric curves due to rarefied gas-flow phenomena. Therefore, the experimental slip-flow correlation served as a bridge between continuum empirical relations and free-molecular theoretical results, but data between $0.10 < Kn < 2$ are required to complete this general correlation.

A complicated nonlinear dependence of the heat-transfer coefficient to the difference between cylinder and recovery temperature ΔT is reported. The heat-transfer coefficient h increased with increasing ΔT for $Kn < 0.02$; while for $Kn > 0.02$, h decreased with increasing ΔT . The Mach number had a secondary effect on this ΔT phenomenon. For cylinders operated at $\Delta T > 200^{\circ}$ F and over the entire range of this research, an increase in air temperature increased the heat-transfer coefficient. The preceding were second-order effects that caused deviations of up to 20 percent from the general correlation.

Finally, the application of these research results to hot-wire anemometry is discussed.

INTRODUCTION

Fine metal wires, 0.00005 to 0.001 inch in diameter, have been widely used in aerodynamic research as anemometers. The use of hot-wire anemometers for mean flow measurements began with the early work of King (ref. 1), while the investigation of fluctuations in airflows started with the classical research of Dryden and Kuethe (ref. 2). In every application, the sensitivity of the electrically heated anemometer to the flow properties is determined by the heat-transfer characteristics of cylinders in forced convection. Assuming potential flow over the wire, King derived an equation for steady flow that relates the electrical power input to the heat loss by convection:

$$I^2 \Omega_w = (A + B \sqrt{U})(T_w - T_a) \quad (1)$$

where

$$A = a \lambda k$$

$$B = b \lambda \sqrt{D_w \rho c_p k}$$

(All symbols are defined in appendix A.) In usual practice, the constants in King's equation, A and B, are obtained experimentally from a calibration curve of $I^2 \Omega_w / (\Omega_w - \Omega_a)$ as a function of \sqrt{U} for each wire used. The sensitivity predicted by King's equation is the basis for hot-wire-anemometer techniques that have become rather elaborate (e.g., ref. 3) in slow subsonic flows.

As aerodynamic research progressed into transonic and supersonic flows, it was natural to investigate the heat-loss characteristics of hot wires and to attempt extension of this research tool. In order to describe the influence of flow parameters over a wide range, recent investigators have used dimensionless groups to generalize heat-loss correlations. Hot-wire heat-loss studies not only supply anemometer sensitivity, but also have furnished the bulk of the heat-transfer measurements for cylinders in slip and near-free-molecule flows. Interest in this phase of aerodynamics has grown greatly as it has become necessary to compute heat transfer to missiles and satellites that fly at high altitudes. Though these objects generally fly at very high speeds, the actual flow over the body is subsonic in many cases, because shock waves occur near forward surfaces. This investigation follows some excellent research in this field during the past eight years; therefore, it is appropriate to outline the problem studied here in terms of what previous workers have established.

1111

02-1 pack

Review of Previous Investigations

The Reynolds number (based on cylinder diameter) and Mach number are the usual dimensionless groups chosen to specify the regimes for airflow over normal cylinders. Figure 1 is a convenient summary of recent heat-transfer experiments with normal cylinders. The Mach number of the ordinate is based on free-stream velocity and static temperature; the abscissa is the Reynolds number based on the cylinder diameter and on free-stream density, velocity, and viscosity. The shaded areas indicate the experimental ranges of previous work, and these areas are keyed by numbers to the reference list of this report (refs. 4 to 16). Figure 1 also shows the research region of this paper.

The two constant Knudsen number lines in figure 1 provide a guide to the flow regimes. Though the boundaries of free-molecule, slip, and continuum flows probably are not sharply defined, reference 15 proposed the following definitions for flow over normal cylinders:

- (1) Continuum flow: $Kn < 0.001$
- (2) Slip flow: $0.001 < Kn < 2$
- (3) Free-molecule flow: $Kn > 2$

The Knudsen number Kn is defined as the ratio of the mean free path of the gas λ to the cylinder diameter D_w . Kinetic theory of gases relates the Knudsen number to the ratio of the Mach number to the Reynolds number; for air, this proportionality is as follows:

$$Kn \equiv \frac{\lambda}{D_w} \approx 1.45 \frac{M}{Re_t} \sqrt{\frac{T}{T_t}} \quad (2)$$

At atmospheric pressure with anemometer wires 0.0002 inch or smaller in diameter, the flow region for the hot wires in much of the early turbulence work would fall below M of 0.10 and between Re of 3 and 30.

King's equation can be written in terms of nondimensional groups as

$$Nu = A' + B' \sqrt{Pr} \sqrt{Re} \quad (1a)$$

The 0.5-power dependence on Reynolds number is well established in slow subsonic continuum flows (ref. 11). However, Lowell (ref. 10) was the first to point out that the Reynolds number alone does not correlate fine-wire heat-transfer data over an appreciable velocity range. He reported that the Mach number was a parameter at $M = 0.375$ and 0.575 . Then, Laurence and Landes (ref. 9) found that their data correlated if Nu was plotted as a function of \sqrt{Re} , but the Mach number remained a

parameter even in the range of $M = 0.1, 0.2, \text{ and } 0.3$. Since the work being reviewed is limited to room-temperature airflows over cylinders (i.e., viscosity is constant), the use of both Re and M simply shows that ρD_w and U are not interchangeable in the product $\rho D_w U$. This has been noted by later investigators (refs. 12, 14, and 16). It is well established that the maximum separation of the constant Mach number lines on a plot of Nu against \sqrt{Re} occurs at the lowest Mach numbers; in fact, by proper choice of fluid properties, this "Mach number effect" can be almost eliminated in supersonic flow (refs. 7, 8, 14, and 15).

The Knudsen number was introduced as a correlating parameter in reference 14. The effect of ρ and D_w in the product ρD_w was found to be fully equivalent over the wide experimental range of reference 14. Since conditions of constant ρD_w are constant Knudsen number flows, the Knudsen and Reynolds numbers were shown to be the governing parameters in the incompressible range. The nonequivalence of ρD_w and U in attempted Reynolds number correlations was most pronounced for very fine wires that exhibited low sensitivity to velocity.

Nearly all the anemometer heat-loss investigators have varied the operating temperature of the wire (refs. 9, 10, 14, and 16). The most extensive research has been reported by reference 14, which found that the Nu varied with wire temperature at a given flow condition, and that this variation depended on both M and ρ . However, no simple correlation was found to cover all of the effects observed when the wire temperature was varied.

Reference 16 reports measurements of the nonlinear variation with wire temperature of the heat-transfer rate from hot wires from $M = 0.5$ to 2.5 and $Re = 18$ to 144. The reference proposed a nonlinear overheat ratio ξ defined as

$$h = h_0(1 - \xi \bar{a}_w) \quad (3)$$

where h_0 is the heat-transfer coefficient extrapolated to $\Delta T = 0$, and $\bar{a}_w \equiv (\Omega_w - \Omega_e) / \Omega_e$. The overheat ratio ξ was found to be a function of Mach and Reynolds numbers. Like reference 14, reference 16 found that the nonlinearity reverses under some flow conditions. That is, for some Reynolds numbers in the subsonic region the heat-transfer coefficient increased with increasing wire temperature; and, depending on M and Re , the heat-transfer coefficient was observed to decrease with increasing wire temperature under other flow conditions.

The work of reference 16 is the nearest approach to formulating clearly the important parameters affecting the nonlinear variation of heat-transfer rate with wire temperature. However, the results are

T111

limited to transonic and supersonic Mach numbers and to three values of Reynolds number. Additional data are required to verify the predicted trends at lower subsonic Mach numbers.

Objectives of This Research

The primary objective of this research was to examine the nonlinear variation of heat transfer with wire and air temperatures. The effect of wire temperature is complicated and not fully clarified by previous work, while there appears to be no systematic variation of air temperature in heat-transfer experiments from fine wires. Besides providing an additional insight into the nonlinearity of heat transfer with ΔT , data taken at various air temperatures are important for some hot-wire-anemometer applications (e.g., appendix E of ref. 17).

Furthermore, sufficient heat-transfer data from normal cylinders have been published in recent years that it should be possible to show clearly the effect of continuum, slip, and free-molecule flows on heat-transfer characteristics. An attempt to find a preliminary general correlation based on the results of this and earlier work is also an objective of this report.

APPARATUS AND PROCEDURE

Apparatus

Tunnel and air facility. - A sketch of the variable-density, low-turbulence tunnel used in this research is shown in figure 2. The incoming air passed through a cone-shaped filter screen covered with filter paper and wool felt. The air then entered the 6-inch-diameter inlet section where a total-pressure probe and heater control thermocouple were located. The tunnel contracted to the 1.50-inch-diameter circular test section in 6 inches; both the inlet and test sections were polished machined steel, "Pentrated" to prevent rust formation. Four static-pressure taps (1/64-in. holes) were located in the plane of the hot-wire probe. Static taps also extended along the length of the contracted area. As shown in the sketch, the hot-wire probe was mounted in a probe actuator that moved the wire out of the airflow into a small dead-air volume for protection when flow conditions were adjusted. A high-pressure valve packing gland acted as the vacuum seal but allowed the in and out motion of the probe. This simple feature was the primary reason for the long test life of the fine tungsten wire probe (number 109) reported here; the design evolved during the breaking of the first 108 wires.

The tunnel was serviced by the central laboratory air facilities. Test-section static pressure could be varied between 3 and 110 inches of mercury absolute. Mass-flow rate was independently adjustable; in this manner, the corresponding test-section Mach number could be varied between 0 and 0.85. For low mass-flow rates, the air mass flow was metered with a calibrated sonic orifice. The measured tunnel total and static pressures were used to calculate the Mach number assuming isentropic relations for all mass flow above 0.014 pound per second. A water U-tube manometer was used for total-static differences less than 2 inches of mercury; all other pressure readings were read from calibrated mercury manometers. Pressures were measured to at least three significant figures on both water and mercury manometers. Some uncontrollable fluctuations occurred in the inlet air supply, which may have resulted in a random error in reading of the third significant figure.

The total temperature of the air could be varied between -10° and 300° F by alternate use of refrigerator coils and electrical heaters. Total temperature was calculated from the measured recovery temperature of a calibrated thermocouple located in the probe test-section plane (see fig. 2). This temperature was read to the nearest half degree on a self-balancing indicator. Although the tunnel and inlet piping were well insulated, it was difficult to control the air total temperature as closely as desired over all the flow conditions. Deviations from the nominal air temperatures in day-to-day operation were $\pm 10^{\circ}$ F. However, the air temperature listed in table I is probably accurate within $\pm 1^{\circ}$ F of the total air temperature for each data point; uncertainty in total air temperature did not contribute significantly to uncertainty of the calculated Nusselt numbers except for wire temperatures only 50° F above recovery temperature. The effect of air-temperature fluctuations during any tunnel flow setting was minimized by making a linear interpolation between the two temperatures measured at the beginning and end of each set of six wire heat-loss measurements.

Probe design and tungsten wire. - A sketch of the probe used throughout this research is shown in figure 3. Several features of this design bear mentioning. One of the prime requirements is that the wire-supporting prongs do not substantially interfere with the airflow over the wire. Evidence that the design used met the requirement has been supplied by reference 12. Several probes of similar design were used in an experimental determination of the effect of yaw angle of attack on fine-wire heat transfer in reference 12, which concluded that no effect of probe interference could be noted in the results. Another important feature is that the four-wire lead design has matched metal junctions; that is, all unlike metal contacts occur symmetrically. Since the probe body was occasionally in a large temperature gradient (e.g., 300° F at fine-wire supports to 80° F at lead connector), it was important that no unbalanced thermocouple electromotive force exist in

the probe, especially when the wire was operated only 50° F above air temperature. Although some of the early probe designs did not satisfy this requirement, the probe reported here did not show any direct-current unbalance at zero power input for all operating temperatures. Finally, the four-lead-wire design and the use of a Kelvin double bridge minimized the electrical resistance of the probe and its influence on the accuracy of the hot-wire heat-loss measurements. This point is clarified further in the discussion of anemometer electrical equipment.

Tungsten wire with a nominal diameter of 0.0002 inch served as the heat-transfer element of the probe. The mounting technique is described in reference 9. Briefly, the wire is copper-plated at the ends for ease in soldering to the Inconel prongs; a high-temperature soft solder (m.p., 650° F) was used. One of the major drawbacks in the use of fine wires as heat-transfer elements is the uncertainty in the wire diameter (e.g., see ref. 9). In an attempt to decrease this uncertainty, electron micrographs were taken of samples from the spool of wire used on probe 109. These photographs are shown in figure 4; each is a different wire sample. An average diameter was calculated from several diameter measurements near the central position of each photograph. The necked-down section of sample C was not included in this average, which was 0.00022 inch. It can only be hoped that any wire sample as irregular as sample C would be eliminated after its room-temperature resistance was measured. That is, annealed tungsten wires of equal lengths have nearly identical resistance if the wire diameter is uniform. Many probes were discarded as a control procedure when their measured resistance deviated ± 5 percent from the average. Though the average diameter obtained from these samples is not necessarily the diameter of the 0.077-inch-long sample used in probe 109, the average is more probable than the manufacturer's nominal diameter, and 0.00022 inch was used in all calculations.

One of the most important physical properties of tungsten for the calculation of heat loss is the relation between temperature and electrical resistance. Early in the research it was apparent that each wire required calibrating if consistent data of the temperature loading effect on heat-transfer coefficient were to be obtained. Therefore, a small calibration heater was constructed, a sketch of which is given in figure 5. Several wires were silver-soldered to probes so the solder junction was unaffected at 650° F. These wires were then annealed by supplying sufficient current to heat the wire to about twice their room-temperature resistance for 30 minutes. The annealing caused the room-temperature resistance to drop several percent, but after 30 minutes no further change was observed. The probes were then inserted into the heater, and a complete calibration curve was obtained from 32° to 600° F. Two sample curves are given in figure 6(a). In all cases, a 1-milliampere detection current was used with the Kelvin bridge; therefore, negligible heating above air temperature resulted from the resistance measurement.

A least-square solution for the best parabola through these points gave the coefficients shown in figure 6(a); the curve was represented by $\Omega_w = \Omega_0 [1 + \alpha(T_w - 32) + \beta(T_w - 32)^2]$. From ten such complete resistance-temperature calibration curves, an average value of the second-order coefficient β was calculated to be $3.40 \times 10^{-7} (\text{°F})^{-2}$. Then a partial calibration curve was measured for the soft-soldered wire reported here (probe 109). As shown in figure 6(b), a least-square parabola was determined from the data points assuming $\beta = 3.40 \times 10^{-7} (\text{°F})^{-2}$; the resulting empirical equation was used for all calculations to relate measured wire resistance to wire temperature.

Anemometer electrical equipment. - A sketch of the primary circuit is shown in figure 7. The desired operating wire resistance was set on a Leeds and Northrup Kelvin Double Bridge (Model 4285) to four significant figures. With the switch in "hot" position the constant-average-temperature anemometer circuit varied the power input to the bridge until the wire was heated to the desired resistance and the "error" or galvanometer signal was a minimum. A hand-balanced volt-range potentiometer connected to the potential leads of the double bridge was used to measure the voltage across the hot wire. The power input to the wire element could be reproduced at a given flow setting to at least three significant figures in this manner. To measure the resistance of the unheated wire, the anemometer circuit was switched to "cold" position. This supplied the bridge with about 1-milliampere detection current, and the resistance was found by varying the bridge resistance until a 1.65-microvolt-per-millimeter galvanometer indicated balance.

The use of the Kelvin bridge and four-lead probes made it possible to measure the resistance and voltage drop of only the wire element, solder junction, and support prongs. Since the combined resistance of the junctions and prongs was less than 0.2 ohm, these lead resistances were less than 3 percent of the measured resistances in the worst case.

Procedure

The tunnel was operated at nominal Mach numbers of 0.05, 0.10, 0.20, 0.30, and so on to 0.80. At each Mach number, six static-density settings were used corresponding to nominal wire Knudsen numbers of 0.00916, 0.0143, 0.0256, 0.0416, 0.0555, and 0.0770. Most of these combinations were set at all four nominal total air temperatures of tunnel operation: 0° , 80° , 180° , and 280° F. An important feature of the test procedure was the somewhat random schedule of data taking. The run numbers in tables I and II are chronological. As will be emphasized in the RESULTS section, this procedure decreases the probability of systematic error in the measurements.

After the tunnel had been set at the desired condition and the probe moved into the test section, the manometer readings and test-section total temperature were recorded. The unheated or recovery resistance of the wire was measured next. Then, five or six hot-wire resistances were set and the voltage across the wire was recorded at each setting. About 5 minutes were required for all these heat-loss measurements. Finally, the recovery resistance and manometer-temperature readings were recorded again to complete the procedure.

The measured wire recovery resistance was used as a check of the wire temperature-resistance calibration. At no time during the reported runs did the measured Ω_e differ from that predicted by figure 6(b), nor the calculated T_e by more than 1 percent and on the average within 0.5 percent; T_e was calculated from the measured air total temperature in a manner discussed in the next section.

DIMENSIONLESS GROUPS OF CORRELATION

In this section, the dimensionless groups used in correlating the data are related to the physical measurements. An energy balance considering convection, conduction, and radiation for a hot wire in steady operation is

$$Q_P = Q_C + Q_K + Q_R \quad (4)$$

The heat input per unit time is simply

$$Q_P = J^2 I^2 \Omega_w \quad (5)$$

The convective heat-loss rate defines the heat-transfer coefficient h :

$$Q_C = h\pi D_w l (T_w - T_e) \quad (6)$$

Equation (6) has equilibrium or recovery temperature T_e of an insulated wire in the temperature difference $(T_w - T_e)$. Therefore, as the wire temperature approaches its recovery value, the convective heat-transfer rate goes to zero. Figure 8 (from ref. 10) is the equilibrium temperature ratio used to obtain T_e from the measured air total temperature. It is well established that, for Knudsen numbers less than 0.10, the equilibrium temperature ratio for normal wires in both slip and continuum flow is a function only of Mach number (refs. 10 and 13 to 16).

The conduction loss rate to the supporting prongs Q_K is discussed in detail in appendix B. The radiation rate Q_R was calculated to be

less than 0.1 percent of the power input Q_p , and no correction for radiation was made. However, since the heat loss to the supports was appreciable, an "end-loss" correction was made.

The Nusselt number is defined as

$$Nu = \frac{hD_w}{k} \quad (7)$$

The air thermal conductivity k has been evaluated at various temperatures by previous investigators. Some use static, others equilibrium or recovery, or total temperature; frequently in engineering work an arithmetic average "film" temperature is used (ref. 11). The guiding principle for empirical data fitting is, of course, to obtain the best correlation. The DISCUSSION section shows that the nonlinear temperature effect on heat-transfer coefficient of both air and wire temperature is too complicated in the slip-flow region for any of these choices to eliminate either "Mach number" or temperature effects. Therefore, for convenience, the air conductivity has been evaluated at total air temperature (k_t). Since the tunnel was operated at set values of total temperature, this choice introduces no Mach number variation into the Nusselt number correlation at constant Knudsen number:

$$Nu_t = \frac{hD_w}{k_t} \quad (7a)$$

The Nusselt number can be expressed in terms of heat loss using equation (6):

$$Nu_t = \frac{Q_C}{\pi l k_t (T_w - T_e)} \quad (8)$$

The convective heat loss Q_C is the difference between the measured power input Q_p and a calculated correction for Q_K . A convenient way to make this correction is to define an uncorrected Nusselt number Nu_t'' , which is completely determined from measured quantities:

$$Nu_t'' \equiv \frac{Q_p}{\pi l k_t (T_w - T_e)} = \frac{J^2 I^2 \Omega_w}{\pi l k_t (T_w - T_e)} \quad (9)$$

Two published end-loss correction procedures were used, as discussed in appendix B; each gave a correction factor ψ , defined as

$$\psi = \frac{Nu_t}{Nu_t''} \quad (10)$$

5111

Therefore, the tabulated Nusselt numbers were obtained from

$$Nu_t = \psi \frac{J' I^2 \Omega_w}{\pi l k_t (T_w - T_e)} \quad (11)$$

The wire temperature was obtained from measured Ω_w and the resistance-temperature calibration:

$$\Omega_w = \Omega_0 [1 + \alpha(T_w - 32) + \beta(T_w - 32)^2] \quad (12)$$

The equilibrium wire temperature was calculated from figure 8 and the measured total air temperature. The air conductivity k_t was taken from reference 18. All calculations were performed with an IBM 653 digital computer.

The Reynolds number Re_t for the wire was defined by the free-stream (or static) density and velocity; the air viscosity was evaluated at total air temperature (ref. 18):

$$Re_t = \frac{\rho U D_w}{\mu_t} \quad (13)$$

The Knudsen number was calculated from free-stream density and the wire diameter using the formula suggested by reference 14:

$$Kn = \frac{\lambda}{D_w} = \frac{1.5870 \times 10^{-8}}{\rho D_w} \quad (14)$$

The constant 1.5870×10^{-8} has the units pounds(mass) × square feet. Equation (14) assumes that the mean free path for air λ is given by elementary kinetic theory and that $\rho \lambda$ is a constant.

The Mach number was calculated from the velocity measured with a sonic orifice and static temperature:

$$M = \frac{U}{49.02 \sqrt{T}} \quad (15)$$

The measured total-static pressures were used in the isentropic relations ($\gamma = 1.40$) for high-range mass flows to find Mach number.

Finally, the dimensionless turbulent intensity v'/U is known to affect the heat transfer from normal cylinders. However, the excellent work of reference 19 has shown that intensities as high as 20 percent

have negligible effect on heat transfer from fine wires if the scale of turbulence is large compared with cylinder diameter. The intensity of turbulence varied in the test section but was always less than 1 percent. The scale was large compared with D_w . Therefore, turbulence was not a factor in these tests.

RESULTS

Twenty-three plots using all 1100 data points are presented in this section. These figures are intended to show the general consistency and the scope of the data. In the following section, these plots are used to point out some of the complicated effects observed in slip flow. Figure 9 shows the Nusselt number variation with Mach number for specified values of Knudsen number and wire and air temperatures. Figure 9(a) gives results for increasing wire temperatures at a total air temperature of 0° F. Similarly, figures 9(b), (c), and (d) are for air temperatures of 80° , 180° , and 280° F, respectively.

With the exception of the lowest wire temperature at each air temperature, the general consistency of the data is good. There are two experimental checks that can be used as a guide to data reliability. The first has already been discussed in the Procedure section; that is, the recovery resistance of the wire at a given air temperature and Mach number can be checked against the measured air temperature and the resistance-temperature calibration. The fact that these measurements usually checked predicted values within 0.5 percent is evidence that the critical Ω -T calibration did not vary during the course of the experiment. Another check for consistency is reproducibility. To demonstrate this feature, the chronological run numbers are shown with the data points in figure 9(b) for T_w of 583.8° F. The fact that the agreement between check points is good is evidence that the heat-transfer characteristics of the wire were unaffected by dirt accumulation, oxidation, or other uncontrollable factors during the experiment.

The data scatter at the lowest wire temperature for each air temperature is reasonable, because in equation (11) it is clear that constant percentage errors in T_w or T_e are magnified when the difference $(T_w - T_e)$ is small. However, the scatter at $Kn = 0.0770$ and also at $M > 0.50$ is puzzling. No satisfactory explanation for this scatter has been found. The high Knudsen number suggests that the poor correlation may be associated with the rarefied gas flow. For example, reference 20 calculated a "correction" for the temperature-jump phenomenon of slip flow. Accepted slip theory (ref. 21) was used to calculate the temperature jump. Then, by redefining the heat-transfer coefficient in terms of the difference between jump temperature and recovery temperature, a Nusselt number "correction" that depends only Knudsen number was obtained.

The jump phenomenon does not account for the data scatter observed here at low wire temperatures, because the temperature jump is assumed proportional to $(T_w - T_e)$, going to zero as ΔT vanishes. Furthermore, the correction procedure has dubious value when the slip-flow region is approached from free-molecule flow predictions, because the procedure attempts to force data taken in slip flow to fit the form of continuum-flow observations. In this sense, the correction only confuses the over-all correlation and postpones the inevitable deviation from continuum Reynolds number correlations.

DISCUSSION

In this section some of the non-Reynolds-number effects evident in figure 9 are discussed. Then, the dependence of the Nusselt number on both wire and air temperature is considered. These complicated effects fortunately are relatively small compared with the dependence of Nusselt number on the aerodynamic environment. Therefore, the few generalizations that can be inferred from the data concerning these second-order temperature effects are discussed first. Then, a graphical Nusselt number correlation as a function of Reynolds and Knudsen (or Mach) numbers is presented for the slip-flow data of this research. An attempted general Nusselt number correlation for continuum, slip, and free-molecule flows follows, based on these and earlier data together with free-molecule flow theory. Finally, a fluctuation sensitivity equation for hot-wire anemometers is presented that applies to fine wires in subsonic slip flow.

Preliminary Discussion of Results

The following discussion of figure 9 attempts to point out the deviations from simple \sqrt{Re} dependence of continuum flow that are evident in these slip-flow data. Later in this section, the heat-transfer characteristics of cylinders in continuum, slip, and free-molecule flows are considered. The discussion is limited to air at constant temperature where viscosity is constant. If the Nusselt number were a function only of \sqrt{Re} , lines of constant $\rho D_w U$ on a logarithmic plot of Nu against U would form a family of parallel straight lines with a common slope of 0.50. The argument changes little if a family of constant Knudsen number lines on a log-log plot of Nusselt number against Mach number is considered. Two important deviations from this behavior should be noted in figure 9. The constant Knudsen number lines are linear only for Mach numbers less than 0.4. The decrease in slope and curvature that occurs around $M = 0.4$ is most pronounced at high Knudsen number where the sensitivity of heat-transfer coefficient to changes in Mach number almost disappears. Secondly, even the straight portions of these

constant Kn curves exhibit slopes other than 0.50. For example, the slopes $(\Delta \log Nu_t)/(\Delta \log M)$ in figure 9(b) for $T_w = 583.8^\circ F$ from $M = 0.05$ to 0.4 increase with increasing Kn from 0.25 to 0.35.

Therefore, it is clear that no simple power dependence of Nu_t against Re_t should be expected to apply to these data over any appreciable range of variables. Furthermore, the wire and air temperatures can be expected to have only secondary influence on any correlation of the data, because the characteristics just discussed appear in all 23 parts of figure 9.

Effect of Wire Temperature on Heat-Transfer Coefficient

Many cross plots are necessary in order to show clearly what effect varying the wire temperature has on the heat-transfer coefficient at a given flow condition. Figure 10(a), which presents cross plots of figure 9(a), is a plot of Nusselt number as a function of $(T_w - T_e)$ with Knudsen number as a parameter. All plots are for total air temperature of $0^\circ F$, and each plot is for a particular Mach number. Similarly, figures 10(b), (c), and (d), which are for total air temperatures of 80° , 180° , and $280^\circ F$, respectively, are cross plots of figures 9(b) to (d).

Consider figure 10(b) for $T_t = 80^\circ F$ and $M = 0.10$. The interesting feature is that the Nusselt number increases for the two lowest values of Knudsen number as the wire temperature is increased. For $Kn = 0.0256$ and 0.0416 , Nu_t does not vary appreciably with ΔT , but at the two highest values of Kn , the heat-transfer coefficient decreases as the wire temperature increases. Furthermore, whether Nu_t increases or decreases, the dependence on wire temperature is greatest for ΔT less than $200^\circ F$ and tends to vanish for ΔT greater than $200^\circ F$. This general picture is repeated for all the subsonic Mach numbers at $T_t = 80^\circ$ (fig. 10(b)). The two anomalous points at $M = 0.05$ are probably experimental errors. The percentage change in Nu_t from $\Delta T = 50^\circ F$ to the asymptotic value at $\Delta T > 200^\circ F$ is roughly 20 percent at all Mach numbers for both $Kn = 0.00916$ and $Kn = 0.0770$. There does appear to be a secondary Mach number effect that causes the reversal value of Kn (where the sign of the temperature dependence changes) to increase as M increases. For example, at $M = 0.10$, Nu_t is insensitive to ΔT at $Kn = 0.0256$ and 0.0416 ; but at $M = 0.60$ Nu_t is relatively insensitive to ΔT at higher Kn values (0.0416 and 0.0555).

Therefore, from figure 10(b), the wire temperature appears to affect the heat transfer in a manner primarily dependent on Kn and to a lesser extent on M , over the range of this experiment.

Figures 10(a), (c), and (d) essentially confirm what was observed at $T_t = 80^\circ \text{ F}$ in figure 10(b). The temperature difference ($T_w - T_e$) again appears to correlate the data into families of curves similar to figure 10(b). It is important to note that between $\Delta T = 50^\circ$ and 200° F at all air temperatures the maximum wire-temperature loading effect is evident, and at $\Delta T > 200^\circ \text{ F}$, Nu_t approaches an asymptote.

Had a nondimensional temperature ratio like $\tau \left(\equiv \frac{T_w - T_e}{T_t} \right)$ been used, this regular feature would not have been observed. In figures 10(c) and (d), the increased air temperature tends to decrease the value of the Knudsen number where the sign of the wire-temperature loading effect reverses. That is, the $Kn = 0.0416$ and 0.0555 lines of both figures 10(c) and (d) show Nu_t increasing with increasing ΔT , while at $T_t = 80^\circ \text{ F}$ these data were either unaffected or decreased as ΔT increased. This same effect of air temperature on the wire-temperature loading may also be seen in figure 10(a) for $T_t = 0^\circ \text{ F}$. Disregarding for the moment the $Kn = 0.00916$ and 0.0143 lines in figure 10(a), it is apparent that the insensitivity to ΔT at $M = 0.40$ to 0.80 persists at lower values of Kn in figure 10(a) than in figure 10(b). No explanation for the apparently anomalous behavior of the $Kn = 0.00916$ and 0.0143 curves in figure 10(a) has been discovered.

However, though the air temperature seems to have a secondary role in the wire-temperature loading phenomenon, it should not confuse the primary observation. That is, for $Kn < 0.02$, the heat-transfer coefficient increases with increasing ΔT up to $\Delta T \approx 200^\circ \text{ F}$, where it assumes an asymptotic value. On the other hand, for $Kn > 0.02$, the heat-transfer coefficient is unaffected or decreases with increasing ΔT to $\Delta T \approx 200^\circ \text{ F}$, where it again assumes an asymptotic value. The Mach number has a secondary role in this wire-temperature loading effect, generally causing the reversal Knudsen number to assume higher values (>0.02) as the Mach number increases in the subsonic range.

The trends reported here have been noted by previous investigators. The work of reference 16 was mentioned in the INTRODUCTION. The nonlinear overheat coefficient ξ defined by equation (3) is given as a function of Reynolds and Mach number by figure 8 of reference 16. For convenience, this figure is included herein as figure 11, and lines of constant Kn are superimposed. Now, it is clear from figure 10 that the heat-transfer coefficient observed in this research is not a linear function of ΔT (or related \bar{a}_w or τ). However, the sign of the overheat coefficient ξ and its dependence on Kn and M is the important feature of figure 11. In general, in subsonic flow for low Kn , figure 11 predicts an increase in Nu_t with ΔT ; a reversal of sign occurs

between $Kn = 0.015$ and 0.020 ; while for Kn greater than these latter values, ξ predicts Nu_t will decrease with increasing ΔT . Furthermore, the Mach number has a secondary role causing the reversal value of Kn to increase. With the exception of the asymptotic behavior at large ΔT observed in this research, the work of reference 16 generally substantiates the results reported here. Since similar effects were noted in reference 14, there can be no doubt that these complicated wire-temperature effects are real, even though of second-order magnitude. Appendix B discusses the sole correction to the primary data (conduction loss) at some length to emphasize the fact that the wire-temperature loading effect cannot be traced to improper handling of the primary data.

Effect of Air Temperature on Heat-Transfer Coefficient

In order to isolate the effect of air temperature on the heat-transfer coefficient, it is of course necessary to eliminate the influence of wire-temperature loading. A logical way to accomplish this distinction would be to extrapolate the Nusselt number curves of figure 10 to $\Delta T = 0$. However, this is the region of maximum curvature, and extrapolation to zero overheat would be very uncertain. The asymptotic value of Nu_t for $\Delta T > 200^\circ F$ is a more direct Nu_t value that is independent of wire-temperature loading. Therefore, plots of the asymptotic Nu_t ($\Delta T > 200^\circ F$) are presented in figure 12 as a function of total air temperature at various Mach numbers. Over the entire range of this experiment, the Nu_t decreases with increasing air temperature. The magnitude of this general trend in figure 12 appears to depend primarily on the value of the Nusselt number, being the order of 5 to 10 percent per $100^\circ F$ for Nu_t between 3.0 and 4.0 but decreasing to 1 to 2 percent per $100^\circ F$ near $Nu_t = 1.0$. No clear dependence of the air-temperature loading of Nu_t on either Mach or Knudsen number is discernible in this experimental range.

In figure 12, the Nusselt number decreases with increasing temperature, but it is not clear what dependence the heat-transfer coefficient h has on air temperature. Figure 13, which clarifies this point, is a copy of figure 12(b) for $M = 0.50$ with lines of constant heat-transfer coefficient superimposed. If the heat-transfer coefficient were constant and equal to the value observed in $80^\circ F$ air, then Nu_t would vary with air temperature as shown by the dashed lines in figure 13. That is, the variation in air thermal conductivity k , which causes the T_t dashed-line dependence, is counterbalanced by an increase in heat-transfer coefficient h as the air temperature is increased. However, since h

is not as temperature-dependent as k in this experimental range, the result is a net decrease in Nu_t with rising T_t .

Reference 6 reports good agreement of data taken at $1540^\circ < T_t < 3000^\circ$ F with the room-temperature correlation of reference 13. Thus, in the range of this work ($450 < Re < 3000$, $0.3 < M < 0.8$), air temperature had little effect on the Nusselt number, though there is a possibility that the high-temperature correlation is slightly lower than the room-temperature results. Therefore, it appears well established that increasing air temperature causes an increase in heat-transfer coefficient for all subsonic conditions where $Re > 1.0$.

The Prandtl number $c_p\mu/k$ varies from about 0.72 at 0° F to 0.68 at 280° F (ref. 18). Several correlations of Nu_t with Pr were attempted in order to eliminate the air-temperature effect shown in figure 13. However, none of these was successful, although plots of Nu_t/Pr_t^2 or Nu_t/Pr_t^3 did generally reduce the air-temperature dependence. The air-temperature range of this research is too small for any valid conclusions concerning Prandtl number correlations to be inferred.

Correlation of Slip-Flow Heat-Transfer Data

The heat-transfer characteristics of cylinders in slip flow are complicated by second-order dependence on body and air temperature. Nevertheless, a correlation of Nusselt number with the flow parameters is desirable as a first approximation in engineering work even though it does not account for the temperature phenomena. The Preliminary Discussion of Results pointed out what deviations from simple \sqrt{Re} dependence are evident in the data, but figure 9 is not a satisfactory substitute for the conventional correlation of Nu and \sqrt{Re} . Figure 14 is an attempt to find a useful correlation. It shows the logarithmic variation of Nu_t with Re_t ; constant M and Kn parametric lines are shown solid and dashed, respectively. Data for $T_t \approx 80^\circ$ F and $T_w = 584^\circ$ F are plotted in this slip-flow correlation.

The increasing necessity for an additional parameter other than the Reynolds number to correlate these experimental heat-transfer data shows clearly on this plot as Re decreases. This additional parameter is either the Mach number or the Knudsen number. The graphical correlation (fig. 14) makes no distinction between $Nu = f(Re, M)$ or $Nu = f(Re, Kn)$, because both forms are shown. However, only one additional parameter (M or Kn) is independent (eq. (2)). The remainder of this section is devoted to showing that the use of Knudsen number as the additional parameter is preferable. Note that the Kn lines decrease in slope as

Kn increases. However, these constant Kn curves are approaching the slope of the constant Mach number lines at $Kn = 0.00916$. That is, ρD_w is approaching equivalence to U as required for simple Re correlation as Kn decreases; but the decreasing slopes of the Kn curves as $Kn \rightarrow 0.0770$ cause a wide divergence of the constant Mach number lines that is most pronounced at low subsonic M (and low Re).

The preceding discussion of figure 14 emphasizes the fact that the failure of the Reynolds number alone to correlate the data, which has been termed a "Mach number effect" (e.g., p. 34 of ref. 22) and associated with compressibility, is, in fact, a rarefied-gas phenomenon and should be termed a "Knudsen number effect." This distinction is important and not just an arbitrary matter of viewpoint, even though equation (2) may make it so appear. When viewed as a rarefied-gas effect, the large separation of subsonic Mach number lines on a plot of Nu_t against Re_t loses its anomalous features and becomes theoretically predictable. Figure 15 was taken from an approximate slip-flow analysis published in 1953 (ref. 23). The qualitative agreement with the data in figure 14 is excellent, considering the approximations made in the theoretical analysis.

Attempted General Correlation for Nusselt Number in Continuum, Slip, and Free-Molecule Flows

Figure 16 combines the correlation of the slip-flow data of this research (fig. 14) with the continuum experimental results of reference 13 and the free-molecular-flow theoretical predictions of references 15 and 24. A brief review of these latter reports is followed by a discussion of figure 16 as a whole.

The experimental range of reference 13 is shown in figure 1. The transient response of thermocouples in air was measured, and the results were correlated within 7.4-percent average deviation of a single observation by the following equation:

$$Nu_t = 0.431 \sqrt{Re_t^*} \quad (16)$$

where Re_t^* is a Reynolds number defined by free-stream velocity, total-temperature viscosity, wire diameter, and a density based on static pressure and total temperature. In terms of the Reynolds number defined by equation (13), the Nusselt number correlation of reference 13 is

$$Nu_t = 0.431 \sqrt{Re_t} \left(\frac{T}{T_t} \right)^{1/2} \quad (16a)$$

where

$$\frac{T}{T_t} = \left(1 + \frac{\gamma - 1}{2} M^2\right)^{-1}$$

The equation applies in range of the experiment: $250 < Re < 30,000$ and $0.1 < M < 0.9$. A partial plot of equation (16a) is shown in figure 17. The important feature is the small effect that changing the subsonic Mach number has on heat transfer at constant Reynolds number. This Mach number effect increases with increasing M and is practically zero below $M = 0.3$. It is reasonable to expect that a compressibility phenomenon would behave in this manner.

An equation for the free-molecular-flow heat transfer from an infinite cylinder in a diatomic gas stream was derived in reference 24. Evaluating all air properties at $80^\circ F$ and assuming an accommodation coefficient of 0.90, this equation may be written as

$$Nu_t = 0.0297 \frac{g(s)}{Kn} \left(\frac{T}{T_t}\right)^{1/2} \quad (17)$$

where $g(s)$ is a defined function of Mach number plotted in figure 18. Equation (17) applies to all $Kn > 2$. Figure 19 is a plot of equation (17) for $Kn > 2$; it also gives the predictions of slip theory for $Kn < 2$. Although several of the essential features of this free-molecule analysis have been confirmed experimentally, equation (17) has not been tested over an appreciable range of variables. However, free-molecule-analysis theoretical predictions are generally believed reliable. The two essential features of figure 19 for $Kn > 2$ are the first-power dependence on Re and the large separation of subsonic M lines.

Returning to figure 16, the slip-flow experimental data extrapolate smoothly into the continuum-flow empirical curve. However, the slip-flow correlation at $Kn = 0.0770$ cannot be extrapolated to the free-molecule-flow correlation at $Kn = 2$. Nevertheless, several of the trends required by the rarefied-gas analysis are evident in the data. The slip-flow data constant M lines increase in slope and may be approaching first-power Re_t dependence at $Kn = 0.0770$. Furthermore, the increasing Kn dependence causes a spread of the constant M lines at $Kn = 0.0770$ that is most pronounced at low subsonic M . Before the attempted correlation in figure 16 can be reliably extended below $Re = 1.0$, it will be necessary to obtain experimental data between Kn of 0.10 and 10.0. Until these data are published, the theoretical curves from the approximate slip-flow analysis of reference 23 between Kn of 0.04 and 2 shown in figure 19 may be used as a first approximation together with the free-molecule-flow prediction for $Kn > 2$.

Finally, the suggested curve of reference 11 is shown in figure 16 for easy comparison. The low Reynolds number data used to obtain this curve were for very low velocities ($Kn < 0.01$). Furthermore, the attempted general correlation and the reference 11 correlation are not comparable, strictly speaking, because total air temperature was used for calculating conductivity and viscosity in the proposed correlation, while an average "film" temperature was used in reference 11.

Hot-Wire-Anemometer Sensitivity

One application of the heat-transfer correlations presented in the preceding section is for hot-wire-anemometer sensitivity. King's equation (1) sensitivity for wire $Re < 250$ is a crude approximation because the Knudsen number effect complicates the Reynolds number correlation. In the following paragraphs, a sensitivity equation based on dimensionless group correlations is proposed. However, as in the past, the only reliable hot-wire sensitivity is a direct calibration of the particular wire over the flow range of operation. The sensitivity equation serves as a guide to performing this calibration.

The Nusselt number correlation given in figure 14 may be expressed in a general manner as

$$Nu_t = f(M, Kn, \Delta T, T_t) \quad (18)$$

The dependence on ΔT and T_t causes up to 20-percent deviations from figure 14 in a complicated manner. The following derivation assumes that the anemometer wire operates at constant temperature (e.g., see ref. 9). This eliminates the functional dependence of Nu_t on ΔT . It is convenient to express the remaining T_t dependence in equation (18) with a dimensionless temperature ratio τ :

$$\tau = \frac{T_w - \eta T_t}{T_t} = \frac{\Delta T}{T_t} \quad (19)$$

The recovery temperature ratio η (fig. 8) will be assumed a function only of Mach number; this is true for $Kn < 0.10$.

The general sensitivity for a constant-temperature anemometer wire to fluctuating flow velocity, density, and total temperature may be written as

$$2I\Omega_w dI = \frac{\partial}{\partial U} \left[\frac{\pi}{J} \lambda k_t Nu_t (T_w - \eta T_t) \right] dU + \frac{\partial}{\partial \rho} \left[\frac{\pi}{J} \lambda k_t Nu_t (T_w - \eta T_t) \right] d\rho + \frac{\partial}{\partial T_t} \left[\frac{\pi}{J} \lambda k_t Nu_t (T_w - \eta T_t) \right] dT_t \quad (20)$$

5111

Recalling that it is assumed that the wire temperature is maintained constant by a fluctuating feedback current, denoted by i ($=dI$), then equation (20) becomes

$$i = \frac{I}{200} \left[- \left(1 + \frac{\gamma - 1}{2} M^2 \right) \frac{M}{\tau} \frac{\partial \eta}{\partial M} - \frac{\eta}{\tau} (\gamma - 1) M^2 + \left(1 + \frac{\gamma - 1}{2} M^2 \right) \frac{\partial \log Nu}{\partial \log M} \right] \\ \times \frac{100 \delta U}{U} + \frac{I}{200} \left(- \frac{\partial \log Nu}{\partial \log Kn} \right) \frac{100 \delta \rho}{\rho} + \frac{I}{200} \left(\frac{\partial \log k}{\partial \log T_t} - \frac{\eta}{\tau} - \frac{\tau + \eta}{Nu} \frac{\partial Nu}{\partial \tau} \right) \frac{100 \delta T}{T_t} \quad (21)$$

Appendix C gives the derivation of equation (21), which relates the fluctuating current i of a constant-temperature anemometer wire to the fluctuating flow variables velocity fluctuation δU , density fluctuation $\delta \rho$, and total-air-temperature fluctuation δT . The average wire current I refers to an infinitely long wire if the sensitivity slopes are taken from Nu_t rather than Nu_t'' plots. The second-order dependence of the general correlation (fig. 14) on air and wire temperatures complicates generalizations concerning the major sensitivity slopes:

$\frac{\partial \log Nu}{\partial \log M}$, $\frac{\partial \log Nu}{\partial \log Kn}$, and $\frac{\partial Nu}{\partial \tau}$. However, since over a small range of variables each of the logarithmic slopes is linear and approximately independent of the magnitude of the independent variable, it is possible to make two limited generalizations. Figure 20 gives the measured slopes from figure 9(b) for T_w of 583.8° F and its cross plot; these terms are applicable at $T_t \approx 80^\circ$ F and $\Delta T > 200^\circ$ F.

The utility of equation (21) is limited by the lack of a precise universal correlation. However, if the turbulent velocity intensity is the quantity of interest in airflows of $M < 0.4$, equation (21) simplifies considerably. Under these circumstances, density fluctuations are frequently negligible; and, unless heat is added to or taken from the airstream, the total-air-temperature fluctuations are also negligible. The predominant term in the velocity sensitivity is $(\partial \log Nu)/(\partial \log M)$, and this term is as easily obtained experimentally as the usual King's equation calibration curve, perhaps requiring only a larger range of velocity variation.

Finally, it should be pointed out that reference 22 presents sensitivity equations similar to equation (21) for constant-current anemometry, with special emphasis on supersonic-flow applications. In subsonic and transonic applications, equation (21) has the advantage that the Reynolds number was not chosen as an independent variable (M and Kn , rather than M and Re). The use of Reynolds number introduces additional terms in the velocity sensitivity.

CONCLUDING REMARKS

The following conclusions can be drawn from the heat-transfer measurements for cylinders in slip flow presented in this report:

1. An attempted Nusselt number correlation for heat transfer from normal cylinders in subsonic continuum, slip, and free-molecule air-flows is given as figure 16. Slip-flow experimental data of this paper extrapolate into existing continuum-flow experimental data for low values of Knudsen number ($Kn < 0.01$). The slip-flow data qualitatively verify trends predicted by free-molecule-flow theory ($Kn > 2$) at Kn approaching 0.10; but extrapolation does not give quantitative agreement. Further experiments in the transition region between slip and free-molecule flows are necessary to complete the general correlation.

2. Empirical equations that give the Nusselt number as a constant power of Reynolds number, familiar in continuum flow, are progressively in error for $Re < 250$ because of increasing Kn dependence in the slip-flow region. The correlation of Nusselt number for this slip-flow experiment is shown graphically in figure 14 as a function of Reynolds and Knudsen or Mach numbers. This dependence is too complicated for an empirical equation with engineering utility, although simple equations have previously been proposed in both continuum and free-molecule flows.

3. The approximate slip-flow analysis of reference 23 correctly predicts the trends observed but fails to fit the data quantitatively.

4. For air temperatures between 80° and 280° F, the heat-transfer coefficient h increases with increasing temperature difference ΔT at low Kn (< 0.02). This nonlinearity in h with ΔT has commonly been observed in continuum-flow experiments. However, with air temperatures between 0° and 280° F, at high Kn (> 0.02) the heat-transfer coefficient decreases with increasing ΔT . In both cases, the effect of ΔT was greatest for ΔT below 200° F, tending to disappear at ΔT greater than 200° F. A secondary Mach number effect causes the reversal Knudsen number of about 0.02 to shift to larger values as M increases. The major trends are corroborated by the work of reference 16.

5. For wires operated at ΔT greater than 200° F, an increase of air temperature causes the heat-transfer coefficient h to increase. This occurs for all flow conditions of this research. The increase in air thermal conductivity with total air temperature tends to cancel the variation of Nusselt number $Nu_t (=hD_w/k_t)$ with air temperature. However, Nu_t decreases slightly with increasing air temperature because the thermal conductivity has a greater temperature-dependence than the heat-transfer coefficient in the range of this research.

6. Constant-temperature hot-wire-anemometer sensitivity to velocity, density, and total-air-temperature fluctuations is extremely complicated with the probe in subsonic slip flow. General sensitivity equations together with a few generalizations observed in this research have been presented. However, individual calibration of wires in the flow range of interest is the only reliable technique for subsonic applications because (a) King's law is a very special case of hot-wire sensitivity ($Kn < 0.001$, $M < 0.3$), and (b) complicated nonlinearity of heat transfer with wire and air temperature prevents accurate generalizations using dimensionless groups.

Lewis Flight Propulsion Laboratory
National Advisory Committee for Aeronautics
Cleveland, Ohio, August 28, 1958

APPENDIX A

SYMBOLS

A	King's equation intercept (eq. (1)), $A = a\lambda k$
A'	dimensionless King's equation intercept (eq. (1a)), $A' = a/\pi\Omega_0\alpha$
A_w	cross-sectional area of wire, sq ft
a,b	dimensionless empirical constants (eq. (1))
a^*	dimensionless term in eq. (B24)
a_s	speed of sound
\bar{a}_w	resistance ratio, $(\Omega_w - \Omega_e)/\Omega_e$
B	King's equation slope (eq. (1)), $B = b\lambda\sqrt{D_w\rho c_p k}$
B_1, B_2	empirical constants (eq. (B16))
B'	dimensionless King's equation slope (eq. (1a)), $B' = b/\pi\Omega_0\alpha$
B^*	dimensionless term defined by eq. (B18)
C	ratio of heat lost by conduction to supports to heat lost to air by convection (eq. (B13))
c_p	isobaric specific heat
D_s	support diameter, ft or in.
D_w	wire diameter, ft or in.
e,G	dimensionless terms defined by eq. (B20)
g_c	conversion factor to engineering units, $(\text{lb(M)})(\text{ft})/\text{lb(F)}\text{-sec}^2$
h	convective heat-transfer coefficient (eq. (6))
h_0	heat-transfer coefficient extrapolated to $\Delta T = 0$
I	wire current, amp
J	conversion of Btu to ft-lb(F)

J'	conversion of watts to Btu/sec, 9.484×10^{-4}
K_S	thermal conductivity of Inconel support, Btu/(sec)(ft)($^{\circ}$ F)
K_W	thermal conductivity of tungsten wire, Btu/(sec)(ft)($^{\circ}$ F)
Kn	Knudsen number, λ/D_W
k	thermal conductivity of air, Btu/(sec)(ft)($^{\circ}$ F)
l	length of wire, ft
M	Mach number
Nu	Nusselt number, hD_W/k
Nu''	Nusselt number uncorrected for heat loss to supports (eq. (9))
Pr	Prandtl number, $c_p\mu/k$
Q	length-average heating rate, Btu/sec
q	heating rate per unit length, Btu/(ft)(sec)
Re	Reynolds number, $\rho D_W U/\mu$
$Re_{f,s}$	Reynolds number of support, $\rho U D_S/\mu_{f,s}$
S	dimensionless term defined by eq. (B25)
T	static or free-stream air temperature
ΔT	temperature difference, $T_W - T_e$
T_a	air temperature
T_e	recovery or equilibrium wire temperature
T_t	total air temperature
T_W	length-average wire temperature
$T_{W,\infty}$	length-average temperature of infinitely long wire, $T_{W,\infty} \equiv \sigma_1/\sigma$
t^*	dimensionless ratio (eq. (B18))
t_w	local wire temperature at any point x

U	free-stream air velocity, ft/sec
v'	rms turbulent velocity, ft/sec
x	any position along length of wire, $x = 0$ at wire center
Y	dimensionless term defined by eq. (B18)
z	factor in end-loss correction procedure, defined by eq. (B19)
α	first-order coefficient of electrical resistance - temperature relation (eq. (12)), $^{\circ}\text{F}^{-1}$
β	second-order coefficient of electrical resistance - temperature relation (eq. (12)), $^{\circ}\text{F}^{-2}$
γ	ratio of specific heats, 1.4 for air
δ	perturbation component
η	recovery temperature ratio, $\eta \equiv T_e/T_t$
λ	mean free path of air, ft
μ	air viscosity, $\text{lb(M)}/(\text{ft})(\text{sec})$
ξ	nonlinear overheat coefficient (eq. (3))
ρ	air density, $\text{lb(M)}/\text{cu ft}$
σ	coefficient defined in eq. (B7)
σ_1	coefficient defined in eq. (B8)
τ	temperature ratio, $\tau \equiv (T_w - T_e)/T_t$
ψ	end-loss correction ratio, $\psi \equiv \text{Nu}/\text{Nu}''$
Ω_a	length-average wire resistance at air temperature T_a , ohms
Ω_e	length-average wire resistance at recovery air temperature T_e , ohms
Ω_w	length-average wire resistance at hot-wire temperature T_w , ohms
Ω_0	length-average wire resistance at 32°F , ohms
ω	wire resistance per unit length, ohms/ft

Subscripts:

C	convection
f	film temperature, $T_f \equiv (T_s + T_e)/2$
K	conduction
m	measured
P	production
R	radiation
s	support (except a_s)
t	total air temperature T_t
w	wire or cylinder
O	evaluated at 32° F (except h_0)

APPENDIX B

CORRECTIONS FOR CONDUCTION TO SUPPORTS

Linear Correction

The steady-state heat transfer from a hot wire having negligible radiant heat loss is treated by Lowell in reference 10, where equations for making precise corrections for finite wire length are presented. Except for a minor innovation, the following analysis is that of reference 10.

The energy-balance equation at any cross section x for this problem is simply

$$q_P = q_C + q_K \quad (B1)$$

The convection heat loss per unit length of wire at x can be expressed as

$$q_C = hD_w \pi (t_w - T_e) = \pi k_t Nu_t (t_w - T_e) \quad (B2)$$

The expression for conduction of heat to the supports can be simplified if it is assumed that the heat flow through the wire is one-dimensional and that the wire thermal conductivity K_w is not affected by temperature:

$$q_K = - K_w A_w \frac{d^2 t_w}{dx^2} \quad (B3)$$

Neglecting the second-order term $\beta(t_w - 32)^2$, the resistance per unit length of wire can be written in terms of the local wire temperature:

$$\omega = \omega_0 [1 + \alpha(t_w - 32)] \quad (B4)$$

where ω_0 is the resistance per unit length in ohms per inch at 32° F. Substituting equations (B2) to (B4) into (B1),

$$J^2 I^2 \omega_0 [1 + \alpha(t_w - 32)] = \pi k_t Nu_t (t_w - T_e) - K_w A_w \frac{d^2 t_w}{dx^2} \quad (B5)$$

Equation (B5) can be written more simply as

$$\frac{d^2 t_w}{dx^2} - \sigma t_w = -\sigma_1 \quad (\text{B6})$$

where the constants are defined as follows:

$$\sigma \equiv \frac{\pi k_t \text{Nu}_t - J' I^2 \omega_0 \alpha}{K_w A_w} \quad (\text{B7})$$

$$\sigma_1 \equiv \frac{\pi k_t \text{Nu}_t T_e + J' I^2 \omega_0 \alpha \left(\frac{1}{\alpha} - 32 \right)}{K_w A_w} \quad (\text{B8})$$

The lengthwise variation of $k_t \text{Nu}_t$ or its equivalent hD_w is ignored; that is, h is assumed unaffected by t_w or T_e .

Equation (B6) is a second-order, ordinary differential equation with constant coefficients. The following boundary conditions are used to find the temperature distribution along the wire length:

(1) The wire is symmetrical; therefore, at the center of the wire (at $x = 0$), the temperature gradient must be zero: $\left. \frac{dt_w}{dx} \right|_{x=0} = 0$.

(2) The temperature at each support, $x = \pm l/2$, is $T_{w,s}$ (an as yet undetermined temperature, but physically it is known that $T_e \geq T_{w,s} \geq T_w$).

The solution of equation (B6) satisfying these conditions is

$$t_w = T_{w,\infty} - (T_{w,\infty} - T_{w,s}) \frac{\cosh \frac{\sigma^{1/2} x}{2}}{\cosh \frac{\sigma^{1/2} l}{2}} \quad (\text{B9})$$

The measured mean resistance Ω_w is related to the length-average wire temperature ($\omega_0 l = \Omega_0$):

$$\Omega_w = \Omega_0 [1 + \alpha(T_w - 32)] \quad (\text{B10})$$

Here, T_w is obtained from integration of (B9) over the wire length:

$$T_w = T_{w,\infty} - \frac{T_{w,\infty} - T_{w,s}}{\frac{\sigma^{1/2} l}{2}} \tanh \frac{\sigma^{1/2} l}{2} \quad (B11)$$

Having obtained the wire-temperature distribution, the next step is to write an energy balance on the entire wire. The power input is now written in terms of equation (B10), the convection loss in terms of (B11), and the conduction loss in terms of the derivative of (B9) evaluated at the point of attachment ($x = l/2$):

$$\begin{aligned} J^2 I^2 \omega_0 [1 + \alpha(T_w - 32)] \\ = \pi k_t \text{Nu}_t (T_w - T_e) + \frac{2K_w A_w \sigma^{1/2}}{l} (T_{w,\infty} - T_{w,s}) \tanh \frac{\sigma^{1/2} l}{2} \end{aligned} \quad (B12)$$

At this point, it is convenient to define a quantity C as the ratio of the heat lost by conduction to the supports to that lost directly to the airstream by convection:

$$C \equiv \frac{4K_w A_w}{l^2} \frac{(T_{w,\infty} - T_{w,s}) \left(\frac{\sigma^{1/2} l}{2} \right) \tanh \frac{\sigma^{1/2} l}{2}}{\pi k_t \text{Nu}_t (T_w - T_e)} \quad (B13)$$

Equation (B12) can be expressed in terms of C as follows:

$$J^2 I^2 \omega_0 [1 + \alpha(T_w - 32)] = \pi k_t \text{Nu}_t (T_w - T_e) (1 + C) \quad (B14)$$

The only unknown in C (other than Nu_t) is the temperature at the support $T_{w,s}$. An energy balance on the support is made to determine $T_{w,s}$. The problem is analogous to the wire treatment just outlined except that the heat input is the conduction from the wire, the output is convection from the support, and the electrical power input is assumed zero in the supports. Solving this energy balance for $T_{w,s}$ and approximating $\tanh(\sigma^{1/2} l/2)$ as 1.0 give the following:

$$T_{w,s} = \frac{2\text{Nu}_{f,s}^{1/2} k_f^{1/2} K_s^{1/2} D_s T_e + K_w D_w^2 \sigma^{1/2} T_{w,\infty}}{2\text{Nu}_{f,s}^{1/2} k_f^{1/2} K_s^{1/2} D_s + K_w D_w^2 \sigma^{1/2}} \quad (B15)$$

Since the objective of the foregoing analysis of the heat transfer from the support was to determine $T_{w,s}$ in terms of known quantities (so that ultimately the end loss ratio C could be found), it appears that the introduction of $Nu_{f,s}$ in equation (B15) has simply replaced one unknown by another. Fortunately, the Nusselt number of the support can be adequately represented by the following empirical relation, because the support is large and in continuum flow:

$$Nu_{f,s} = B_1 + B_2(Re_{f,s})^n \tag{B16}$$

where

$$Re_{f,s} = \frac{\rho U D_s}{\mu_{f,s}}$$

Equation (B16) neglects the small Mach number effect observed at $Re > 250$. Following are values of n , B_1 , and B_2 from reference 11 (p. 260, table 10-4):

$Re_{f,s}$ range	n	B_1	B_2
0.1 - 1000	0.52	0.32	0.43
1000 - 50,000	.60	0	.24

Equations (B13), (B15), and (B16) can be combined with equation (B14); the only unknown quantity is the corrected wire Nusselt number Nu_t . Lowell (ref. 10) has shown that the combination of essentially the equations just mentioned can be written as

$$C = \frac{1 - t^*(1 + C)}{B^* [(1 + C)^{-1} - t^*] + Y [(1 + C)^{-1} - t^*]^{1/2} - 1} \tag{B17}$$

where

$$\left. \begin{aligned} t^* &\equiv \frac{T_w - T_e}{\left(\frac{1}{\alpha} - 32\right) + T_w} \\ B^* &\equiv \frac{l k_t Nu_t''}{(B_1 + B_2 Re_{f,s}^n)^{1/2} K_s^{1/2} k_{f,s}^{1/2} D_s} \\ Y &\equiv \left(\frac{k_t}{K_w}\right)^{1/2} \frac{l}{D_w} (Nu_t'')^{1/2} \end{aligned} \right\} \tag{B18}$$

A more usable form of equation (B17) was derived by Lowell after reference 10 was published. Another form of the ratio of corrected to uncorrected Nusselt number was defined as follows:

$$\frac{Nu_F}{Nu_F^*} = \frac{1}{1+C} \equiv (1-t^*) \left(\frac{t^*}{1-t^*} + z^2 \right) \quad (B19)$$

Then, by letting

$$\left. \begin{aligned} e &\equiv Y(1-t^*)^{1/2} \\ G &\equiv B^*(1-t^*) \end{aligned} \right\} \quad (B20)$$

an algebraically simpler expression for equation (B19) is obtained:

$$Gz + e = \frac{1}{z - z^3} \quad (B21)$$

The procedure used to calculate Nu_t for table I was to solve (B21) for the root of z between $z = 0.5$ and $z = 1.0$. This solution is straightforward once the physical constants in both G and e are evaluated. The following values were used in the electronic digital computer data-reduction program:

Tungsten wire: $l = 0.077$ in.

$$D_w = 2.2 \times 10^{-4} \text{ in.}$$

$$\alpha = 2.24 \times 10^{-3} \text{ } ^\circ\text{F}^{-1}$$

$$K_w = 3.43 \times 10^{-2} \text{ Btu}/(\text{sec})(\text{ft})(^\circ\text{F})$$

Inconel support: $D_s = 0.027$ in. (at point of attachment)

$$K_s = 2.19 \times 10^{-3} \text{ Btu}/(\text{sec})(\text{ft})(^\circ\text{F})$$

Air properties: $\left. \begin{aligned} \mu_{f,s} &\approx \mu_t \\ k_{f,s} &\approx k_t \end{aligned} \right\} \text{ (ref. 18)}$

Another method of making end-loss corrections on hot-wire data has been widely used by investigators at other laboratories. Essentially, it is a limiting case of the more general method just outlined. Kovásznay originally published the method (without derivation) in reference 7; reference 25 gives a more complete presentation.

The problem is identical to that treated by Lowell, except that Kovásznay uses the mathematically simpler boundary condition $T_{w,s} = T_e$. Since the recovery temperature T_e is immediately available, equations (B7) and (B12) can be solved without further ado for Nu_t . A further simplification can be gained if the reference temperature of the calibration of wire temperature and resistance is taken at T_e rather than at 32° F as in the previous section. If these substitutions are made in equations (B13) and (B14), it can be shown that the following equation is the desired solution for ψ :

$$\frac{Nu_t}{Nu_t''} = \frac{\bar{a}_w + a_w^*}{1 + \bar{a}_w} \quad (B22)$$

where

$$\bar{a}_w = \frac{\Omega_w - \Omega_e}{\Omega_e} \quad (B23)$$

$$\frac{\bar{a}_w}{a_w^*} = 1 - S \left(\frac{a_w^*}{\bar{a}_w} \right)^{1/2} \tanh \frac{1}{S} \left(\frac{\bar{a}_w}{a_w^*} \right)^{1/2} \quad (B24)$$

$$S = \frac{D_w}{l} \left(\frac{K_w}{k_t} \right)^{1/2} Nu_t''^{-1/2} (1 + \bar{a}_w)^{1/2} \quad (B25)$$

This procedure was also used in the data-reduction program. The results of this end-loss correction agreed with those obtained using equation (B21) within a small fraction of 1 percent of Nu_t for all flow conditions of this research. Therefore, the probe supports did act effectively as an infinite sink. That is, the wire-support junction was effectively maintained at recovery temperature, $T_e \approx T_{w,s}$.

Nonlinear Correction

The linear correction procedures just outlined are rather elaborate. However, the methods differ only in the manner used to treat the temperature of the wire-support junction. Both procedures assume that the wire has no second-order temperature dependence ($\beta = 0$), that the heat-transfer coefficient is not dependent on wire temperature, and that the wire thermal conductivity is constant. Generally, none of these

assumptions are true. So, it is conceivable that the end-loss correction is incorrect and that this mistake causes the nonlinearity of Nu_t with ΔT and T_t . An excellent discussion of this problem is published in reference 16. Mechanically integrated solutions of the nonlinear equation that includes β , ξ (eq. (3)), and $K_w = f(t_w)$ are compared with the linear solution, and it is concluded that the linear solution of Kováshay differs by only 1/2 percent from the nonlinear solutions for any realistic probe design. Therefore, the procedure used to correct for finite wire length in this report is adequate.

APPENDIX C

DERIVATION OF HOT-WIRE-ANEMOMETER SENSITIVITY EQUATIONS

Assume that the general heat-loss characteristics of normal cylinders are known in terms of Nusselt number corrected for conduction loss to supports. Specifically, the Nusselt number is a function of the Mach and Knudsen (or Reynolds) numbers, and the effect of air temperature at constant wire temperature is assumed described by a single parameter τ :

$$Nu_t = f(M, Kn, \tau) \quad (C1)$$

$$\tau = \frac{T_w - T_e}{T_t} \quad (C2)$$

The subscript t on Nu and k will be dropped here and understood throughout appendix C. The recovery temperature ratio η will be assumed to be independent of Kn , as in figure 8; this is valid at least to $Kn = 0.10$:

$$\eta = \frac{T_e}{T_t} = f(M) \quad (C3)$$

The heat loss from a wire may be written as

$$J^2 I^2 \Omega_w = \pi l k (T_w - \eta T_t) Nu \quad (C4)$$

Equation (C4) assumes that Nu is corrected for finite wire length so that I^2 is the square of the measured wire current times the end-loss correction factor, ψI_m^2 . Naturally, if a calibration curve for a particular wire is being used, it is possible to set $\psi = 1$ and correlate data as Nu'' .

It will be assumed that the hot-wire resistance (and temperature) is maintained constant by a fluctuating feedback current:

$$2J^2 I \Omega_w dI = \frac{\partial}{\partial U} [\pi l k (T_w - \eta T_t) Nu] dU + \frac{\partial}{\partial \rho} [\pi l k (T_w - \eta T_t) Nu] d\rho + \frac{\partial}{\partial T_t} [2l k (T_w - \eta T_t) Nu] dT_t \quad (C5)$$

5111

CS-5 back

If the fluctuating current dI is set equal to i and small finite flow fluctuations are approximated by δ to replace the derivatives, equation (C5) can be written as

$$\begin{aligned}
 i = & \left[\frac{\pi l}{2J'I\Omega_w} kNuT_t \left(- \frac{\partial \eta}{\partial U} \right) + \frac{\pi l}{2J'I\Omega_w} kNu\eta \left(- \frac{\partial T_t}{\partial U} \right) + \frac{\pi l}{2J'I\Omega_w} k(T_w - \eta T_t) \frac{\partial Nu}{\partial U} \right] \delta U \\
 & + \left[\frac{\pi l}{2J'I\Omega_w} k(T_w - \eta T_t) \frac{\partial Nu}{\partial \rho} \right] \delta \rho \\
 & + \left[\frac{\pi l}{2J'I\Omega_w} (T_w - \eta T_t) Nu \frac{\partial k}{\partial T_t} - \frac{\pi l}{2J'I\Omega_w} kNu\eta + \frac{\pi l}{2J'I\Omega_w} k(T_w - \eta T_t) \frac{\partial Nu}{\partial T_t} \right] \delta T_t
 \end{aligned} \tag{C6}$$

It will be convenient to introduce the following dimensionless groups to generalize equation (C6) for numerical evaluation of the various sensitivity derivatives:

$$\frac{\partial}{\partial \rho} = \frac{\partial Kn}{\partial \rho} \frac{\partial}{\partial Kn} = - \frac{Kn}{\rho} \frac{\partial}{\partial Kn} \tag{C7}$$

$$\frac{\partial}{\partial U} = \frac{\partial M}{\partial U} \frac{\partial}{\partial M} = \frac{1 + \frac{\gamma - 1}{2} M^2}{a_s} \frac{\partial}{\partial M} \tag{C8}$$

$$\frac{\partial T_t}{\partial U} = \frac{U}{c_p g_c J} \tag{C9}$$

$$\frac{\partial}{\partial T_t} = \frac{\partial \tau}{\partial T_t} \frac{\partial}{\partial \tau} = - \frac{\tau + \eta}{T_t} \frac{\partial}{\partial \tau} \tag{C10}$$

Substituting (C7) to (C10) into equation (C6) and recalling that

$M = \frac{U}{a_s}$ and $\frac{I}{2Nu} = \frac{\pi l}{2J'I\Omega_w} k(T_w - \eta T_t)$, the following form may be written:

$$\begin{aligned}
 i = & \frac{I}{2} \left[- \left(1 + \frac{\gamma - 1}{2} M^2 \right) \frac{M}{\tau} \frac{\partial \eta}{\partial M} - \frac{\eta}{T_w - \eta T_t} \frac{U^2}{c_p g_c J} + \left(1 + \frac{\gamma - 1}{2} M^2 \right) \frac{M}{Nu} \frac{\partial Nu}{\partial M} \right] \frac{\delta U}{U} \\
 & + \frac{I}{2} \left(- \frac{Kn}{Nu} \frac{\partial Nu}{\partial Kn} \right) \frac{\delta \rho}{\rho} + \frac{I}{2} \left(\frac{T_t}{k} \frac{\partial k}{\partial T_t} - \frac{\eta T_t}{T_w - \eta T_t} - \frac{\tau + \eta}{Nu} \frac{\partial Nu}{\partial \tau} \right) \frac{\delta T_t}{T_t}
 \end{aligned} \tag{C11}$$

Replacing $\left(\frac{u}{v} \frac{\partial v}{\partial u}\right)$ by $\frac{\partial \log v}{\partial \log u}$ and using a familiar identity, the sensitivity equation can be written in its final form, which is given as equation (21) of the text.

REFERENCES

1. King, Louis Vessot: On the Convection of Heat from Small Cylinders in a Stream of Fluid. Proc. Roy. Soc. (London), ser. A, vol. 214, no. 14, Nov. 12, 1914, pp. 373-432.
2. Dryden, H. L., and Kuethe, A. M.: The Measurement of Fluctuations of Air Speed by the Hot-Wire Anemometer. NACA Rep. 320, 1929.
3. Corrsin, Stanley: Extended Applications of the Hot-Wire Anemometer. NACA TN 1864, 1949.
4. Carbon, M. W., Kutsch, H. J., and Hawkins, G. A.: The Response of Thermocouples to Rapid Gas-Temperature Changes. Trans. ASME, vol. 72, no. 5, July 1950, pp. 655-657.
5. Fiock, Ernest: Ninth Monthly Report of Progress on the Development of Thermocouple Pyrometers for Gas Turbines. NBS, Sept. 6, 1946.
6. Glawe, George E., and Johnson, Robert C.: Experimental Study of Heat Transfer to Small Cylinders in a Subsonic, High-Temperature Gas Stream. NACA TN 3934, 1957.
7. Kovásznay, Leslie S. G., and Törmarck, Sven I. A.: Heat Loss of Hot-Wires in Supersonic Flow. Bumblebee Rep. No. 127, Dept. Aero., The Johns Hopkins Univ., Apr. 1950. (Contract Nord 8036 with BuOrd., U. S. Navy.)
8. Laufer, J., and McClellan, R.: Measurement of Heat Transfer from Fine Wires in Supersonic Flows. Jour. Fluid Mech., vol. 1, pt. 3, Sept. 1956, pp. 276-289.
9. Laurence, James C., and Landes, L. Gene: Auxiliary Equipment and Techniques for Adapting the Constant-Temperature Hot-Wire Anemometer to Specific Problems in Air-Flow Measurements. NACA TN 2843, 1952.
10. Lowell, Herman H.: Design and Applications of Hot-Wire Anemometers for Steady-State Measurements at Transonic and Supersonic Airspeeds. NACA TN 2117, 1950.
11. McAdams, William H.: Heat Transmission. Third ed., ch. 10, McGraw-Hill Book Co., Inc., 1954.

12. Sandborn, Virgil A., and Laurence, James C.: Heat Loss from Yawed Hot Wires at Subsonic Mach Numbers. NACA TN 3563, 1955.
13. Scadron, Marvin D., and Warshawsky, Isidore: Experimental Determination of Time Constants and Nusselt Numbers for Bare-Wire Thermocouples in High-Velocity Air Streams and Analytic Approximation of Conduction and Radiation Errors. NACA TN 2599, 1952.
14. Spangenberg, W. G.: Heat-Loss Characteristics of Hot-Wire Anemometers at Various Densities in Transonic and Supersonic Flow. NACA TN 3381, 1955.
15. Stalder, Jackson R., Goodwin, Glen, and Creager, Marcus O.: Heat Transfer to Bodies in a High-Speed Rarefied-Gas Stream. NACA Rep. 1093, 1952. (Supersedes NACA TN 2438.)
16. Winovich, Warren, and Stine, Howard A.: Measurements of the Non-linear Variation with Temperature of Heat-Transfer Rate from Hot Wires in Transonic and Supersonic Flow. NACA TN 3965, 1957.
17. Mickelsen, William R., and Baldwin, Lionel V.: Aerodynamic Mixing Downstream from Line-Source of Heat in High-Intensity Sound Field. NACA TN 3760, 1956.
18. Hilsenrath, Joseph, et al.: Tables of Thermal Properties of Gases. Cir. 564, NBS, Nov. 1, 1955.
19. Van Der Hegge Zijnen, B. G.: Heat Transfer from Horizontal Cylinders to a Turbulent Air Flow. Appl. Sci. Res., sec. A, vol. 7, nos. 2-3, 1958, pp. 205-223.
20. Collis, D. C., and Williams, M. J.: Two-Dimensional Forced Convection from Cylinders at Low Reynolds Numbers. Rep. A. 105, Res. & Dev. Branch, Aero. Res. Labs. (Australia), Nov. 1957.
21. Kennard, Earle H.: Kinetic Theory of Gases. McGraw-Hill Book Co., Inc., 1938, pp. 312-315.
22. Morkovin, M. V.: Fluctuations and Hot-Wire Anemometry in Compressible Flows. AGARDograph 24, North Atlantic Treaty Organization, AGARD, Nov. 1956.
23. Sauer, F. M., and Drake, R. M., Jr.: Forced Convection Heat Transfer from Horizontal Cylinders in a Rarefied Gas. Jour. Aero. Sci., vol. 20, no. 3, Mar. 1953, pp. 175-180.

24. Stalder, Jackson R., Goodwin, Glen, and Creager, Marcus O.: A Comparison of Theory and Experiment for High-Speed Free-Molecule Flow. NACA Rep. 1032, 1951. (Supersedes NACA TN 2244.)
25. Kovásznay, L. S. G.: Turbulence Measurements. Vol. IX of Physical Measurements in Gas Dynamics and Combustion, sec. F, pt. 1, R. Ladenburg, ed., Princeton Univ. Press, 1954, pp. 213-285.

TABLE I. - RESULTS OF STUDY OF HEAT TRANSFER FROM CYLINDERS IN SUBSONIC SLIP FLOW

M	Kn	Re _t	T _t	T _w	Nu _t ^a	Nu _t	Run ^a	M	Kn	Re _t	T _t	T _w	Nu _t ^a	Nu _t	Run					
0.0488	0.0753	0.9763	12.9	33.6	1.054	0.7396	342	0.0503	0.0255	2.867	87.5	133.2	1.303	0.9931	133					
		.9814	11.5	86.6	.9479	.6534	343						183.6	1.325	1.022	134				
		.9874	9.9	183.6	.9212	.6402	344						283.2	1.299	1.013	135				
0.0490	0.0143	4.677	272.9	333.2	1.361	1.089	319	0.0506	0.0442	1.662	85.0	133.2	1.081	0.7928	109					
		4.679	272.7	383.9	1.402	1.133	320						183.6	1.086	.8050	110				
		4.685	272.1	483.4	1.429	1.170	321						283.2	1.066	.7994	111				
		4.689	271.8	583.8	1.450	1.199	322						383.9	1.051	.7947	112				
		4.693	271.4	620.0	1.456	1.208	323						483.4	1.287	1.023	137				
0.0492	0.0142	5.259	8.4	33.6	2.002	1.596	348	0.0507	0.0253	2.762	196.6	233.1	1.281	0.9981	223					
		5.222	9.3	86.6	1.797	1.424	349						2.770	195.5	283.2	1.244	.9717	224		
		5.206	10.1	183.6	1.715	1.370	350						2.779	194.4	383.9	1.236	.9768	225		
		5.190	10.9	383.9	1.698	1.384	351						2.787	193.2	483.4	1.235	.9858	226		
		5.174	11.7	483.4	1.696	1.394	352						2.795	192.1	583.8	1.237	.9967	227		
0.0495	0.0744	0.9724	72.5	132.0	0.9212	0.6468	1	0.0508	0.0403	1.711	265.5	333.2	0.9844	0.7457	288					
		1.308	71.5	133.2	1.021	0.7364	85						1.716	264.2	383.9	.9849	.7514	289		
				183.6	1.003	.7278	86						1.721	262.9	483.4	.9922	.7671	290		
				283.2	.9908	.7280	87						1.726	261.7	583.8	.9945	.7769	291		
				383.9	.9819	.7281	88						1.732	260.4	620.0	.9988	.7830	292		
0.0496	0.0570	1.331	3.5	33.6	1.101	0.7804	396	0.0513	0.0575	1.202	274.3	333.2	0.8621	0.6358	283					
		1.329	3.9	86.6	1.069	.7614	397						1.206	272.9	383.9	.8667	.6447	284		
		1.324	4.8	183.6	1.028	.7374	398						1.209	271.8	483.4	.8680	.6540	285		
		1.321	5.4	383.9	1.010	.7344	399						1.213	270.1	583.8	.8678	.6606	286		
		1.318	6.1	483.4	1.002	.7258	400						1.216	269.2	620.0	.8656	.6606	287		
0.0498	0.0259	2.603	283.8	333.2	1.090	0.8420	309	0.0516	0.0582	1.234	187.2	233.1	0.8849	0.6398	193					
		2.611	282.5	383.9	1.114	.8697	310						1.233	187.6	283.2	.9112	.6692	194		
		2.618	281.3	483.4	1.141	.9045	311						1.232	188.0	383.9	.9110	.6789	195		
		2.626	280.0	583.8	1.151	.9224	312						1.231	188.3	483.4	.9036	.6799	196		
		2.634	278.7	620.0	1.149	.9233	313						1.229	188.7	583.8	.8987	.6815	197		
0.0500	0.0143	5.067	88.5	133.2	1.607	1.270	145	0.0529	0.0142	5.159	182.7	233.1	1.596	1.286	235					
				183.6	1.459	1.145	146						5.168	182.1	283.2	1.581	1.280	236		
				283.2	1.599	1.289	147						5.176	181.5	383.9	1.567	1.281	237		
				383.9	1.590	1.295	148						5.185	180.8	483.4	1.565	1.291	238		
				483.4	1.594	1.310	149						5.193	180.2	583.8	1.569	1.305	239		
0.0501	0.0259	2.951	5.6	33.6	1.517	1.155	360	0.0531	0.0792	0.9231	189.1	233.1	0.8635	0.6211	169					
		2.941	6.5	86.6	1.418	1.078	361						.9249	186.0	283.2	.8398	.6051	170		
		2.929	7.6	183.6	1.374	1.056	362						.9268	187.1	383.9	.8097	.5867	171		
		2.918	8.5	383.9	1.361	1.069	363						.9287	186.2	483.4	.8003	.5846	172		
		2.907	9.5	483.4	1.362	1.078	364						.9305	185.3	583.8	.7923	.5820	173		
0.0502	0.00922	7.896	89.0	133.2	1.903	1.541	151	0.0537	0.0261	3.665	13.7	33.6	1.804	1.417	354					
				183.6	1.898	1.548	152						3.660	13.7	86.6	1.539	1.189	355		
				283.2	1.875	1.545	153						3.654	14.1	183.6	1.466	1.141	356		
				383.9	1.885	1.570	154						3.649	14.5	383.9	1.442	1.146	357		
				483.4	1.886	1.584	155						3.643	14.9	483.4	1.431	1.144	358		
0.0503	0.0442	1.662	85.0	133.2	1.081	0.7928	109	0.0575	1.202	274.3	333.2	0.8621	0.6358	283						
		1.836	1.086	.8050	110	1.206	272.9								383.9	.8667	.6447	284		
		2.026	1.066	.7994	111	1.209	271.8								483.4	.8680	.6540	285		
		2.216	1.051	.7947	112	1.213	270.1								583.8	.8678	.6606	286		
		2.406	1.287	1.023	137	1.216	269.2								620.0	.8656	.6606	287		
0.0504	0.0744	0.9724	72.5	132.0	0.9212	0.6468	1	0.0582	1.234	187.2	233.1	0.8849	0.6398	193						
		1.308	71.5	133.2	1.021	0.7364	85								1.233	187.6	283.2	.9112	.6692	194
				183.6	1.003	.7278	86								1.232	188.0	383.9	.9110	.6789	195
				283.2	.9908	.7280	87								1.231	188.3	483.4	.9036	.6799	196
				383.9	.9819	.7281	88								1.229	188.7	583.8	.8987	.6815	197
0.0505	0.0143	5.067	88.5	133.2	1.607	1.270	145	0.0582	1.234	187.2	233.1	0.8849	0.6398	193						
				183.6	1.459	1.145	146								1.233	187.6	283.2	.9112	.6692	194
				283.2	1.599	1.289	147								1.232	188.0	383.9	.9110	.6789	195
				383.9	1.590	1.295	148								1.231	188.3	483.4	.9036	.6799	196
				483.4	1.594	1.310	149								1.229	188.7	583.8	.8987	.6815	197
0.0506	0.0259	2.951	5.6	33.6	1.517	1.155	360	0.0582	1.234	187.2	233.1	0.8849	0.6398	193						
		2.941	6.5	86.6	1.418	1.078	361								1.233	187.6	283.2	.9112	.6692	194
		2.929	7.6	183.6	1.374	1.056	362								1.232	188.0	383.9	.9110	.6789	195
		2.918	8.5	383.9	1.361	1.069	363								1.231	188.3	483.4	.9036	.6799	196
		2.907	9.5	483.4	1.362	1.078	364								1.229	188.7	583.8	.8987	.6815	197
0.0507	0.0442	1.662	85.0	133.2	1.081	0.7928	109	0.0582	1.234	187.2	233.1	0.8849	0.6398	193						
		1.836	1.086	.8050	110	1.233	187.6								283.2	.9112	.6692	194		
		2.026	1.066	.7994	111	1.232	188.0								383.9	.9110	.6789	195		
		2.216	1.051	.7947	112	1.231	188.3								483.4	.9036	.6799	196		
		2.406	1.287	1.023	137	1.229	188.7								583.8	.8987	.6815	197		
0.0508	0.0403	1.711	265.5	333.2	0.9844	0.7457	288	0.0582	1.234	187.2	233.1	0.8849	0.6398	193						
		1.716	264.2	383.9	.9849	.7514	289								1.233	187.6	283.2	.9112	.6692	194
		1.721	262.9	483.4	.9922	.7671	290								1.232	188.0	383.9	.9110	.6789	195
		1.726	261.7	583.8	.9945	.7769	291								1.231	188.3	483.4	.9036	.6799	196
		1.732	260.4	620.0	.9988	.7830	292								1.229	188.7	583.8	.8987	.6815	197
0.0509	0.0253	2.762	196.6	233.1	1.281	0.9981	223	0.0582	1.234	187.2	233.1	0.8849	0.6398	193						
		2.770	195.5	283.2	1.244	.9717	224								1.233	187.6	283.2	.9112	.6692	194
		2.779	194.4	383.9	1.236	.9768	225								1.232	188.0	383.9	.9110	.6789	195
		2.787	193.2	483.4	1.235	.9858	226								1.231	188.3	483.4	.9036	.6799	196
		2.795	192.1	583.8	1.237	.9967	227								1.229	188.7	583.8	.8987	.6815	197
0.0510	0.0403	1.711	265.5	333.2	0.9844	0.7457	288	0.0582	1.234	187.2	233.1	0.8849	0.6398	193						
		1.716	264.2	383.9	.9849	.7514	289								1.233	187.6	283.2	.9112	.6692	194
		1.721	262.9	483.4	.9922	.7671	290								1.232	188.0	383.9	.9110	.6789	195
		1.726	261.7	583.8	.9945	.7769	291								1.231	188.3	483.4	.9036	.6799	196
		1.732	260.4	620.0	.9988	.7830	292								1.229	188.7	583.8	.8987	.6815	197
0.0511	0.0575	1.202	274.3	333.2	0.8621	0.6358	283	0.0582	1.234	187.2	233.1	0.8849	0.6398	193						
		1.206	272.9	383.9	.8667	.6447	284								1.233	187.6	283.2	.9112	.6692	194
		1.209	271.8	483.4	.8680	.6540	285								1.232	188.0</				

TABLE I. - Continued. RESULTS OF STUDY OF HEAT TRANSFER FROM CYLINDERS IN SUBSONIC SLIP FLOW

M	Kn	Re _t	T _t	T _w	Nu _t ^H	Nu _t	Run	M	Kn	Re _t	T _t	T _w	Nu _t ^H	Nu _t	Run										
0.0990	0.0259	5.199	277.5	333.2	1.279	1.014	314	0.1020	0.00916	16.91	2.0	33.6	2.653	2.194	984										
		5.208	276.7	383.9	1.351	1.086	315			16.90	2.1	86.6	2.555	2.121	985										
		5.217	276.0	483.4	1.391	1.135	316			2.2	183.6	2.505	2.101	986											
		5.226	275.3	583.8	1.406	1.158	317			16.89	2.3	383.9	2.507	2.143	987										
		5.235	274.5	620.0	1.407	1.162	318			0.00917	16.89	2.4	483.4	2.509	2.160	988									
	0.0549	2.628	72.5	133.2	1.207	0.9042	91		16.88	2.5	583.8	2.509	2.172	989											
				183.6	1.180	.8881	92		0.1024	0.0445	3.336	85.0	133.2	1.342	1.028	115									
				283.2	1.152	.8764	93						183.6	1.294	.9931	116									
				383.9	1.131	.8669	94						283.2	1.274	.9896	117									
				483.4	1.113	.8579	95						383.9	1.251	.9798	118									
		583.8	1.098	.8486	96	483.4	1.229	.9682					119												
0.0993	0.0256	5.804	13.8	33.6	2.068	1.658	366	0.0757	1.866	185.5	233.1	1.006	0.7488	163											
		5.802	13.9	86.6	1.780	1.409	367								1.873	185.3	283.2	.9663	.7188	164					
		5.800	14.0	183.6	1.684	1.342	368								1.879	185.1	383.9	.9621	.7252	165					
		5.798	14.1	383.9	1.645	1.336	369								1.886	184.9	483.4	.9455	.7178	166					
		5.797	14.2	483.4	1.634	1.336	370								1.893	184.7	583.8	.9320	.7116	167					
		5.795	14.2	583.8	1.621	1.332	371								1.900	184.5	620.1	.9244	.7062	168					
0.0997	0.0407	3.397	188.5	233.1	1.222	0.9438	211	0.1029	0.0415	3.360	280.4	333.2	1.119	0.8688	293										
		3.406	187.5	283.2	1.242	.9696	212									3.371	278.9	383.9	1.144	.8972	294				
		3.415	186.5	383.9	1.234	.9744	213									3.383	277.5	483.4	1.160	.9216	295				
		3.424	185.6	483.4	1.227	.9784	214									3.394	276.0	583.8	1.164	.9340	296				
		3.433	184.6	583.8	1.221	.9811	215									3.406	274.5	620.0	1.166	.9383	297				
0.1000	0.0569	2.707	-4.0	33.6	1.232	0.8958	390	0.1032	0.0776	1.776	281.9	333.2	0.9775	0.7403	247										
		2.692	-2.5	86.6	1.275	.9442	391									1.788	278.9	383.9	.9868	.7539	248				
		2.676	-1.0	183.6	1.224	.9159	392									1.801	276.0	483.4	.9093	.6919	249				
		2.661	.4	383.9	1.193	.9081	393									1.816	272.3	583.8	.9002	.6904	250				
		2.646	1.9	483.4	1.174	.8953	394									1.829	269.4	620.0	.8909	.6838	251				
		2.631	3.3	583.8	1.156	.8793	395									0.1039	0.0143	10.48	90.5	133.2	1.661	1.319	1035		
0.1008	0.0255	5.704	89.5	133.2	1.553	1.220	522	183.6	1.827	1.482	1036														
				183.6	1.548	1.226	523	283.2	1.913	1.581	1037														
				283.2	1.559	1.253	524	383.9	1.936	1.617	1038														
				383.9	1.556	1.264	525	483.4	1.941	1.635	1039														
				483.4	1.550	1.269	526	583.8	1.952	1.657	1040														
				583.8	1.549	1.278	527	0.0580	2.495	184.4	233.1	1.068	0.8042	181											
0.0564	2.440	259.8	333.2	0.9797	0.7410	273	2.498								183.9	283.2	1.083	.8243	182						
							2.443								259.5	383.9	1.016	.7797	274	2.501	183.5	383.9	1.072	.8259	183
							2.445								259.1	483.4	1.022	.7942	275	2.504	183.0	483.4	1.061	.8248	184
							2.447								258.7	583.8	1.021	.8015	276	2.507	182.6	583.8	1.052	.8230	185
							2.449								258.3	620.0	1.020	.8024	277	2.510	182.1	620.1	1.047	.8214	186
							0.1009	0.0250	5.586	188.1	233.1	1.534	1.229	229	0.1069	0.0141	11.54	-2.0	33.6	2.202	1.778	935			
5.602	187.1	283.2	1.529	1.232	230	86.6			2.180	1.774	936														
5.618	186.0	383.9	1.523	1.241	231	183.6			2.128	1.750	937														
5.634	185.0	483.4	1.513	1.243	232	383.9			2.117	1.776	938														
5.650	183.9	583.8	1.511	1.251	233	483.4			2.110	1.782	939														
5.666	182.8	620.1	1.507	1.250	234	583.8			2.103	1.786	940														
0.1010	0.00917	15.92	90.0	133.2	1.996	1.626	1065	0.1614	0.0613	3.948	6.0	33.6	1.543	1.179	324										
				183.6	2.194	1.821	1066									3.934	6.9	86.6	1.437	1.095	325				
				283.2	2.278	1.920	1067									3.919	7.9	183.6	1.355	1.038	326				
				383.9	2.310	1.968	1068									3.904	8.9	383.9	1.283	.9957	327				
				483.4	2.329	2.000	1069									3.890	9.9	483.4	1.258	.9789	328				
	0.0749	1.960	79.5	132.0	1.127	0.8328	13	3.875	10.9	583.8	1.235	.9609	329												
				183.0	1.064	.7856	14	0.1956	0.0139	21.29	-2.0	33.6	2.919	2.441	923										
				234.5	1.050	.7776	15									86.6	2.790	2.339	924						
				285.1	1.023	.7585	16									183.6	2.680	2.264	925						
				332.6	1.016	.7565	17									383.9	2.611	2.241	926						
386.5	.9997	.7457	18	483.4	2.603	2.248	927																		
437.3	.9886	.7388	19	583.8	2.576	2.235	928																		
488.0	.9792	.7328	20	0.0251	11.75	-2.0	33.6	2.153	1.733	1.733	917														
538.5	.9671	.7254	21									11.76	-2.2	86.6	2.172	1.767	918								
590.2	.9585	.7165	22									-2.4	183.6	2.076	1.702	919									
640.4	.9523	.7110	23									11.77	-2.6	383.9	2.029	1.692	920								
0.1012	0.0411	3.368	269.4									333.2	1.076	0.8283	299	0.1957	0.0746	3.909	11.4	33.6	1.574	1.207	330		
		3.367	269.5	383.9	1.133	.8864	300	3.894	12.4	86.6	1.375	1.039	331												
		3.365	269.8	483.4	1.161	.9218	301	3.880	13.4	183.6	1.290	.9792	332												
		3.364	270.0	583.8	1.169	.9386	302	3.866	14.3	383.9	1.213	.9314	333												
		3.363	270.1	620.0	1.172	.9441	303	3.852	15.3	483.4	1.186	.9121	334												
0.1019	0.0255	5.780	87.0	133.2	1.592	1.256	139	0.1972	0.0735	3.619	259.0	333.2	1.087	0.8386	252										
				183.6	1.623	1.295	140									3.622	258.6	383.9	1.091	.8479	253				
				283.2	1.590	1.281	141									3.625	258.3	483.4	1.079	.8465	254				
				383.9	1.566	1.273	142									3.628	257.9	583.8	1.070	.8457	255				
				483.4	1.556	1.274	143									3.632	257.5	620.0	1.066	.8444	256				
	0.0766	1.928	85.0	133.2	1.112	0.8202	37	0.1986	0.00908	33.03	-3.5	33.6	3.458	2.942	947										
				183.6	1.057	.7782	38									0.00909	33.00	-3.2	86.6	3.334	2.846	948			
				233.1	1.038	.7673	39									32.97	-2.9	183.6	3.209	2.760	949				
				283.2	1.023	.7598	40									0.00910	32.94	-2.6	383.9	3.181	2.779	950			
				333.2	1.010	.7528	41									0.00911	32.91	-2.3	483.4	3.163	2.779	951			
383.9	.9956	.7433	42	32.88	-2.0	583.8	3.163	2.794	952																
433.0	.9823	.7343	43																						
483.4	.9722	.7276	44																						
533.0	.9625	.7206	45																						
583.8	.9480	.7081	46																						

5111 CS-6

TABLE I. - Continued. RESULTS OF STUDY OF HEAT TRANSFER FROM CYLINDERS IN SUBSONIC SLIP FLOW

M	Kn	Re _t	T _t	T _w	Nu _t ¹	Nu _t	Run	M	Kn	Re _t	T _t	T _w	Nu _t ¹	Nu _t	Run																	
0.2975	0.0752	5.172	282.7	333.2	1.234	0.9730	257	0.3088	0.0750	5.536	181.0	233.1	1.295	1.010	175																	
				383.9	1.214	.9614	258						5.542	180.8	283.2	1.270	.9949	176														
				483.4	1.178	.9387	259						5.548	180.6	383.9	1.250	.9888	177														
				583.8	1.159	.9299	260						5.554	180.4	483.4	1.218	.9698	178														
				620.0	1.153	.9271	261						5.559	180.2	583.8	1.188	.9501	179														
															620.1	1.178	.9430	180														
0.2979	0.0550	7.674	82.3	133.2	1.617	1.278	103	0.3183	0.0444	10.09	88.5	133.2	1.763	1.413	486																	
				183.6	1.581	1.256	104						183.6	1.790	1.448	487																
				283.2	1.526	1.222	105						283.2	1.753	1.452	488																
				383.9	1.479	1.191	106						383.9	1.730	1.426	489																
				483.4	1.437	1.163	107						483.4	1.704	1.414	490																
				583.8	1.405	1.141	108																									
0.2980	0.0142	29.57	89.0	133.2	2.434	2.031	1023	0.3948	0.00919	59.46	88.0	133.2	3.334	2.871	1071																	
				183.6	2.674	2.268	1024						183.6	3.549	3.089	1072																
				283.2	2.715	2.329	1025						283.2	3.644	3.206	1073																
				383.9	2.762	2.393	1026						383.9	3.672	3.254	1074																
				483.4	2.758	2.405	1027						483.4	3.683	3.284	1075																
				583.8	2.758	2.419	1028						583.8	3.659	3.278	1076																
0.2983	0.0142	31.23	-3.0	33.6	3.172	2.675	929	0.3961	0.0242	23.94	-8.0	33.6	2.699	2.237	881																	
				86.6	3.151	2.676	930						23.95	-8.1	86.6	2.684	2.240	882														
				183.6	3.044	2.605	931						23.96	-8.2	183.6	2.586	2.177	883														
				383.9	2.990	2.598	932									2.488	2.124	884														
				483.4	2.962	2.589	933									23.97	-8.4	483.4	2.523	2.172	885											
				583.8	2.941	2.582	934												23.98	-8.5	583.8	2.406	2.073	886								
	0.0253	15.91	194.4	194.0	583.8	2.059	1.766	741	0.3977	0.0410	14.15	-6.0	33.6	2.174	1.753	833																
					620.1	2.039	1.751	742						14.14	-5.9	86.6	2.097	1.698	834													
	0.0254	15.86	196.0	233.1	1.776	1.452	737	-5.8	183.6	2.005	1.636	835																				
					15.89	195.2	383.9			2.062	1.742	739	14.13				-5.7	383.9	1.926	1.596	836											
	15.90	194.8	483.4	2.067	1.761	740	0.0411	14.13	-5.6	483.4	1.881	1.565		837																		
	0.2987	0.00922	45.74	89.0	133.2	2.911					2.475	1059	-5.5	583.8	1.842	1.538	838															
183.6					3.236	2.794					1060	0.3982			0.0776	7.082	91.0	133.2	1.498	1.172	426											
283.2					3.314	2.893					1061							183.6	1.369	1.063	427											
383.9					3.339	2.938					1062							283.2	1.376	1.085	428											
483.4					3.339	2.956					1063							383.9	1.332	1.057	429											
583.8					3.356	2.988	1064	483.4	1.295	1.032	430																					
583.8				583.8	1.260	1.007	431																									
0.2990	0.0739	5.714	80.4	133.2	1.437	1.115	61	0.3986	0.00911	63.76	-4.0	483.4	3.919	3.500	994																	
				183.6	1.361	1.055	62						.00912	63.67	-3.5	383.9	3.915	3.477	993													
				233.1	1.330	1.035	63						.00913	63.58	-3.0	183.6	4.017	3.523	992													
				283.2	1.311	1.025	64						.00914	63.49	-2.5	86.6	4.166	3.628	991													
				333.2	1.298	1.019	65						.00915	63.40	-2.0	33.6	4.459	3.881	990													
				383.9	1.268	.9970	66						0.3987	0.0766	7.556	0.5	33.6	1.713	1.332	767												
				433.0	1.245	.9796	67		0.0767	7.554	0.6	86.6						1.593	1.237	768												
				483.4	1.226	.9662	68											7.552	.7	183.6	1.491	1.163	769									
				533.0	1.210	.9553	69											7.550	.8	383.9	1.389	1.094	770									
				583.8	1.194	.9438	70											7.547	.9	483.4	1.351	1.066	771									
				620.1	1.180	.9328	71											7.545	1.0	583.8	1.320	1.041	772									
				0.2994	0.0399	9.843	284.0						483.4	1.557	1.288	699	0.3991	0.0141	41.31	-6.0	33.6	3.559	3.037	941								
9.851	283.5	583.8	1.565					1.307	700	86.6	3.421	2.929	942																			
9.859	285.0	620.0	1.558					1.304	701	183.6	3.273	2.821	943																			
0.3005	0.0254	16.67	89.5					133.2	2.184	1.800	534	0.0254	20.81	190.0	620.1	2.189						1.892	1.892	754								
								183.6	2.190	1.818	535											0.0255	20.71	192.4	483.4	2.209	1.895	752				
								283.2	2.183	1.832	536															0.0256	20.76	191.2	583.8	2.194	1.893	753
				383.9	2.159	1.827	537	0.0257	20.67	173.6	383.9						2.209	1.880	751													
				483.4	2.142	1.824	538										0.4000	0.0407	13.60	87.8	133.2									1.898	1.537	492
				583.8	2.132	1.827	539																							183.6	1.914	1.563
0.3012	0.0253	17.63	0.4	383.9	2.247	1.898	890					283.2	1.880	1.550	494																	
				17.64	.2	483.4	2.223					1.890	891	383.9	1.851	1.538						495										
				17.65	0	583.8	2.205					1.884	892	483.4	1.816	1.519						496										
				0.3019	0.0591	7.574	0	33.6	1.739	1.356	815	583.8	1.794	1.509	1.509	497																
								7.570	.2	86.6	1.640						1.279	816														
								0.3021	0.0564	7.037	282.0						333.2	1.141	0.8888	671	0.4003	0.0143	38.71	88.0	133.2	2.689	2.268	1041				
.0565	7.019	283.5	383.9														1.271	1.013	672	183.6						2.925	2.503	1042				
.0566	7.002	285.0	483.4														1.305	1.056	673	283.2						2.993	2.591	1043				
0.3040	0.0565	7.232	186.0														233.1	1.479	1.178	199						383.9	2.999	2.617	1044	483.4	2.994	2.629
				7.236	185.9	283.2	1.472					1.179	200																			
				7.241	185.6	383.9	1.439					1.164	201																			
				7.245	185.4	483.4	1.396	1.135	202																							
				7.250	185.2	583.8	1.372	1.122	203																							
				7.254	184.9	620.1	1.365	1.118	204																							
0.3056	0.0567	6.997	285.5	583.8	1.306	1.066	674	0.4004	0.0574	9.645	89.5	133.2	1.712	1.366	444																	
				6.991	286.0	620.0	1.312						1.074	675	183.6	1.646	1.316	445														
				0.3064	0.0567	7.232	186.0						233.1	1.479	1.178	199	383.9	2.999	2.617	1044	483.4	2.994	2.629	1045								
													7.236	185.9	283.2	1.472									1.179	200						
													7.241	185.6	383.9	1.439									1.164	201						
													7.245	185.4	483.4	1.396									1.135	202						
7.250	185.2	583.8	1.372					1.122	203																							
7.254	184.9	620.1	1.365					1.118	204																							

5111
CS-6 back

TABLE I. - Continued. RESULTS OF STUDY OF HEAT TRANSFER FROM CYLINDERS IN SUBSONIC SLIP FLOW

M	Kn	Re _t	T _t	T _w	Nu _t ¹	Nu _t	Run	M	Kn	Re _t	T _t	T _w	Nu _t ¹	Nu _t	Run												
0.4007	0.0565	9.116	281.5	333.1	1.241	0.9801	666	0.4931	0.00910	77.03	-5.0	33.6	4.587	4.002	996												
				383.9	1.349	1.085	667																				
				483.4	1.399	1.143	668																				
0.4008	0.0408	12.99	192.2	583.8	1.720	1.447	621	0.4951	0.0143	46.77	87.0	133.2	2.698	2.277	1047												
				192.0	620.1	1.712	1.444									622											
	0.0409	12.97	193.0	233.1	1.647	1.333	617									183.6	3.044	2.615	1048								
			192.8	283.2	1.705	1.395	618																				
			12.98	192.6	383.9	1.739	1.442													619	283.2	3.145	2.735	1049			
192.4	483.4	1.732	1.448	620																							
0.4010	0.0256	21.64	89.0	133.2	2.355	1.959	540	0.4965	0.0143	49.35	-3.0	33.6	3.605	3.081	959												
				183.6	2.384	1.999	541																				
				283.2	2.359	1.996	542																				
				383.9	2.339	1.996	543																				
				483.4	2.309	1.982	544																				
583.8	2.289	1.976	545																								
0.4013	0.0402	12.84	282.0	333.2	1.350	1.080	702	0.4968	0.0249	28.31	-6.0	33.6	2.871	2.397	893												
				383.9	1.568	1.287	703																				
				483.4	1.652	1.377	704																				
				583.8	1.678	1.412	705																				
				620.0	1.677	1.414	706																				
0.4024	0.0749	6.911	283.0	333.2	1.027	0.7852	646	0.4974	0.0398	17.80	-8.0	33.6	2.270	1.842	845												
				6.908	283.2	383.9	1.141									.8950	647										
				6.905	283.5	483.4	1.185									.9451	648										
				6.902	283.8	583.8	1.186									.9550	649										
	0.0750	6.899	284.0	620.0	1.185	0.9571	650																				
0.4028	0.0742	7.503	91.3	133.2	1.494	1.167	73	0.4981	0.0255	26.34	87.0	133.2	2.377	1.980	546												
				183.6	1.458	1.144	74																				
				233.1	1.437	1.134	75																				
				283.2	1.405	1.111	76																				
				333.2	1.377	1.092	77																				
				383.9	1.258	.9878	78																				
				433.0	1.316	1.047	79																				
				483.4	1.288	1.025	80																				
				533.0	1.269	1.011	81																				
				583.8	1.251	.9977	82																				
				620.1	1.240	.9893	83																				
				0.4032	0.0250	20.74	282.0									333.2	1.958	1.641	732	0.4988	0.0403	16.70	84.0	133.2	1.936	1.572	498
																20.69	283.5	383.9	2.064								
					0.0251	20.68	283.7									483.4	2.071	1.768	734								
				20.67	284.0	620.0	2.120									1.831	736										
0.4056	0.0141	38.02	184.5	233.1	2.215	1.857	1113	0.4992	0.0388	18.49	-24.0	33.6	2.295	1.863	869												
				37.99	184.9	283.2	2.583									2.211	1114										
	37.96	185.3	383.9	2.848	2.480	1115																					
	37.93	185.7	483.4	2.862	2.510	1116																					
	37.90	186.1	583.8	2.855	2.518	1117																					
37.87	186.5	620.1	2.860	2.527	1118																						
0.4072	0.0585	10.10	-2.0	33.6	1.843	1.451	809	0.4998	0.0573	11.26	190.0	233.1	1.283	1.001	581												
				0.0586	10.10	-1.8	86.6									1.777	1.405	810									
	10.09	-1.6	183.6	1.699	1.354	811																					
	10.08	-1.4	383.9	1.602	1.293	812																					
	10.07	-1.2	483.4	1.558	1.262	813																					
0.0587	10.07	-1.0	583.8	1.519	1.232	814																					
0.4074	0.0577	9.334	192.0	233.1	1.346	1.058	599	0.5005	0.0254	25.45	188.0	233.1	2.019	1.677	755												
				283.2	1.277	1.002	600																				
				383.9	1.454	1.178	601																				
				483.4	1.445	1.181	602																				
				583.8	1.430	1.177	603																				
620.1	1.422	1.172	604																								
0.4415	0.0570	10.13	194.5	233.1	1.158	0.8870	552	0.5006	0.0401	15.62	280.0	333.2	1.403	1.128	707												
				10.17	192.4	283.2	1.290									1.014	553										
				10.21	190.3	383.9	1.301									1.037	554										
				10.25	188.2	483.4	1.275									1.023	555										
				10.30	186.1	583.8	1.260									1.018	556										
10.34	184.0	620.1	1.248	1.009	557																						
0.4717	0.0647	9.212	280.0	620.0	1.228	0.9970	645	0.5010	0.0565	11.11	282.0	333.2	1.327	1.059	676												
				0.0648	9.200	280.8	583.8									1.241	1.006	644									
	9.190	281.5	483.4	1.249	1.004	643																					
	0.0649	9.179	282.2	383.9	1.230	0.9761	642																				
	0.0650	9.167	283.0	333.2	1.085	.8381	641																				
0.4793	0.00910	75.19	-5.0	33.6	4.549	3.966	995	0.5048	0.0411	15.80	191.0	620.1	1.780	1.508	629												
				75.17	-5.0	86.6	4.390									3.840	997										
	183.6	4.267	3.760	998																							
	383.9	4.161	3.712	999																							
	483.4	4.128	3.700	1000																							
0.4931	0.00910	77.03	-5.0	33.6	4.587	4.002	996	0.5048	0.0412	15.75	192.6	283.2	1.765	1.451	624												
				0.4951	0.0143	46.77	87.0									133.2	2.698	2.277	1047								
				183.6																3.044	2.615	1048					
				283.2																			3.145	2.735	1049		
				383.9																						3.158	2.768
483.4	3.149	2.777	1051																								
583.8				3.136	2.780	1052																					
0.4965							0.0143	49.35	-3.0	33.6	3.605	3.081	959														
86.6														3.520	3.023	960											
183.6																	3.469	3.007	961								
383.9	3.384	2.973	962																								
483.4				3.357	2.966	963																					
583.8							3.315	2.940	964																		
0.4968										0.0249	28.31	-6.0	33.6	2.871	2.397	893											
86.6																	2.788	2.339	894								
183.6	2.702	2.286	895																								
383.9				2.578	2.211	896																					
483.4							2.525	2.175	897																		
583.8										2.484	2.148	898															
0.4974													0.0398	17.80	-8.0	33.6	2.270	1.842	845								
17.79	86.6	2.217	1.809																	846							
17.78				183.6	2.146	1.768															847						
17.77							383.9	2.050	1.713													848					
17.76										483.4	2.011	1.689											849				
17.75													583.8	1.986	1.675	850											
0.4981	0.0255	26.34	87.0														133.2	2.377	1.980	546							
183.6				2.467	2.077	547																					
283.2							2.464	2.095	548																		
383.9										2.445	2.096	549															
483.4													2.418	2.086	550												
583.8	2.387	2.068	551																								
0.4988				0.0403	16.70	84.0										133.2	1.936	1.572	498								
183.6							1.971	1.616	499																		
283.2										1.967	1.632	500															
383.9													1.885	1.571	501												
483.4	1.907	1.604	502																								
583.8				1.877	1.587	503																					
0.4992							0.0388	18.49	-24.0							33.6	2.295	1.863	869								
0.0389										18.46	-23.6	86.6								2.274	1.860	870					
18.44										-23.2	183.6	2.132	1.752	871													
0.0390	18.42	-22.8	383.9				2.027	1.688	872																		
0.4998	0.0573	11.26	190.0	233.1	1.283	1.001	581																				
283.2				1.476	1.185	582																					
383.9				1.499	1.220	583																					
483.4	1.492	1.225	584																								
583.8	1.480	1.223	585																								
620.1	1.476	1.223	586																								
0.5005	0.0254	25.45	188.0	233.1	2.019	1.677	755																				
25.41				188.8	283.2	2.350	1.808	756																			
0.0255				25.37	189.6	383.9	2.226	1.896	757																		
25.33				190.4	483.4	2.258	1.941	758																			
25.29				191.2	583.8	2.271	1.966	759																			
25.26	192.0	620.1	2.283	1.982	760																						
0.5006	0.0401	15.62	280.0	333.2	1.403	1.128	707																				
15.63				280.0	383.9	1.711	1.419	708																			
0.0402				15.60	281.0	483.4	1.728	1.448	709																		
15.57	282.0	583.8	1.733	1.464	710																						
15.55	283.0	620.0	1.740	1.474	711																						
0.5010	0.0565	11.11	282.0	333.2	1.327	1.059	676																				
383.9				1.433	1.163	677																					
483.4				1.456	1.196	678																					
583.8				1.448	1.198	679																					
620.0				1.441	1.195	680																					
0.5016	0.0761	9.316	0.5	33.6	1.828	1.439	773																				
86.6				1.654	1.294	774																					
183.6				1.544	1.213	775																					
383.9				1.457	1.139	776																					
483.4				1.397	1.110	777																					
583.8	1.360	1.080	778																								
0.5048	0.0411	15.80	191.0	620.1	1.780	1.508	629																				
0.0412				15.75	192.6	283.2	1.765	1.451	624																		
15.76				192.2	383.9	1.836	1.533	625																			
15.78				191.8	483.4	1.829	1.539	626																			

TABLE I. - Concluded. RESULTS OF STUDY OF HEAT TRANSFER FROM CYLINDERS IN SUBSONIC SLIP FLOW

M	Kn	Re _t	T _t	T _w	Nu'' _t	Nu _t	Run	M	Kn	Re _t	T _t	T _w	Nu'' _t	Nu _t	Run
0.6932	0.0557	15.05	186.0	233.1	1.502	1.202	593	0.7635	0.0559	15.59	275.2	583.8	1.465	1.216	695
				283.2	1.542	1.247	594				275.0	620.0	1.491	1.243	696
				383.9	1.524	1.245	595				0.0560	15.57	276.0	333.2	1.430
483.4	1.513	1.245	596	275.8	383.9	1.467	1.196	693							
583.8	1.493	1.236	597	15.58	275.5	483.4	1.474	1.214	694						
0.7008	0.0408 .0409 .0410	20.73 20.67 20.61	184.0 185.5 187.0	620.1	1.823	1.550	640	0.7714	0.0759	11.57	276.0	333.2	1.173	0.9194	661
				583.8	1.841	1.562	639				275.9	383.9	1.238	.9850	662
				483.4	1.874	1.582	638				275.8	483.4	1.241	.9982	663
0.0411	20.55 20.57 20.49	188.5 188.0 190.0	383.9 283.1 283.2	1.876	1.571	1.571	637	0.7799	0.0570	15.99	183.0	233.1	1.430	1.136	605
				1.735	1.415	1.415	635				183.2	283.2	1.493	1.202	606
				1.808	1.492	1.492	636				0.0571 .0572	15.96 15.91	184.0	620.1	1.488
1.671	1.330	1.330	474	183.8	483.4	1.511	1.244	608							
1.705	1.372	1.372	475	183.6	383.9	1.525	1.246	607							
0.7012	0.0573	15.42	81.3	283.2	1.685	1.371	476	0.7827	0.0772	11.83 11.82 11.81	185.0	233.1	1.234	0.9575	575
				383.9	1.647	1.351	477				185.4	283.2	1.311	.8710	576
				483.4	1.607	1.325	478				185.8	383.9	1.293	1.031	577
0.7019	0.0761	12.19	-3.7	183.6	1.568	1.235	781	0.0773	11.80 11.79	186.2 186.6	483.4 583.8	1.254 1.233	1.005 .9944	578 579	
			-3.8	383.9	1.454	1.156	782								
			-3.9	483.4	1.407	1.120	783								
0.0762	12.18	-4.0	583.8	1.368	1.088	784	0.0774	11.78	187.0	620.1	1.222	0.9872	580		
				33.8	1.746	1.365								779	
				86.6	1.670	1.309								780	
0.7035	0.0400 0.0402 0.0403 .0404	20.55 20.50 20.44	274.0 275.5 277.0	333.2	1.616	1.326	717	0.7831	0.0386	26.32 26.34 26.36 26.37 26.39	-27.2 -27.4 -27.6 -27.8 -28.0	86.6 183.6 383.9 483.4 583.8	2.568 2.285 2.154 2.073 2.014	1.949 1.897 1.809 1.745 1.699	876 877 878 879 880
				383.9	1.748	1.455	718								
				483.4	1.787	1.504	719								
0.0403 .0404	20.39 20.34	278.3 280.0	583.8 620.0	1.793	1.522	720	0.0387	26.31	-27.0	33.6	2.452	2.009	875		
				1.792	1.524	721									
				1.792	1.524	721									
0.7060	0.0402	23.26 23.28 23.29 23.30 23.32 23.33	-11.0 -11.2 -11.4 -11.6 -11.8 -12.0	33.6	2.330	1.898	863	0.7844	0.0408	22.47 22.46	176.5 176.6	233.1 283.2	1.599 1.830	1.290 1.512	1089 1090
				86.6	2.322	1.908	864								
				183.6	2.222	1.840	865								
0.0402	23.30 23.32 23.33	-11.6 -11.8 -12.0	383.9 483.4 583.8	2.117	1.777	866	0.0409	22.44	176.8 176.9	483.4 583.8	1.860 1.844	1.570 1.565	1092 1093		
				2.060	1.735	867									
				2.017	1.705	868									
0.7077	0.0563	14.67 14.68	276.0 275.8	333.2	1.291	1.027	687	0.7857	0.0254	36.12 36.10 36.09 36.08	176.0 176.2 176.4 176.6	233.1 283.2 383.9 483.4	2.018 2.290 2.594 2.396	1.678 1.940 2.055 2.072	1107 1108 1109 1110
				383.9	1.396	1.130	688								
				483.4	1.466	1.207	689								
0.0563	14.69	275.5 275.2	483.4 583.8	1.480	1.229	690	0.0255	36.06 36.05	176.8 177.0	583.8 620.1	2.400 2.386	2.089 2.081	1111 1112		
				1.479	1.232	691									
				1.479	1.232	691									
0.7091	0.0753	10.99	276.5 276.4 276.2	333.2	1.153	0.9013	656	0.7865	0.0249	40.63	-12.5	33.6 86.6 183.6	2.896 2.883 2.848	2.423 2.429 2.425	911 912 913
				383.9	1.232	.9792	657								
				483.4	1.248	1.004	658								
0.0753	11.00	276.1 276.0	583.8 620.0	1.238	1.004	659	0.7870	0.0570	17.70 17.71	-11.0 -11.1 -11.2 -11.3	33.6 86.6 183.6 383.9	1.988 1.945 1.859 1.729	1.585 1.561 1.504 1.413	827 828 829 830	
				1.228	.9981	660									
				1.228	.9981	660									
0.7127	0.0237	37.68	80.3	133.2	2.299	1.909	1017	0.7888	0.0733	13.09	78.5	133.2 183.6 283.2 383.9 483.4 583.8	1.454 1.498 1.466 1.426 1.384 1.347	1.133 1.182 1.169 1.144 1.116 1.089	462 463 464 465 466 467
				2.582	2.185	1018									
				2.611	2.234	1019									
0.0237	37.68	80.3	133.2 283.2 383.9 483.4 583.8	2.608	2.250	1020	0.7899	0.0557	17.23	80.0	133.2 183.6 283.2 383.9 483.4 583.8	1.672 1.740 1.721 1.693 1.650 1.605	1.331 1.405 1.405 1.393 1.365 1.332	480 481 482 483 484 485	
				2.899	2.542	1021									
				2.521	2.196	1022									
0.7158	0.0408	21.99	82.0	133.2	1.987	1.621	510	0.7928	0.0401	24.00	81.0	133.2 183.6 283.2 383.9 483.4 583.8	2.039 2.111 2.080 2.023 1.993 1.947	1.669 1.748 1.739 1.701 1.687 1.654	516 517 518 519 520 521
				2.145	1.778	511									
				2.036	1.698	512									
0.0408	16.22 16.20	-8.5 -8.1	583.8 483.4	1.599	1.309	826	0.7944	0.0734	13.78	-6.0	33.6 86.6 183.6	1.854 1.753 1.645	1.464 1.385 1.307	785 786 787	
				1.599	1.345	825									
				1.599	1.345	825									
0.0582	16.19 16.17	-7.7 -7.3	383.9 183.6	1.702	1.388	824	0.7944	0.0734	13.78	-6.0	33.6 86.6 183.6	1.854 1.753 1.645	1.464 1.385 1.307	785 786 787	
				1.702	1.388	824									
				1.702	1.388	824									
0.0584	16.15 16.13	-6.9 -6.5	86.6 33.6	1.907	1.526	822	0.7944	0.0734	13.78	-6.0	33.6 86.6 183.6	1.854 1.753 1.645	1.464 1.385 1.307	785 786 787	
				1.907	1.526	822									
				1.907	1.526	822									
0.7240	0.0762	11.36 11.35	184.2 184.6	483.4	1.261	1.011	567	0.7944	0.0734	13.78	-6.0	33.6 86.6 183.6	1.854 1.753 1.645	1.464 1.385 1.307	785 786 787
				583.8	1.246	1.006	568								
				583.8	1.246	1.006	568								
0.0762	11.35	185.0	620.1	1.242	1.005	569	0.7944	0.0734	13.78	-6.0	33.6 86.6 183.6	1.854 1.753 1.645	1.464 1.385 1.307	785 786 787	
				1.242	1.005	569									
				1.242	1.005	569									
0.7373	0.0754	12.17	77.0	133.2	1.470	1.147	456	0.7944	0.0734	13.78	-6.0	33.6 86.6 183.6	1.854 1.753 1.645	1.464 1.385 1.307	785 786 787
				183.6	1.477	1.163	457								
				283.2	1.442	1.146	458								
0.0754	12.17	77.0	133.2 183.6 283.2 383.9 483.4 583.8	1.470	1.147	456	0.7944	0.0734	13.78	-6.0	33.6 86.6 183.6	1.854 1.753 1.645	1.464 1.385 1.307	785 786 787	
				1.477	1.163	457									
				1.442	1.146	458									
0.0754	12.17	77.0	133.2 183.6 283.2 383.9 483.4 583.8	1.414	1.133	459	0.7944	0.0734	13.78	-6.0	33.6 86.6 183.6	1.854 1.753 1.645	1.464 1.385 1.307	785 786 787	
				1.366	1.099	460									
				1.372	1.112	461									
0.7582	0.0141	69.57	-8.5	33.6	3.786	3.353	972	0.7944	0.0734	13.78	-6.0	33.6 86.6 183.6	1.854 1.753 1.645	1.464 1.385 1.307	785 786 787
				86.6	3.849	3.334	973								
				183.6	3.796	3.317	974								
0.0141	69.57	-8.5	33.6 86.6 183.6	3.685	3.261	975	0.7944	0.0734	13.78	-6.0	33.6 86.6 183.6	1.854 1.753 1.645	1.464 1.385 1.307	785 786 787	
				3.685	3.261	975									
				3.636	3.233	976									

1111

TABLE II. - ORGANIZATION OF RESULTS FOR NOMINAL VALUES OF PARAMETERS

Nominal Knudsen number, Kn	Nominal Mach number, M								
	0.05	0.10	0.20	0.30	0.40	0.50	0.60	0.70	0.80
Run numbers ^a for $T_t \approx 0^\circ \text{ F}$									
0.0770	342 420	336 414	330 408	402	767	773	761	779	785
0.0555	396	390	324 384	815	809	791 803	797	821	827
0.0416	378	372	857	839	833	845 869	851	863	875
0.0256	354 360	366	917	887	881	893	899 905	---	911
0.0143	348	935	923	929	941	959	965	---	972
0.00916	---	984	947	953 978	990	995	---	---	---
Run numbers ^a for $T_t \approx 80^\circ \text{ F}$									
0.0770	1	13 37	25 49	61	73 426	432	438	456	462
0.0555	85	91	97	103	444	450	468	474	480
0.0416	109	115 127	121 262	486	492	498	504	510	516
0.0256	133	139 522	528	534	540	546	1005	1011 1017	---
0.0143	145	1035	1029	1023	1041	1047	1083	----	---
0.00916	151	1065	1053	1059	1071	1077	----	----	---
Run numbers ^a for $T_t \approx 180^\circ \text{ F}$									
0.0770	169	163	157	175	---	---	---	567	575
0.0555	193	181	187	199	552 599	558 581	587	593	605
0.0416	217	211	205	611	617	623	630	635	1089
0.0256	223	229	743	737	749	755	1095	1101	1107
0.0143	235	---	---	---	1113	1119	----	----	----
Run numbers ^a for $T_t \approx 280^\circ \text{ F}$									
0.0770	278	247	252	257	646	---	651	656	661
0.0555	283	273	268	671	666	641 676	681	687	692
0.0416	288	293 299	304	697	702	707	712	717	---
0.0256	309	314	722	727	732	---	---	---	---
0.0143	319	---	---	---	---	---	---	---	---

^aEach run number is the first of a group of runs in table I at the indicated nominal values of M, Kn, and T_t .

5111

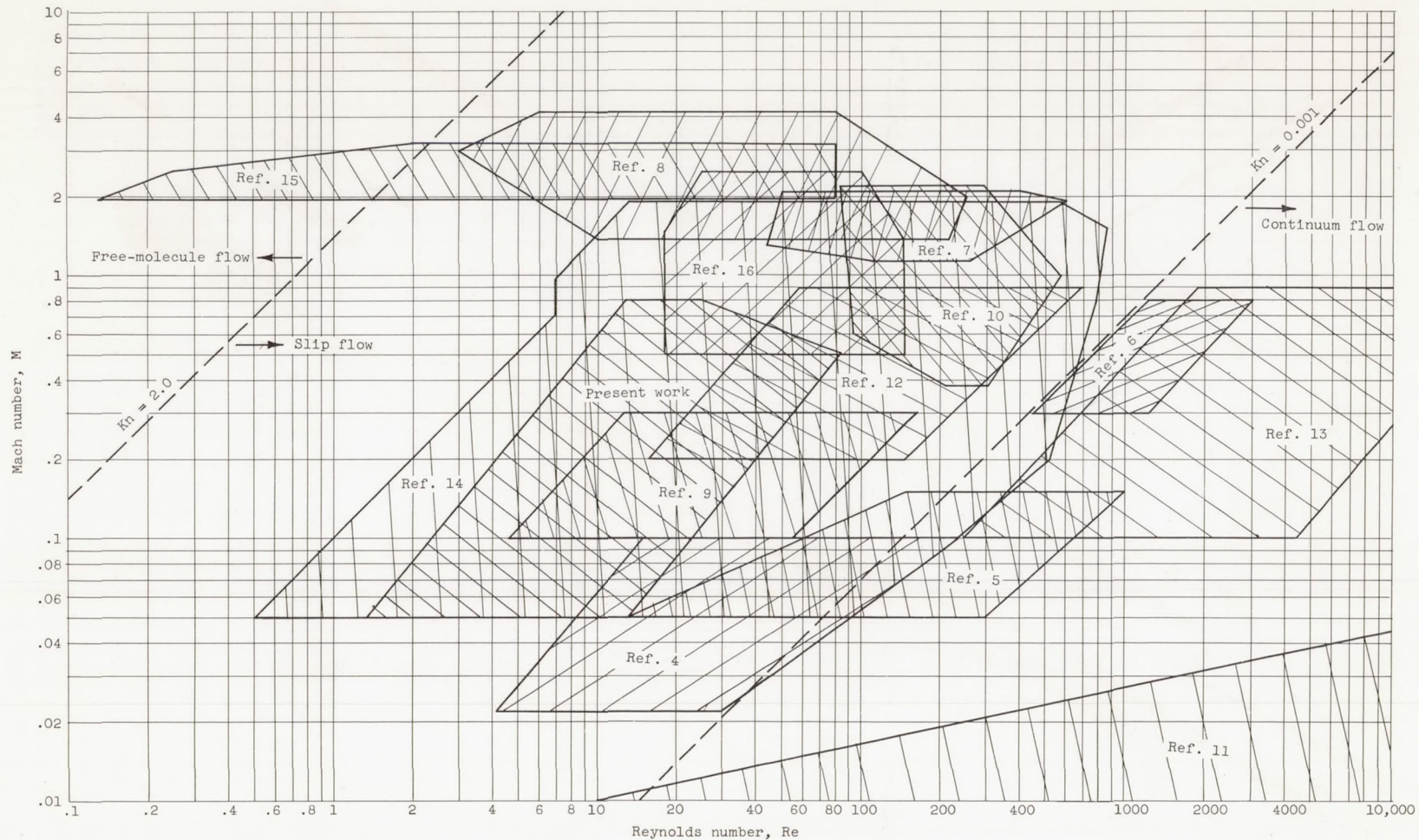


Figure 1. - Comparison of Mach and Reynolds number ranges of heat-transfer experiments with normal cylinders. Flow regions after reference 15.

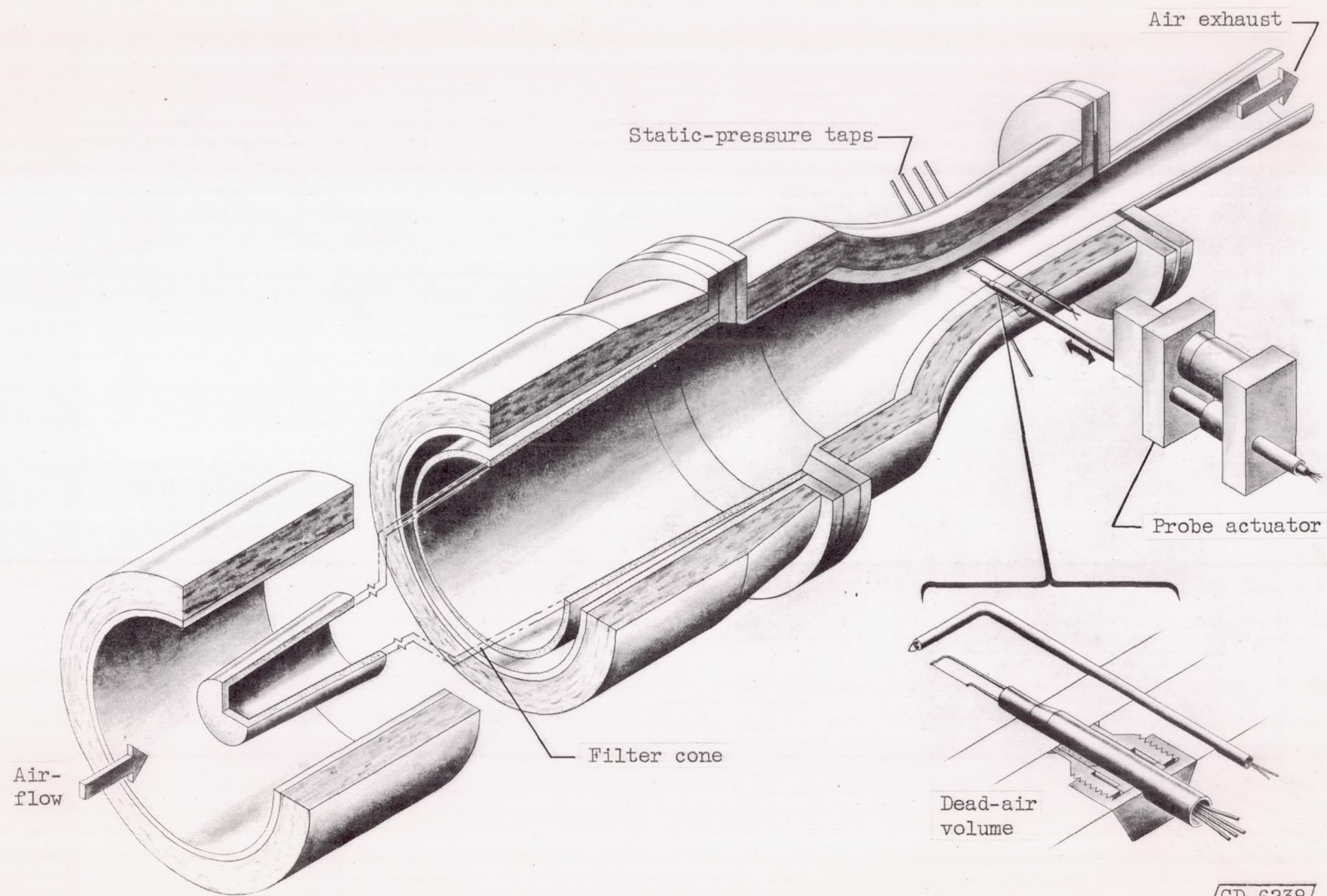


Figure 2. - Variable-density subsonic tunnel.

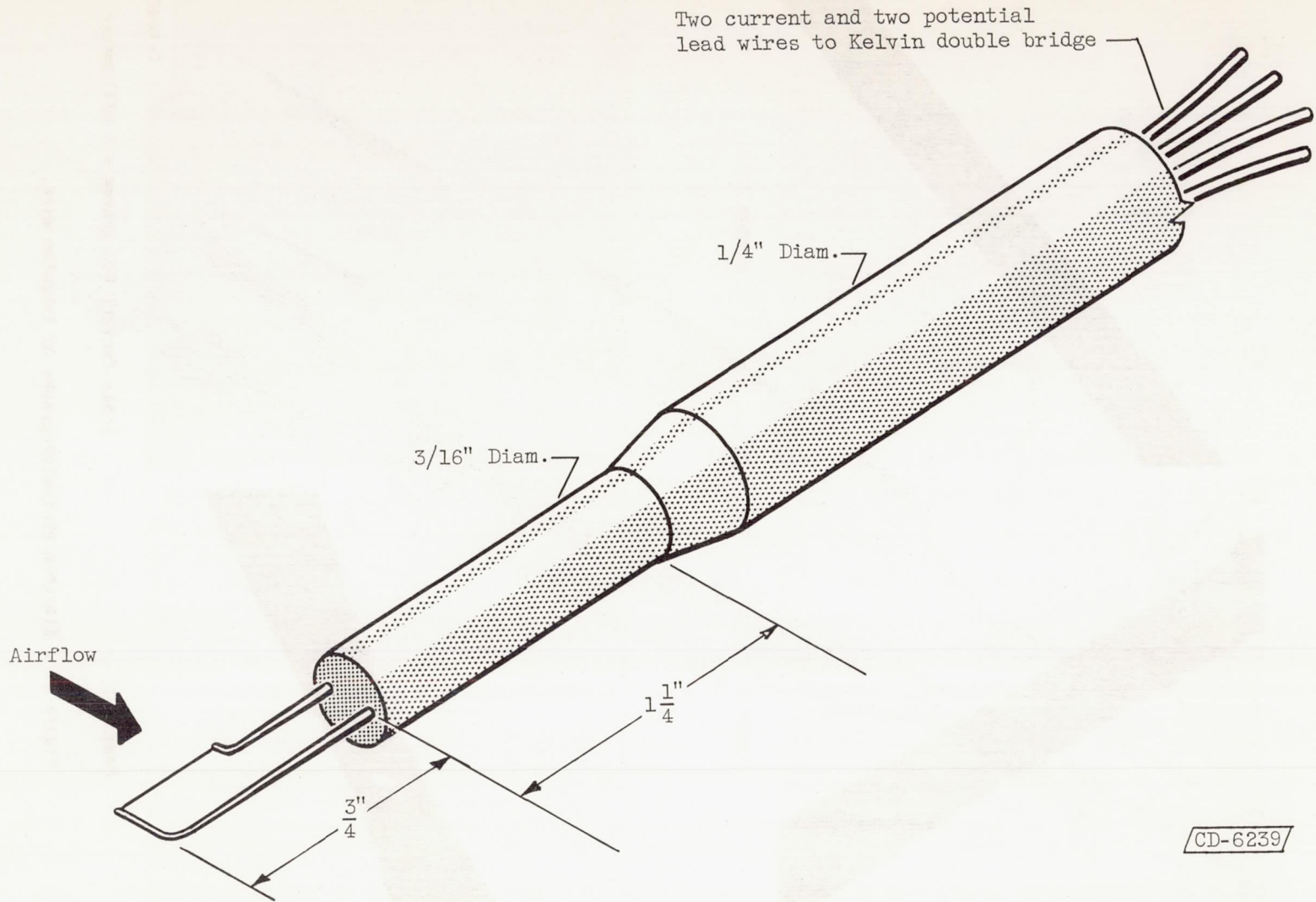
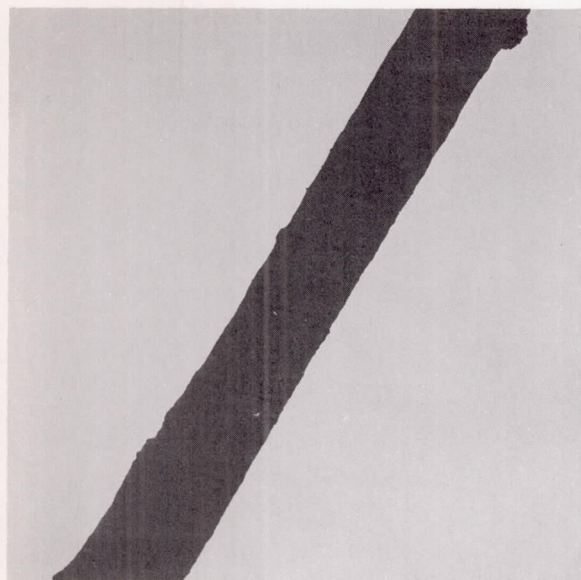
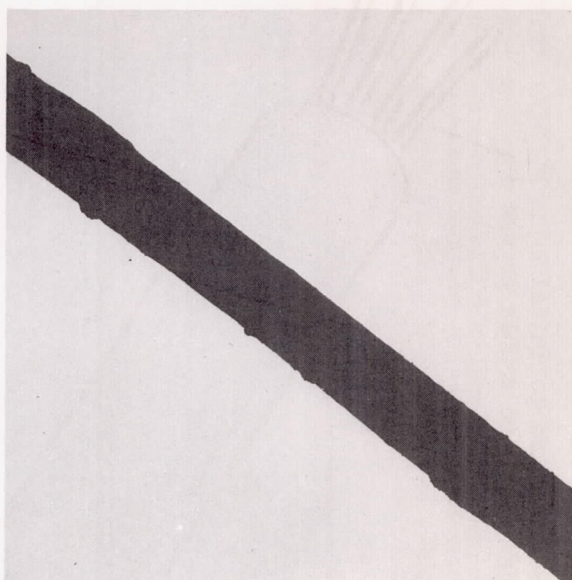


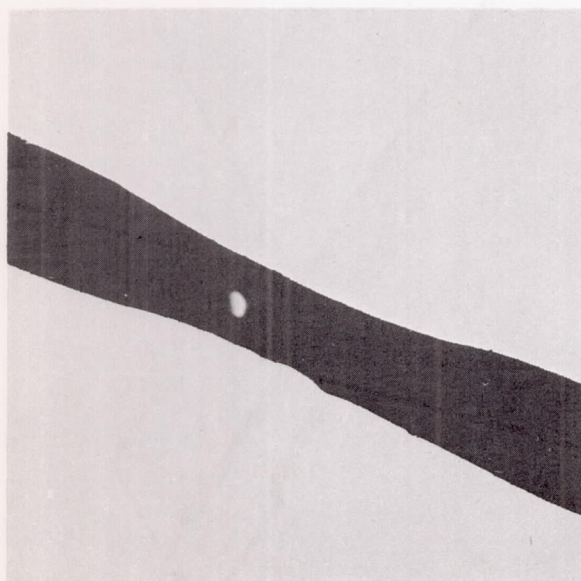
Figure 3. - Tungsten-wire supporting probe.



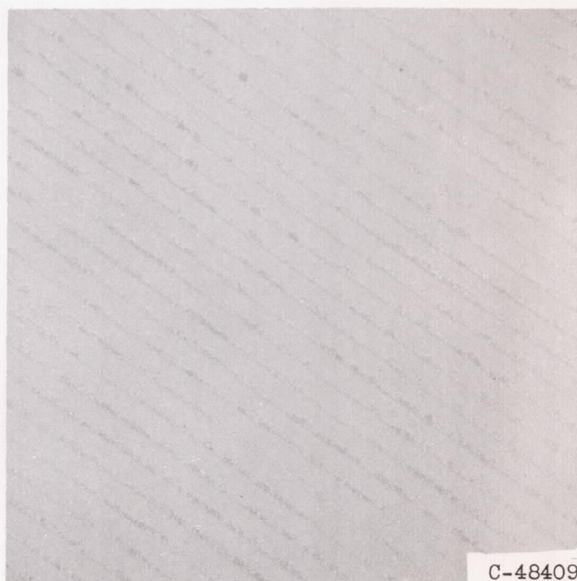
Sample A



Sample B



Sample C



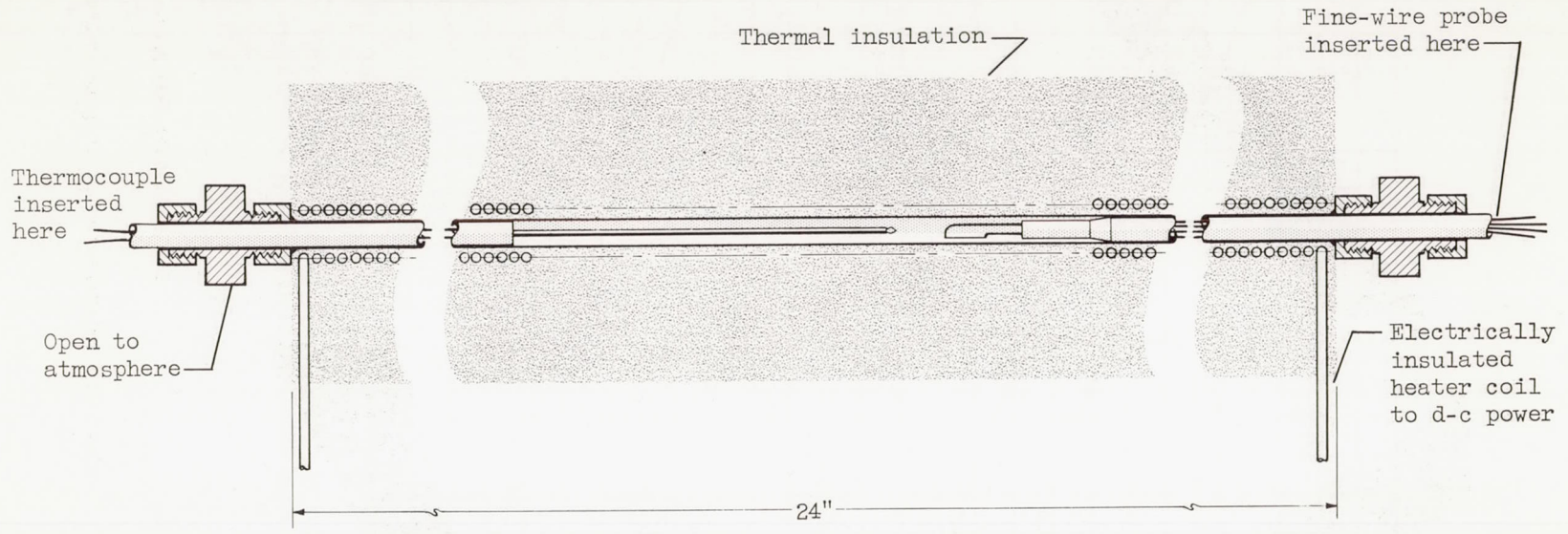
C-48409

Scale factor; 600 grates = 1 millimeter

Figure 4. - Electron photomicrographs of tungsten wire.

5111

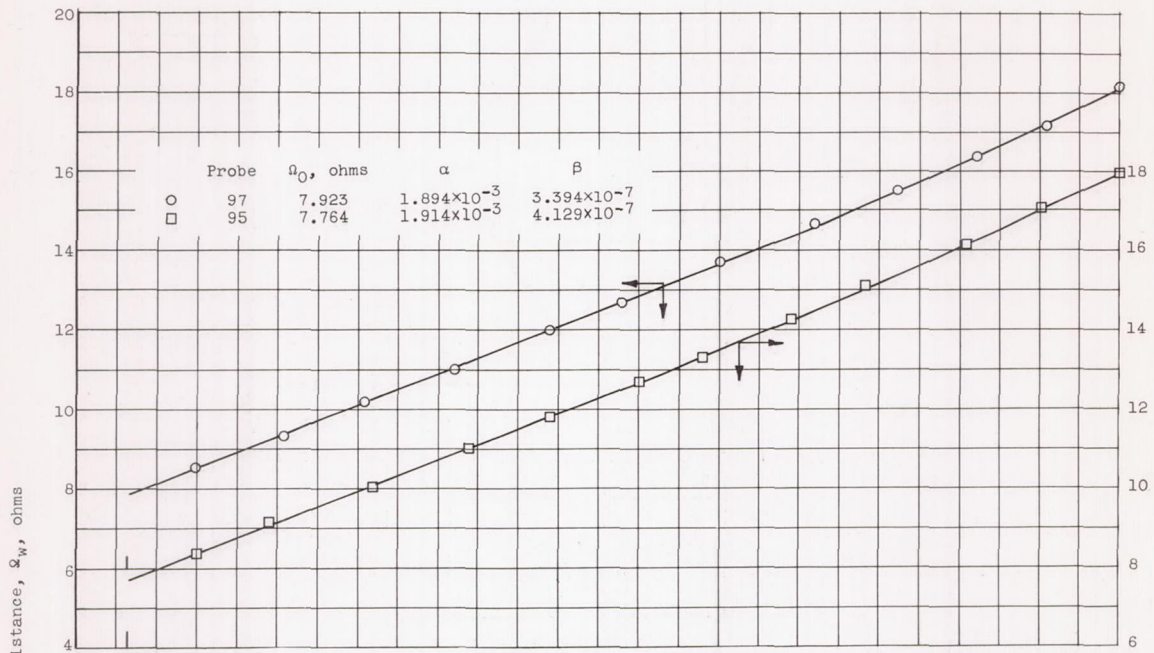
CS-7 back



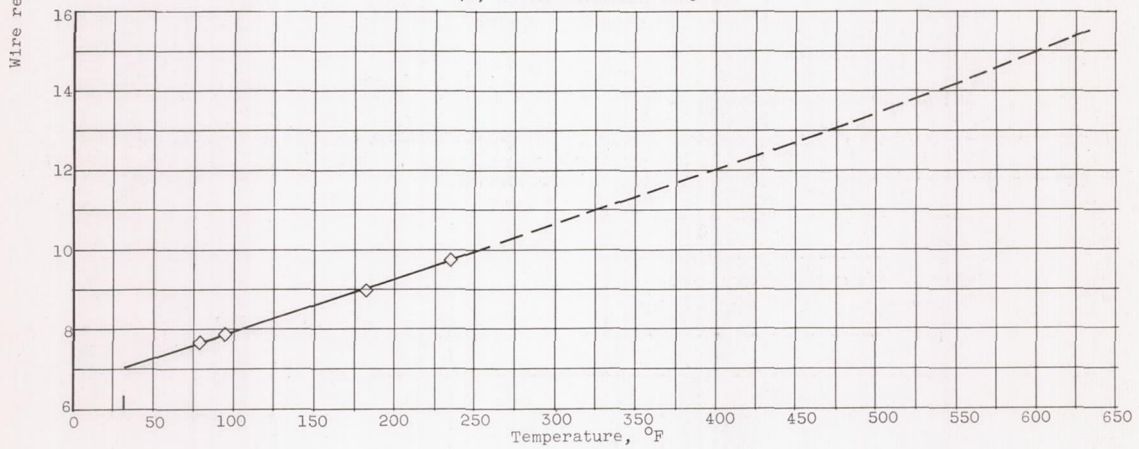
CD-6240

Figure 5. - Resistance-temperature calibration tank.

5111

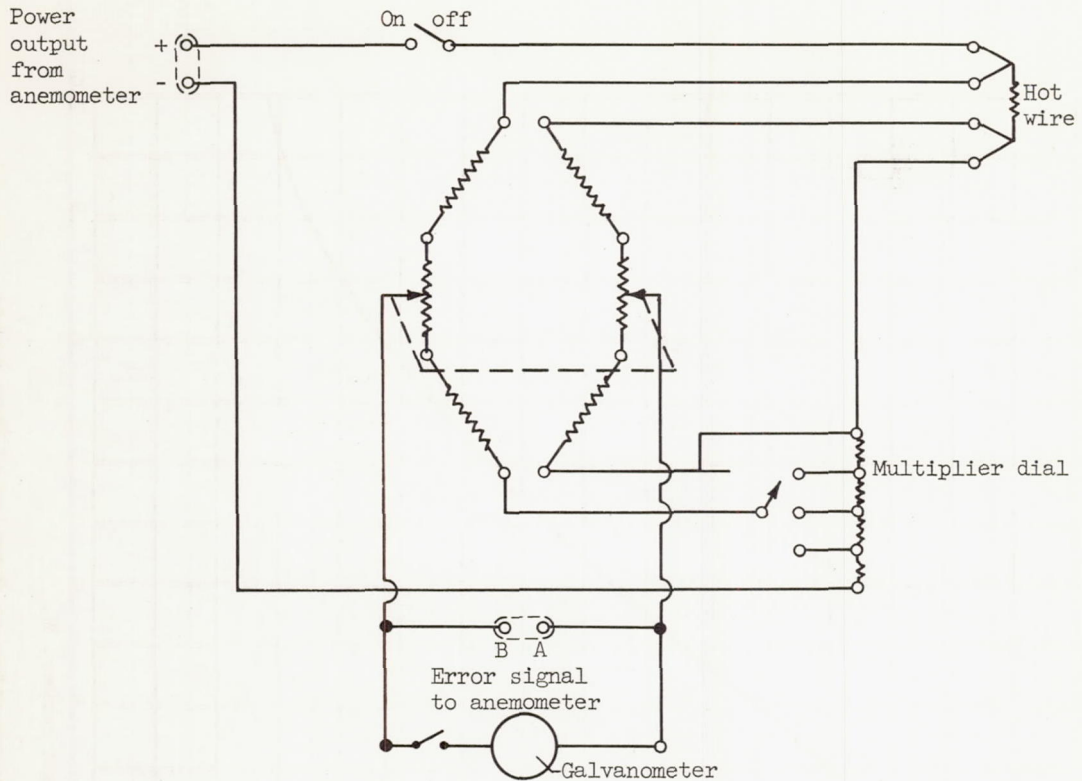


(a) Silver-soldered samples.

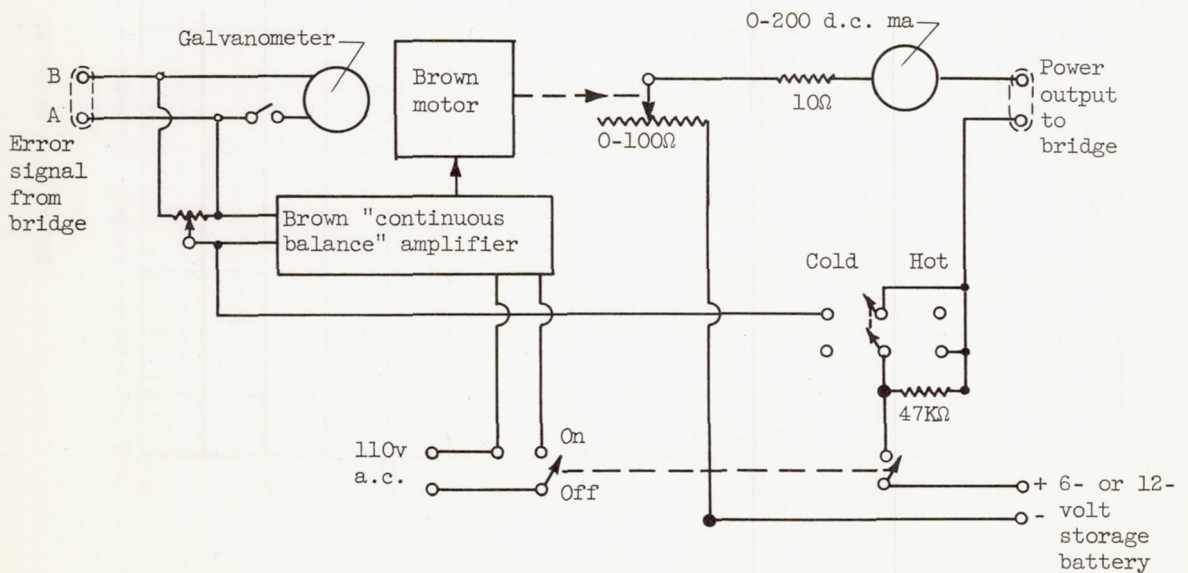


(b) Probe 109: $\mathcal{R}_0 = 7.054$ ohms; $\alpha = 1.833 \times 10^{-3}$; assumed $\beta = 3.40 \times 10^{-7}$.

Figure 6. - Calibration of wire electrical resistance and temperature.



(a) Kelvin bridge ohmmeter.



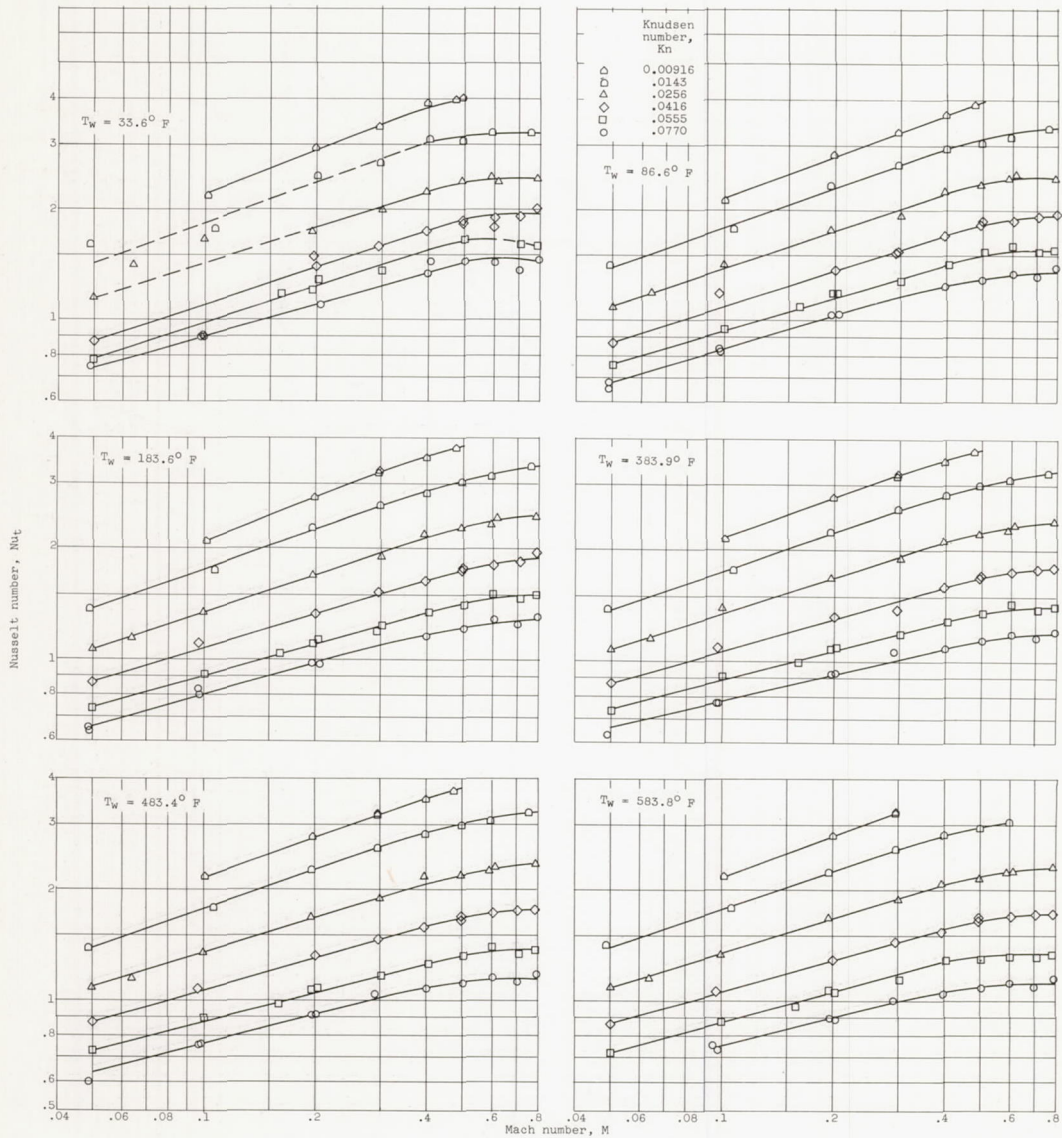
(b) Constant-average-temperature anemometer.

Figure 7. - Anemometer electrical equipment.

5111



Figure 8. - Recovery temperature ratio as function of Mach number.



(a) Total air temperature, 0° F .
 Figure 9. - Variation of Nusselt number with Mach number for constant Knudsen number and constant total air and cylinder temperatures.

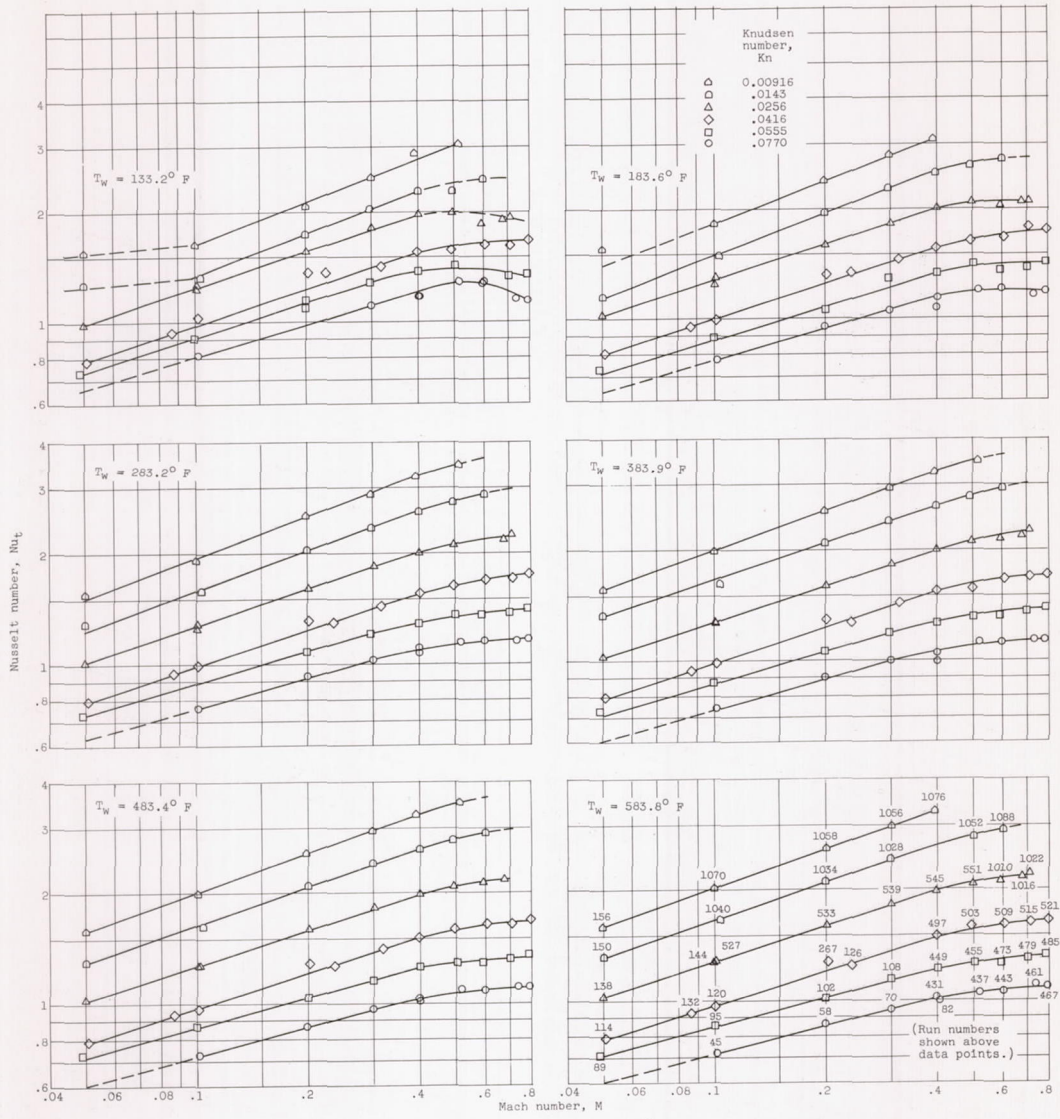


Figure 9. - Continued. Variation of Nusselt number with Mach number for constant Knudsen number and constant total air and cylinder temperatures.

5111

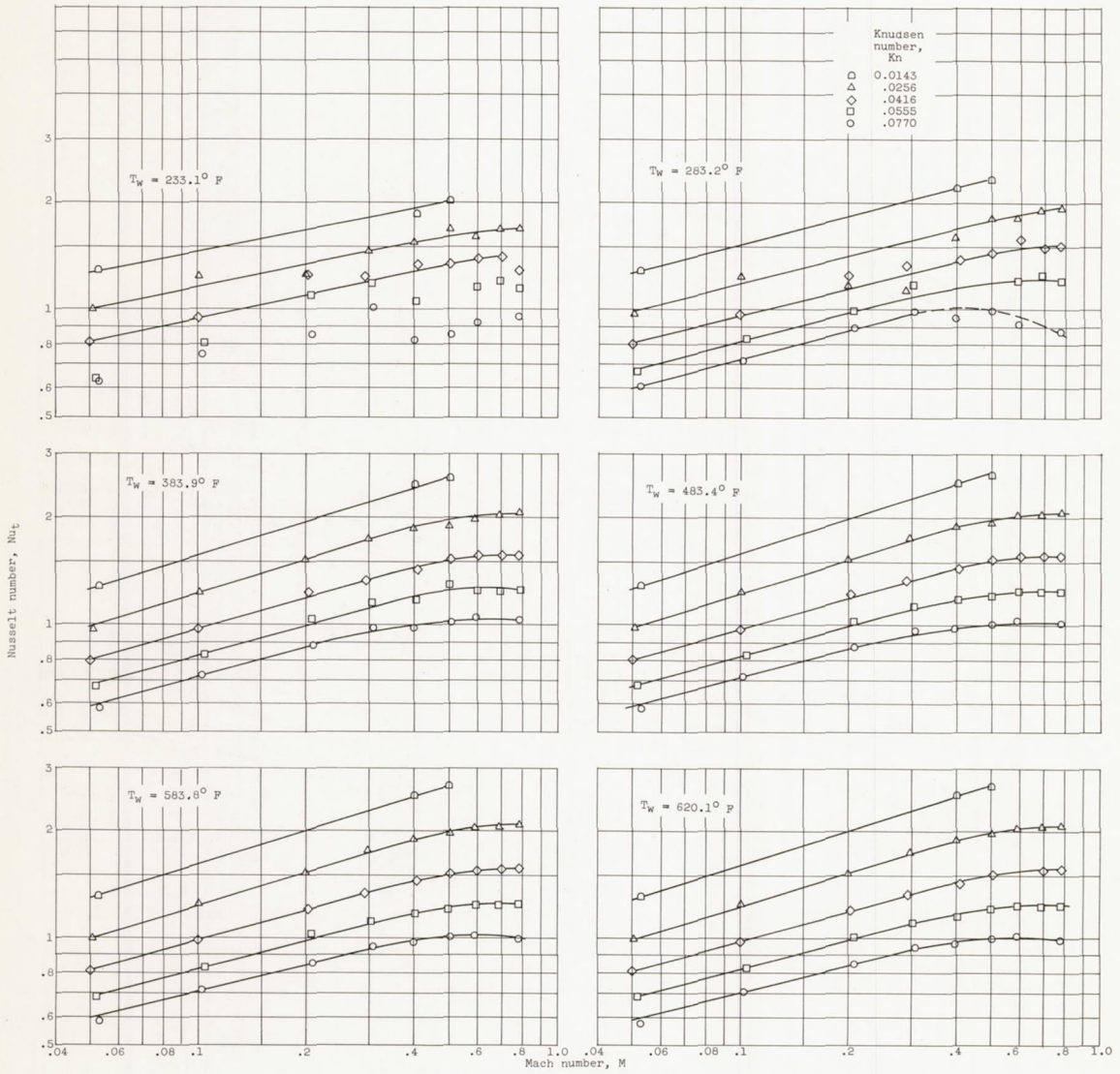
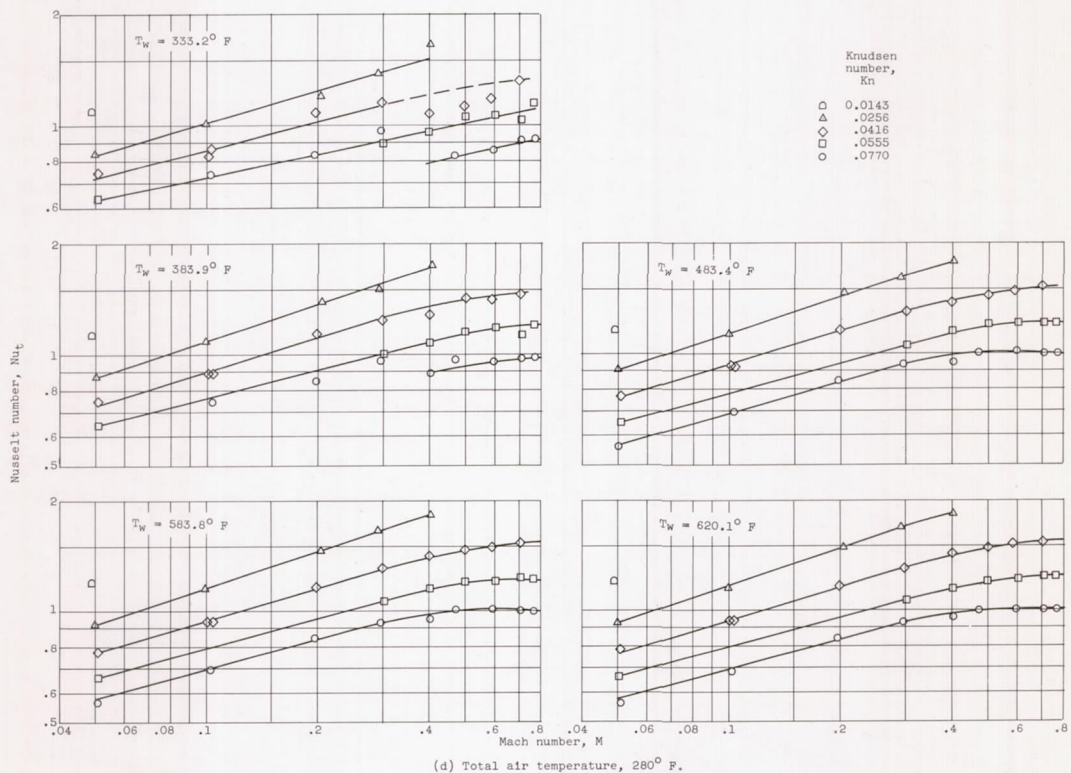


Figure 9. - Continued. Variation of Nusselt number with Mach number for constant Knudsen number and constant total air and cylinder temperatures.

5111

CS-8 back 5111



(d) Total air temperature, $280^\circ F$.
 Figure 9. - Concluded. Variation of Nusselt number with Mach number for constant Knudsen number and constant total air and cylinder temperatures.

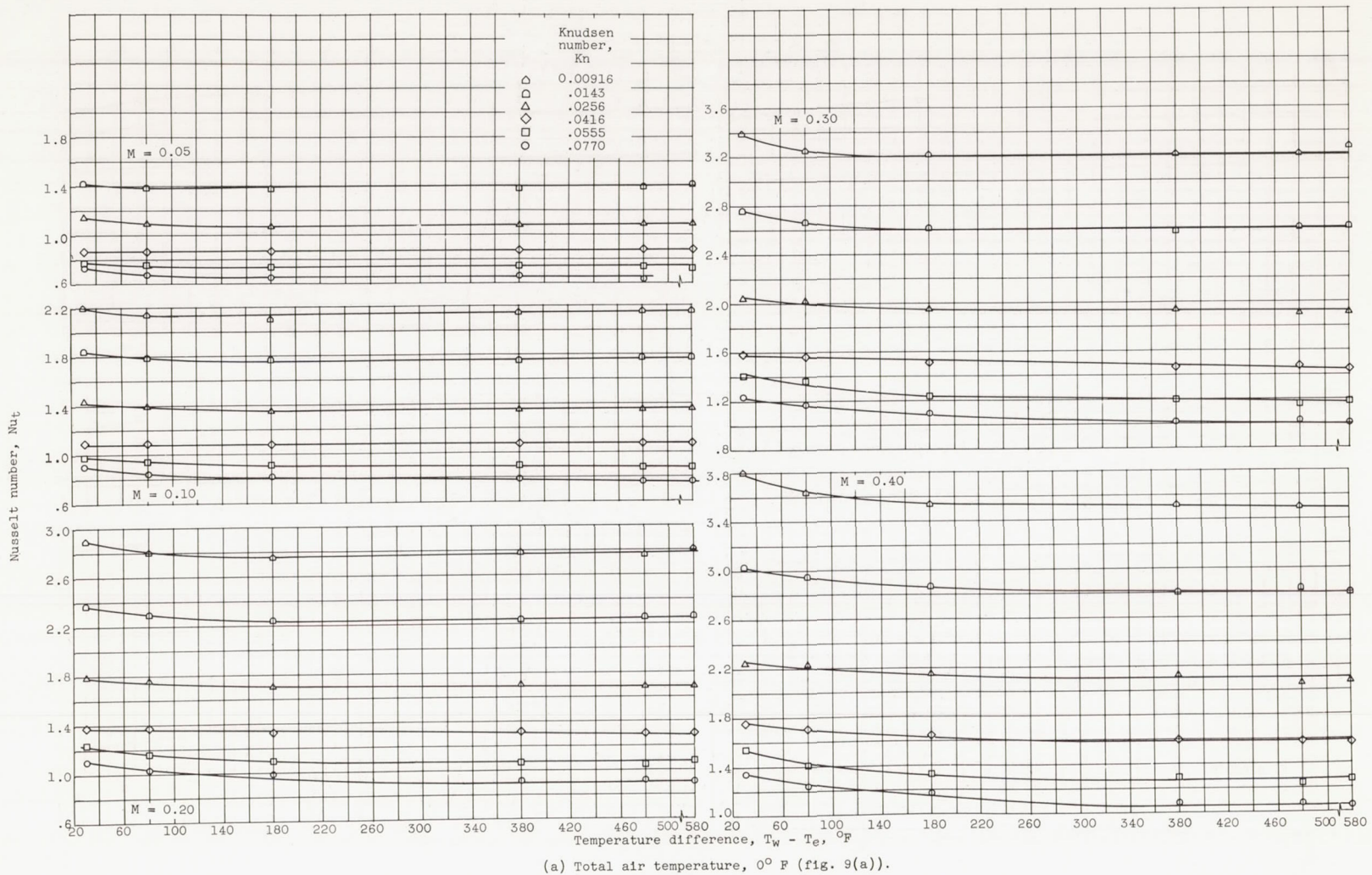
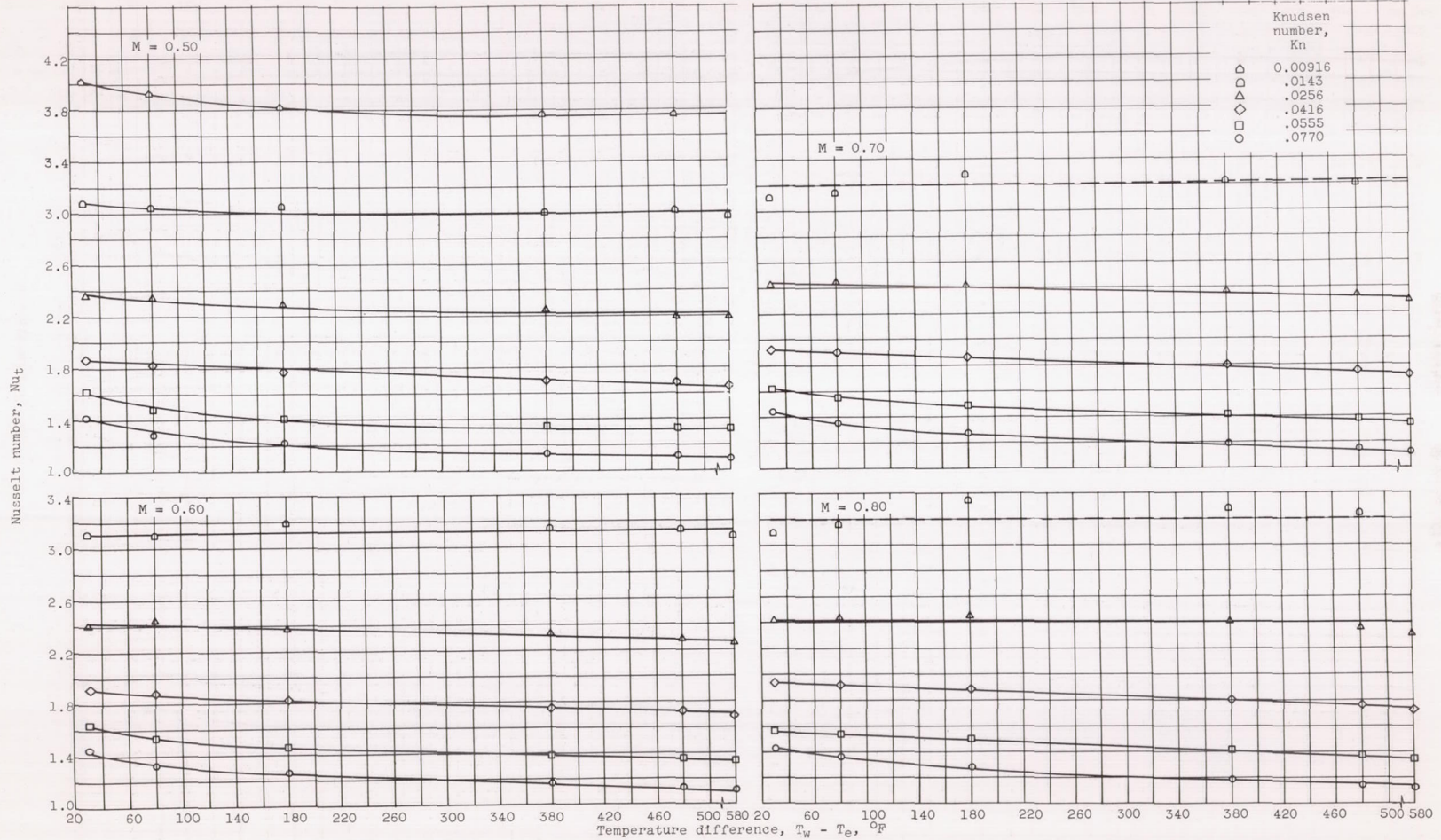


Figure 10. - Crossplots of figure 9 showing Nusselt number variation with cylinder temperature.



(a) Concluded. Total air temperature, $^{\circ}F$ (fig. 9(a)).

Figure 10. - Continued. Crossplots of figure 9 showing Nusselt number variation with cylinder temperature.

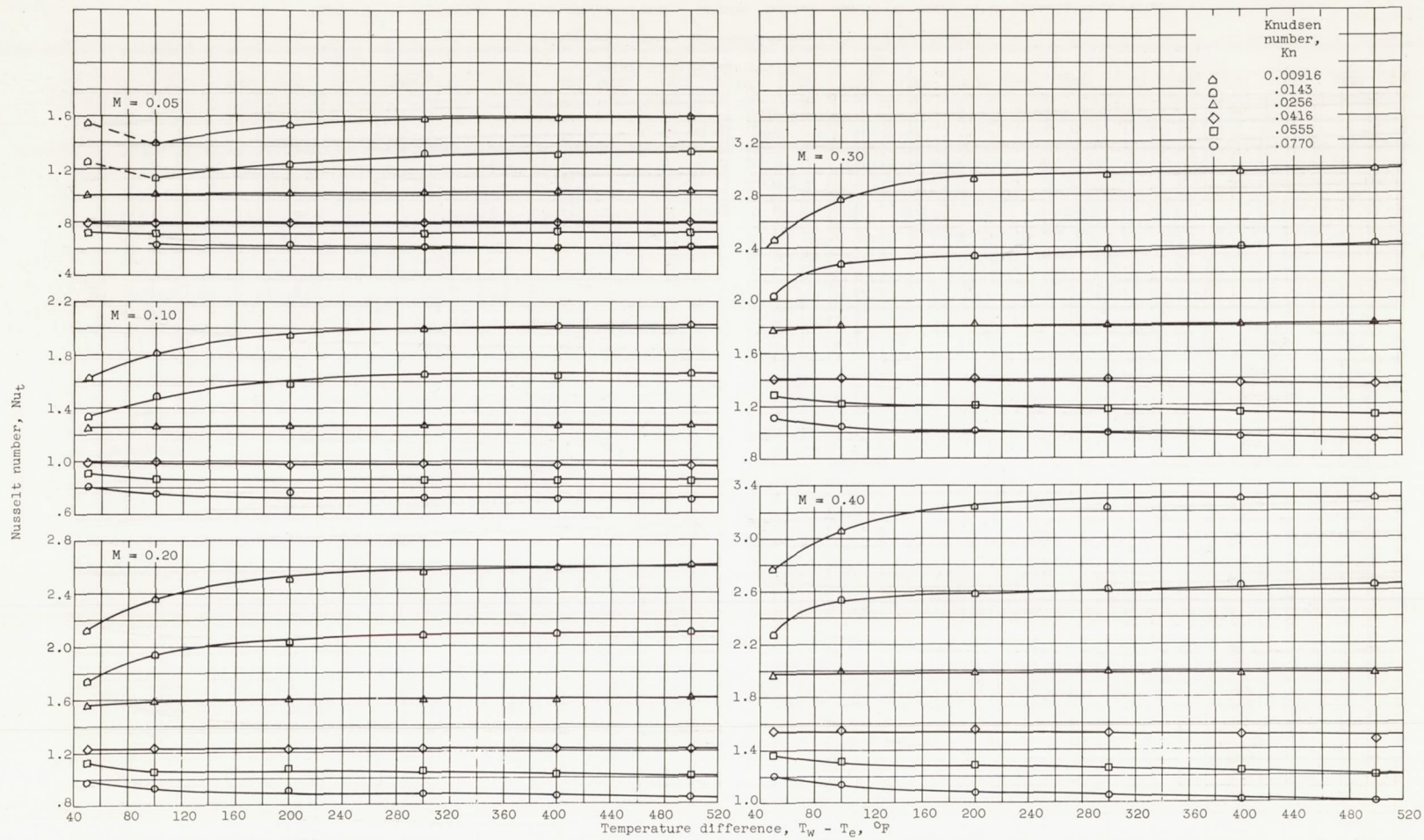
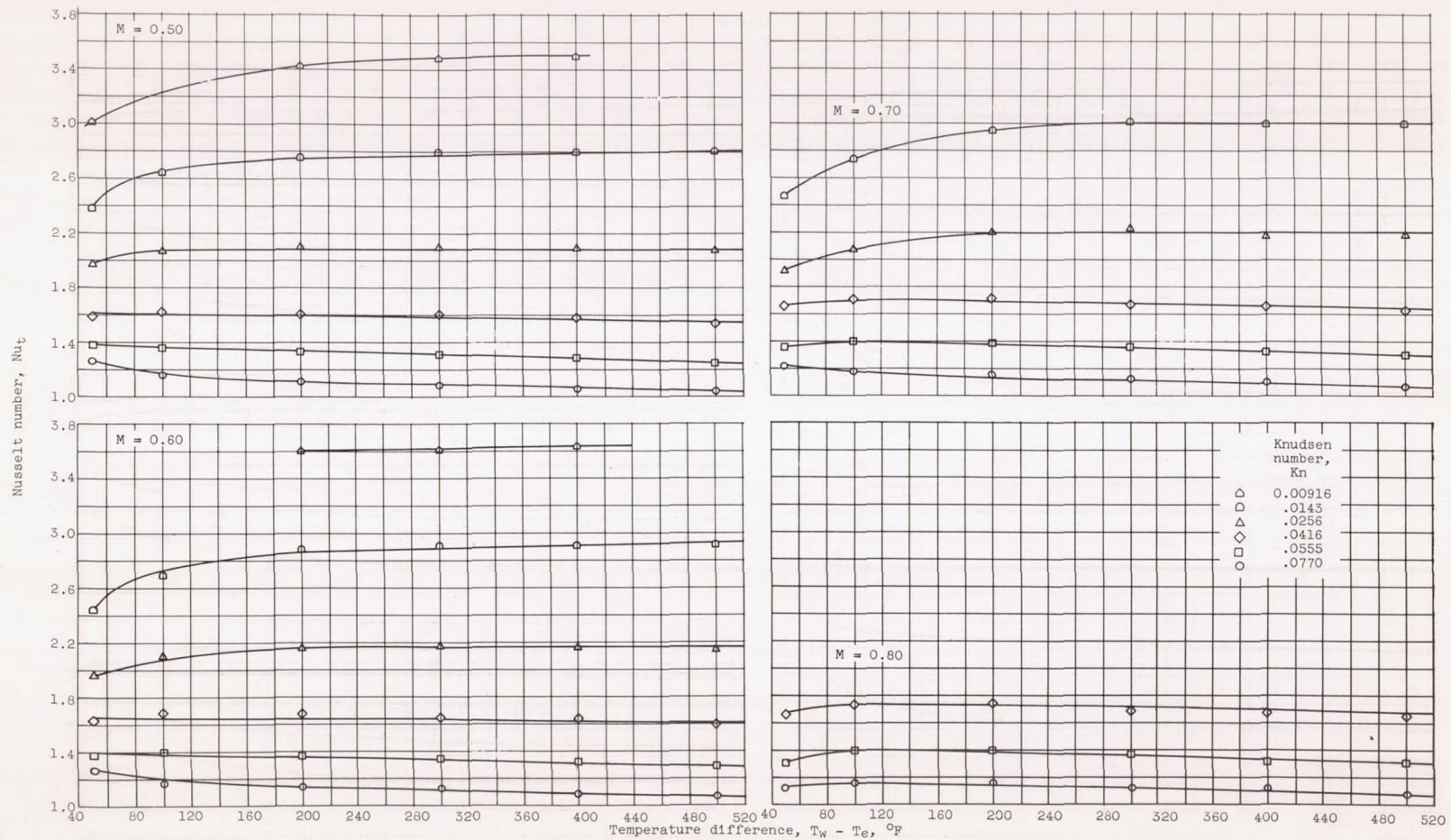
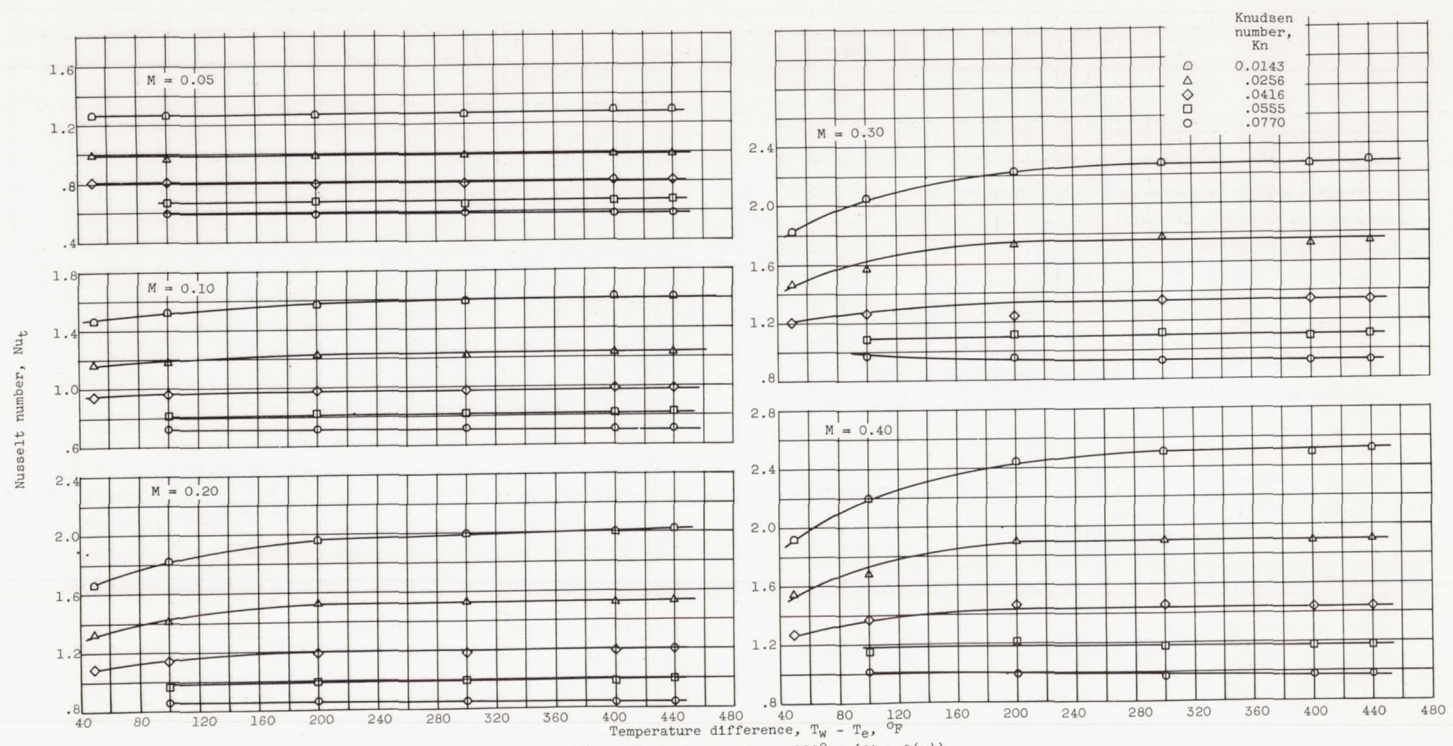


Figure 10. - Continued. Crossplots of figure 9 showing Nusselt number variation with cylinder temperature.



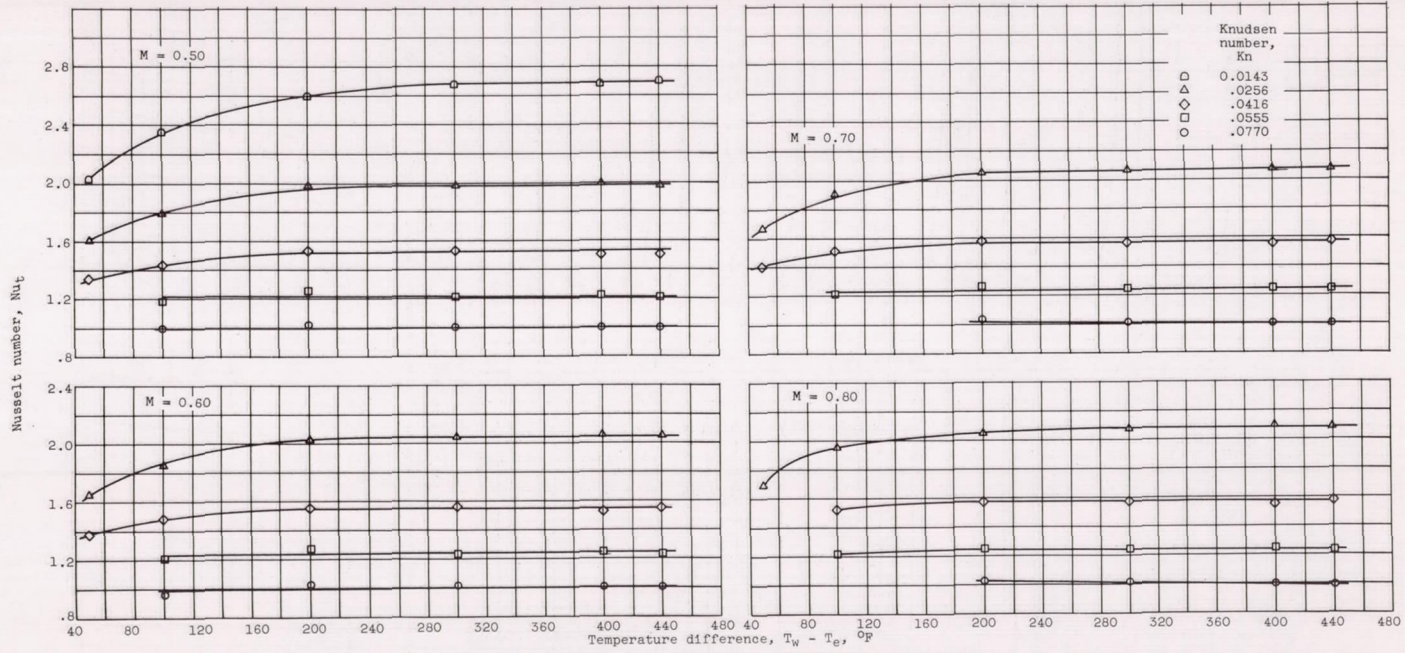
(b) Concluded. Total air temperature, 80°F (fig. 9(b)).

Figure 10. - Continued. Crossplots of figure 9 showing Nusselt number variation with cylinder temperature.



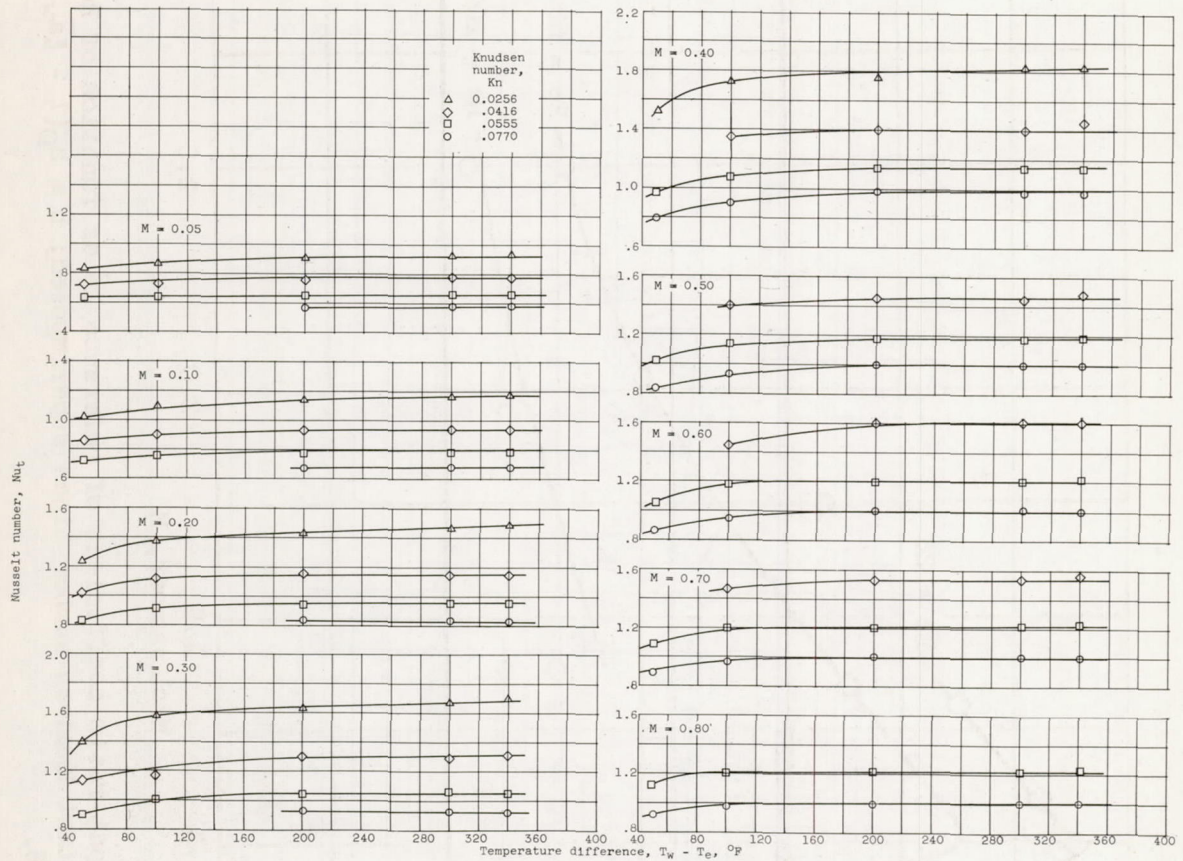
(c) Total air temperature, 180° F (fig. 9(c)).

Figure 10. - Continued. Crossplots of figure 9 showing Nusselt number variation with cylinder temperature.



(c) Concluded. Total air temperature, 180° F (fig. 9(c)).

Figure 10. - Continued. Crossplots of figure 9 showing Nusselt number variation with cylinder temperature.



(d) Total air temperature, 280° F (fig. 9(d)).

Figure 10. - Concluded. Crossplots of figure 9 showing Nusselt number variation with cylinder temperature.

1111

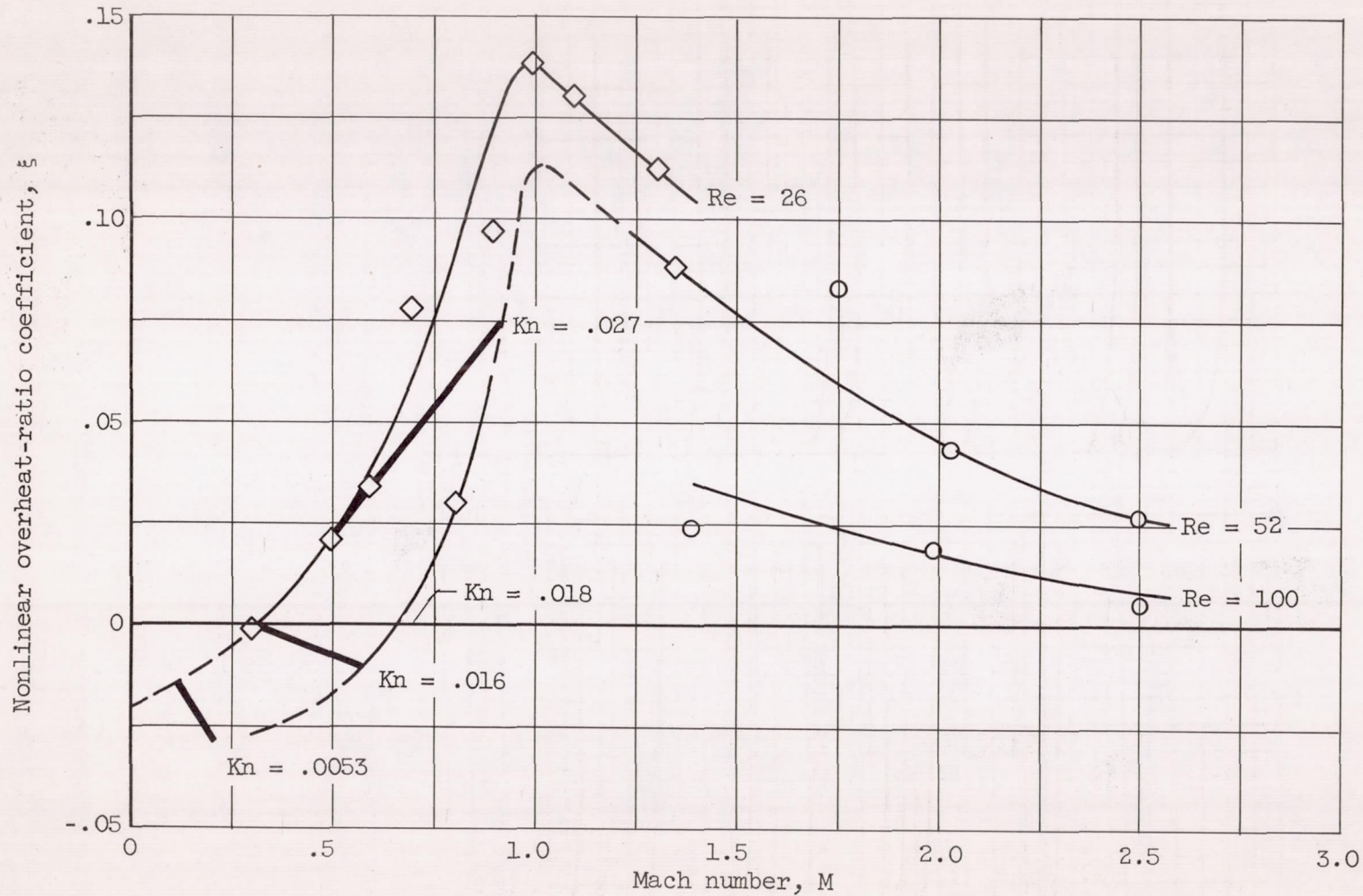


Figure 11. - Nonlinear overheat-ratio coefficient of reference 16 as function of Reynolds and Mach numbers with constant Knudsen number lines superimposed; $h = h_0(1 - \xi a_w)$. Data points of reference 16.

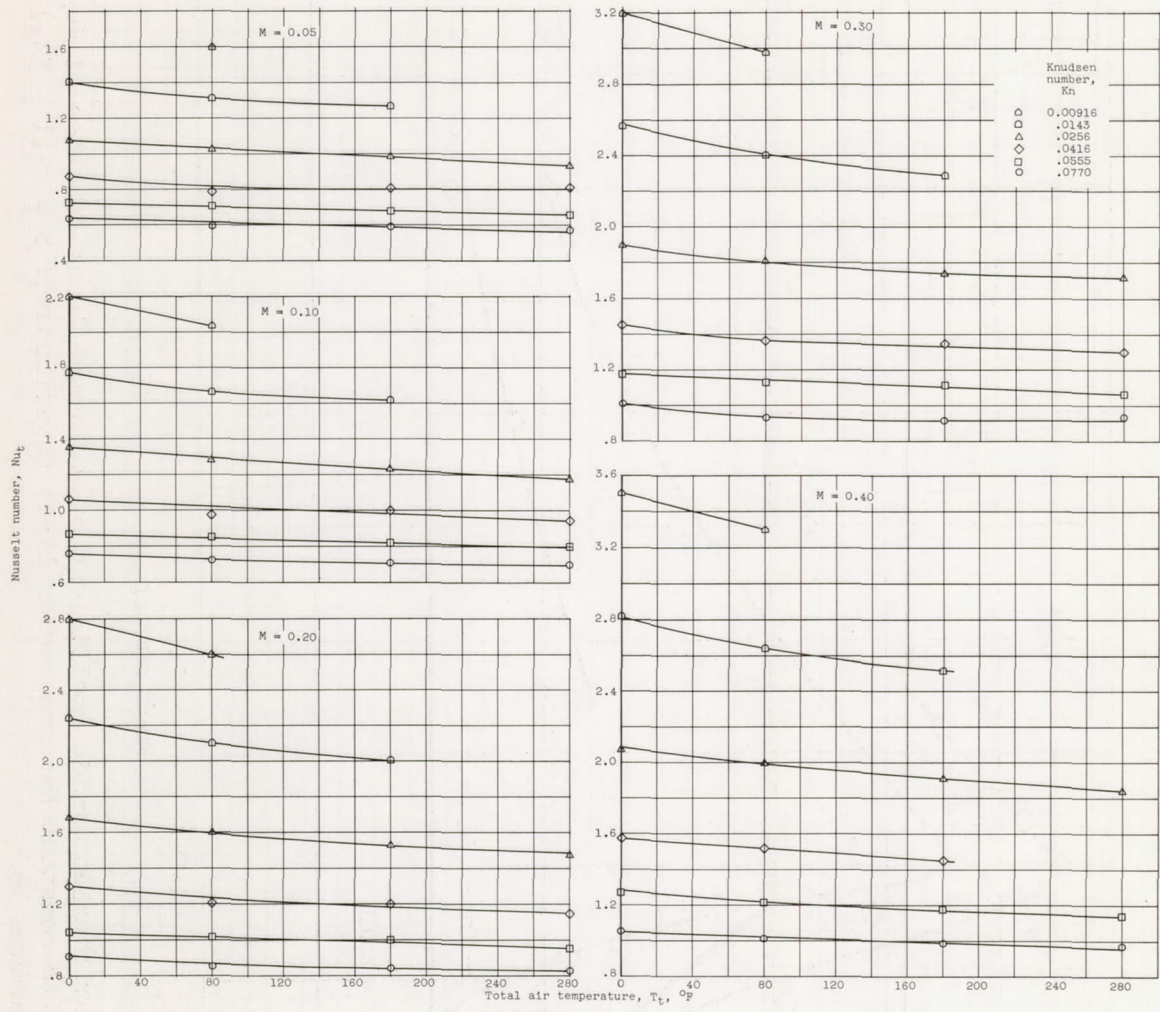


Figure 12. - Variation of Nusselt number with total air temperature. Crossplots of figure 10 showing asymptotic Nusselt number at $\Delta T > 200^{\circ} F$.

5111

5111

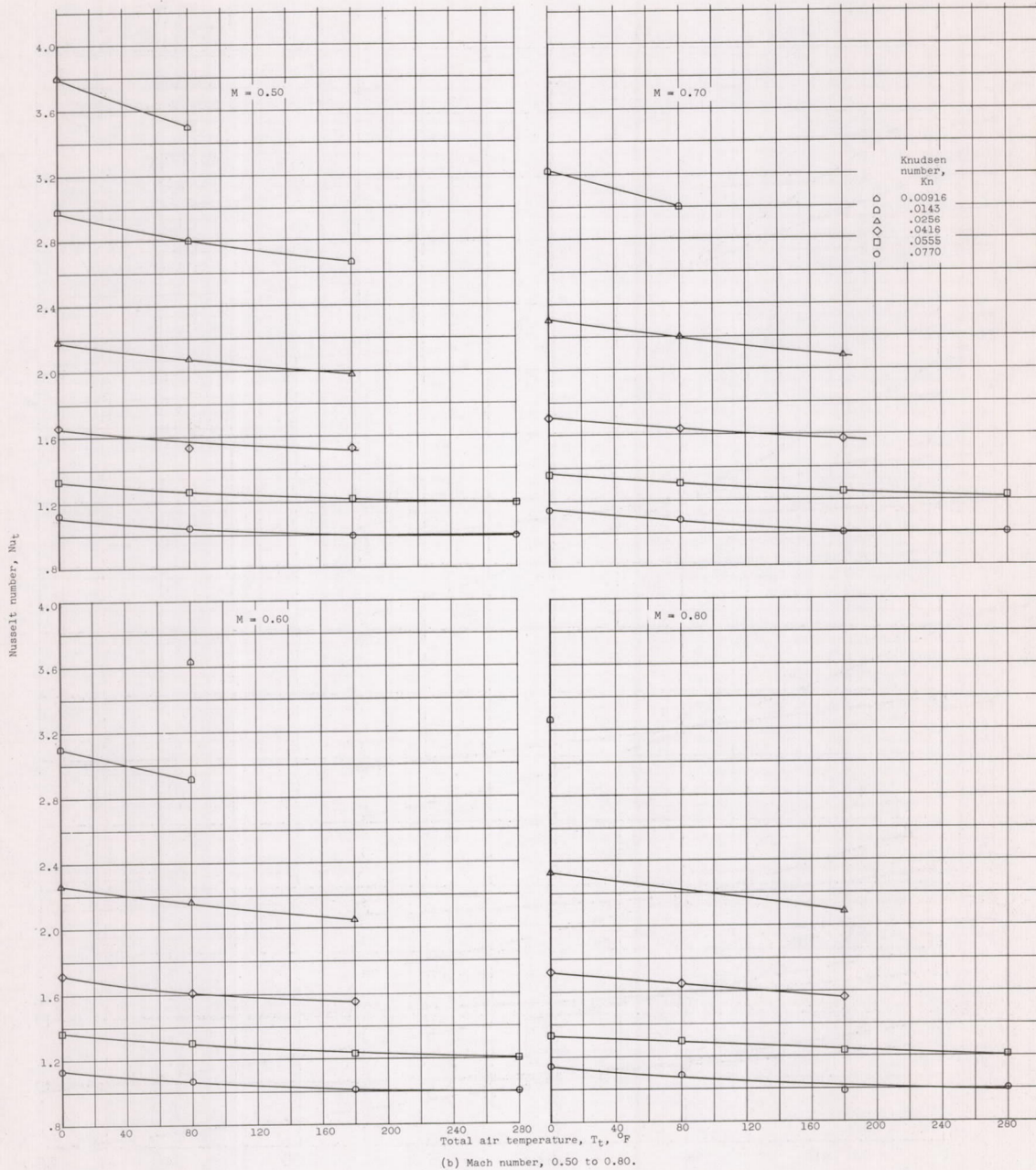


Figure 12. - Concluded. Variation of Nusselt number with total air temperature. Crossplots of figure 10 showing asymptotic Nusselt number at $\Delta T > 200^{\circ} F$.

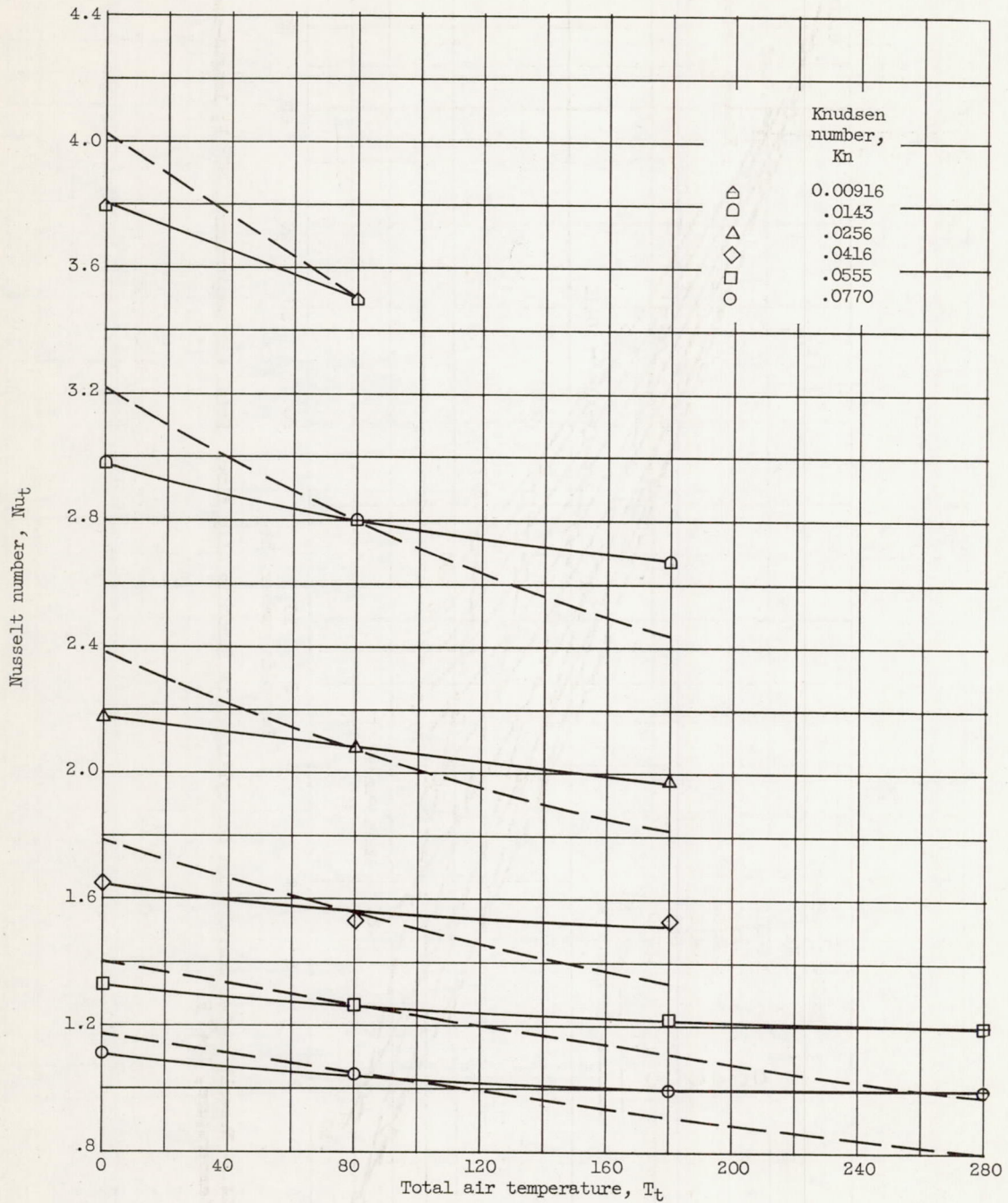


Figure 13. - Variation of Nusselt number with total air temperature. Curves of constant heat-transfer coefficient h_{80F} superimposed on figure 12(b) for $M = 0.50$.

5111

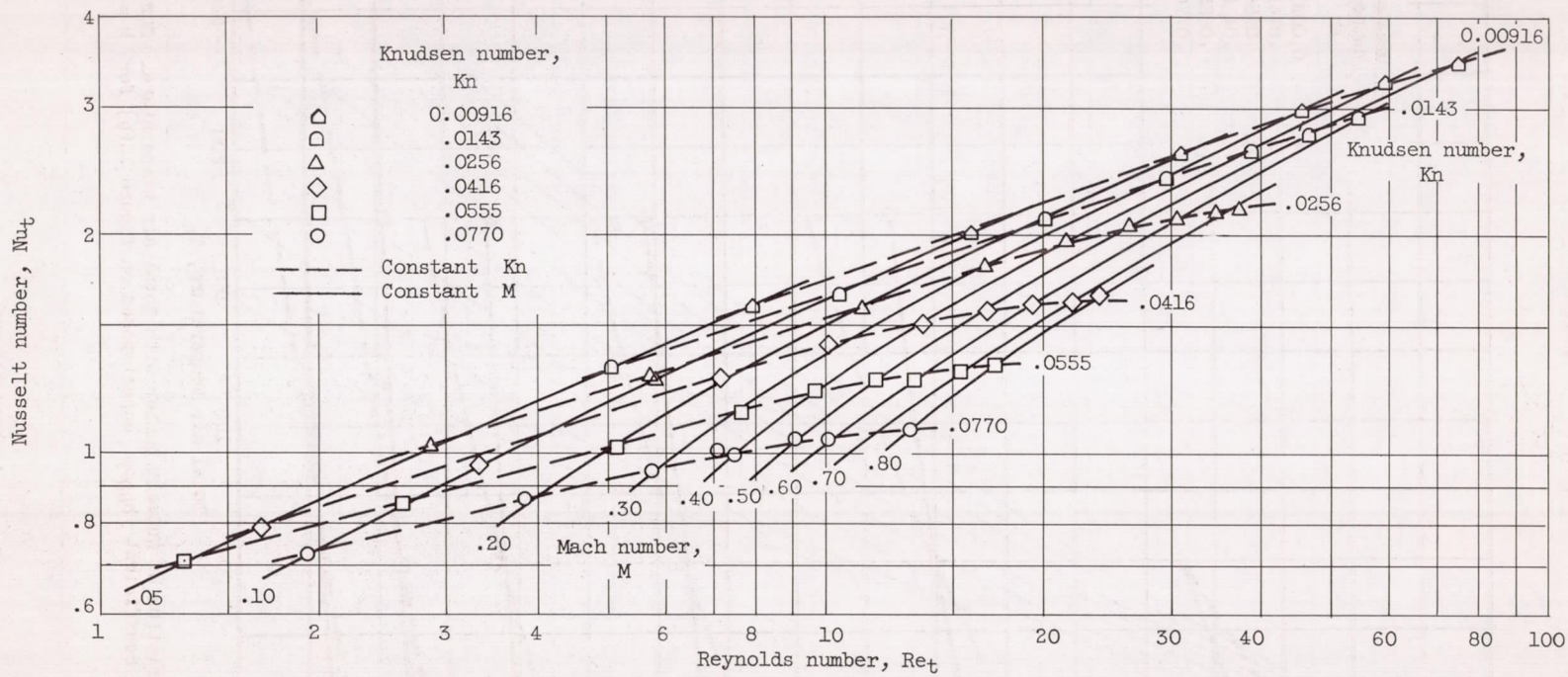


Figure 14. - Nusselt number correlation for cylinders in subsonic slip flow. Total air temperature, 80° F; length-average wire temperature, 584° F.

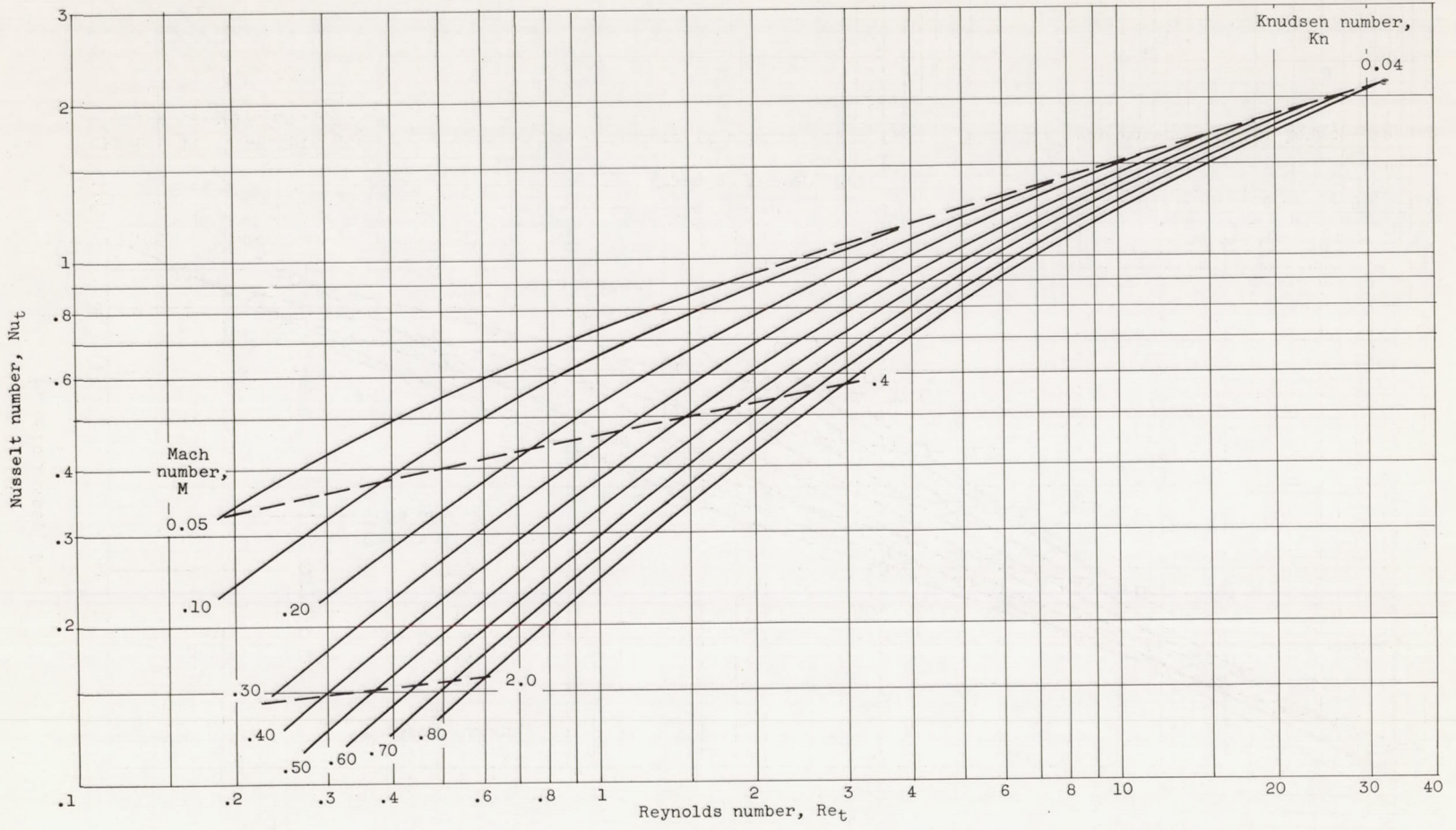


Figure 15. - Predicted Nusselt number correlation from approximate slip-flow theory (after ref. 23).

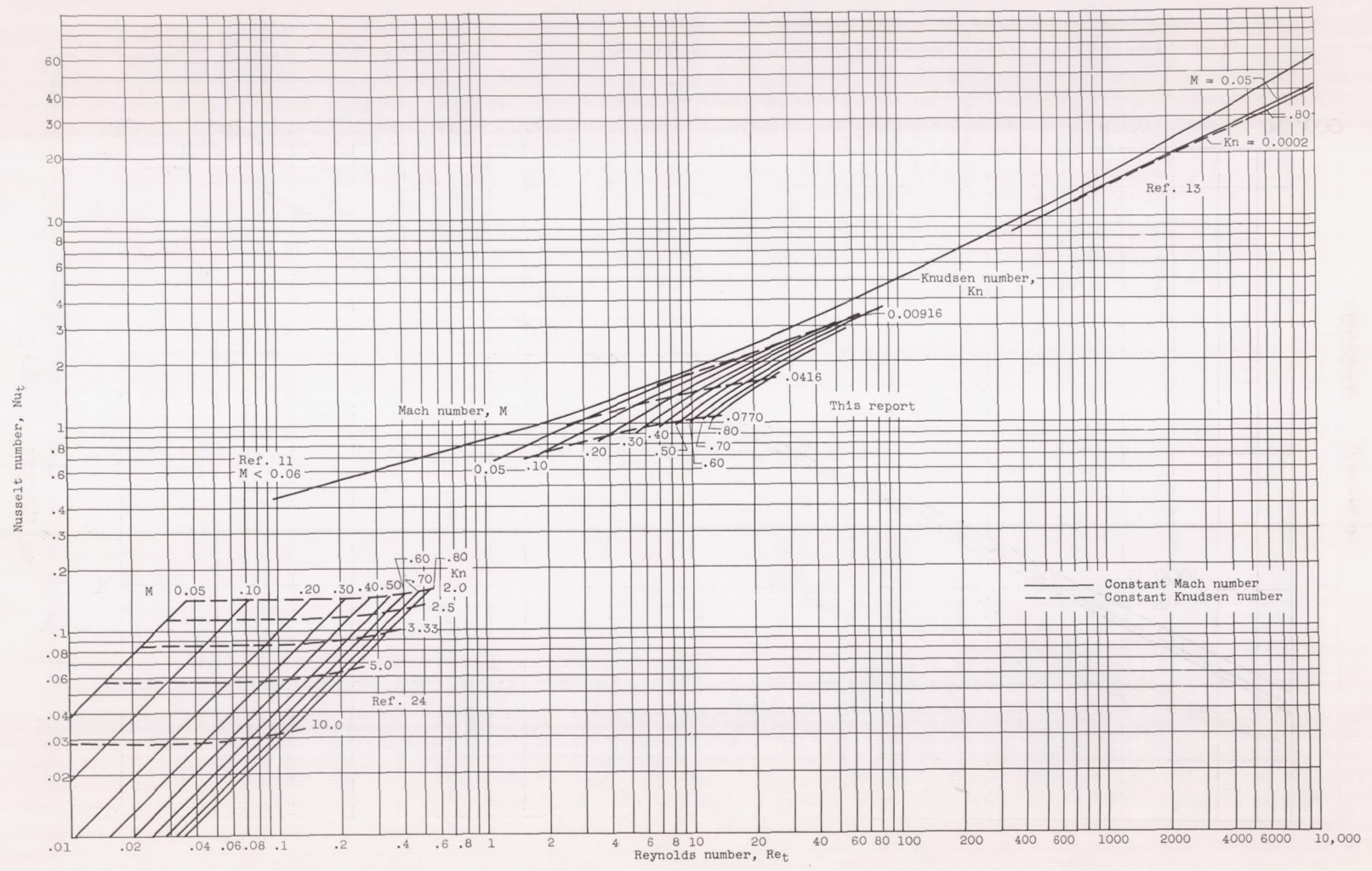


Figure 16. - Attempted Nusselt number correlation for cylinders in subsonic continuum, slip, and free-molecule flows.

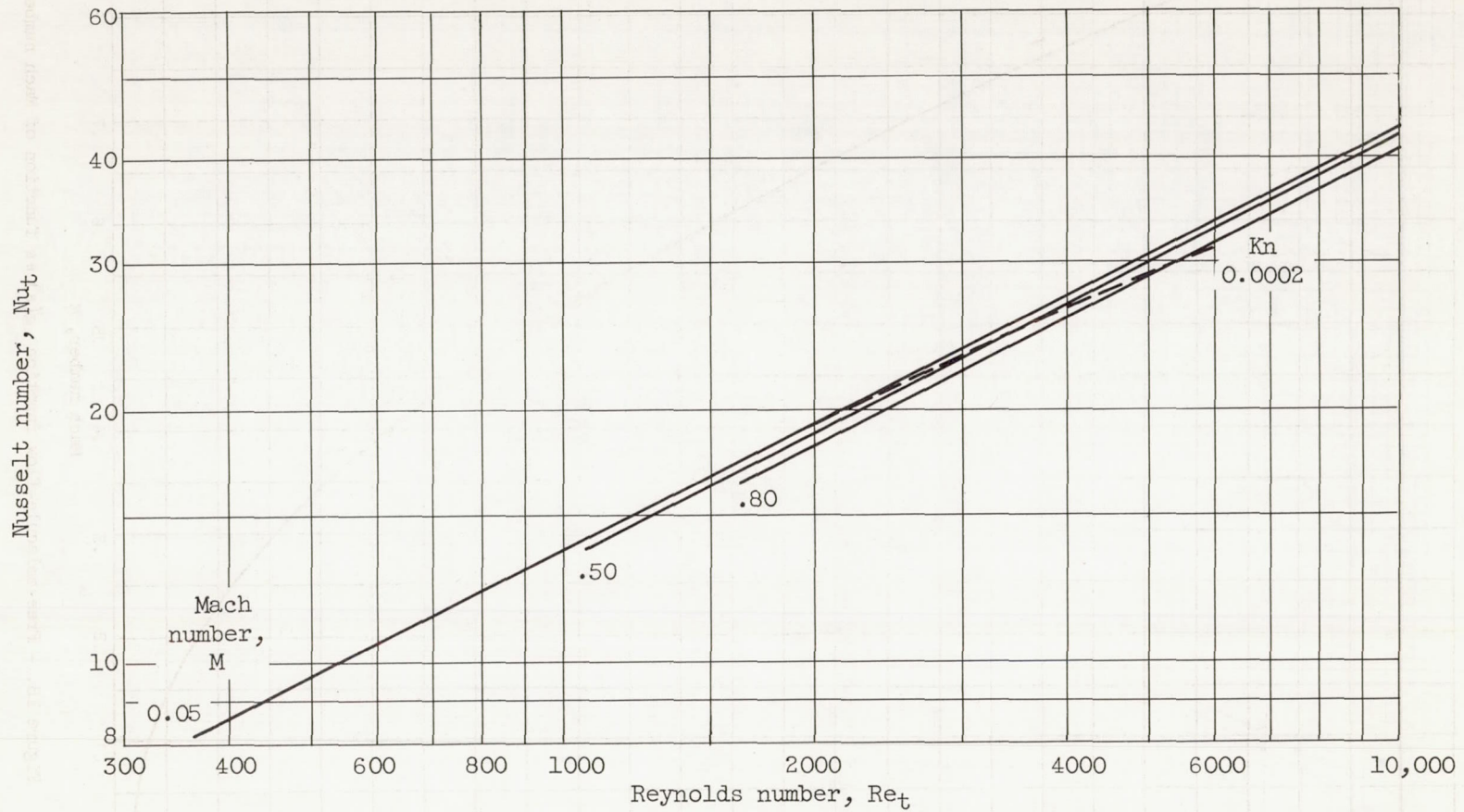


Figure 17. - Continuum-flow experimental Nusselt number correlation (after ref. 13).

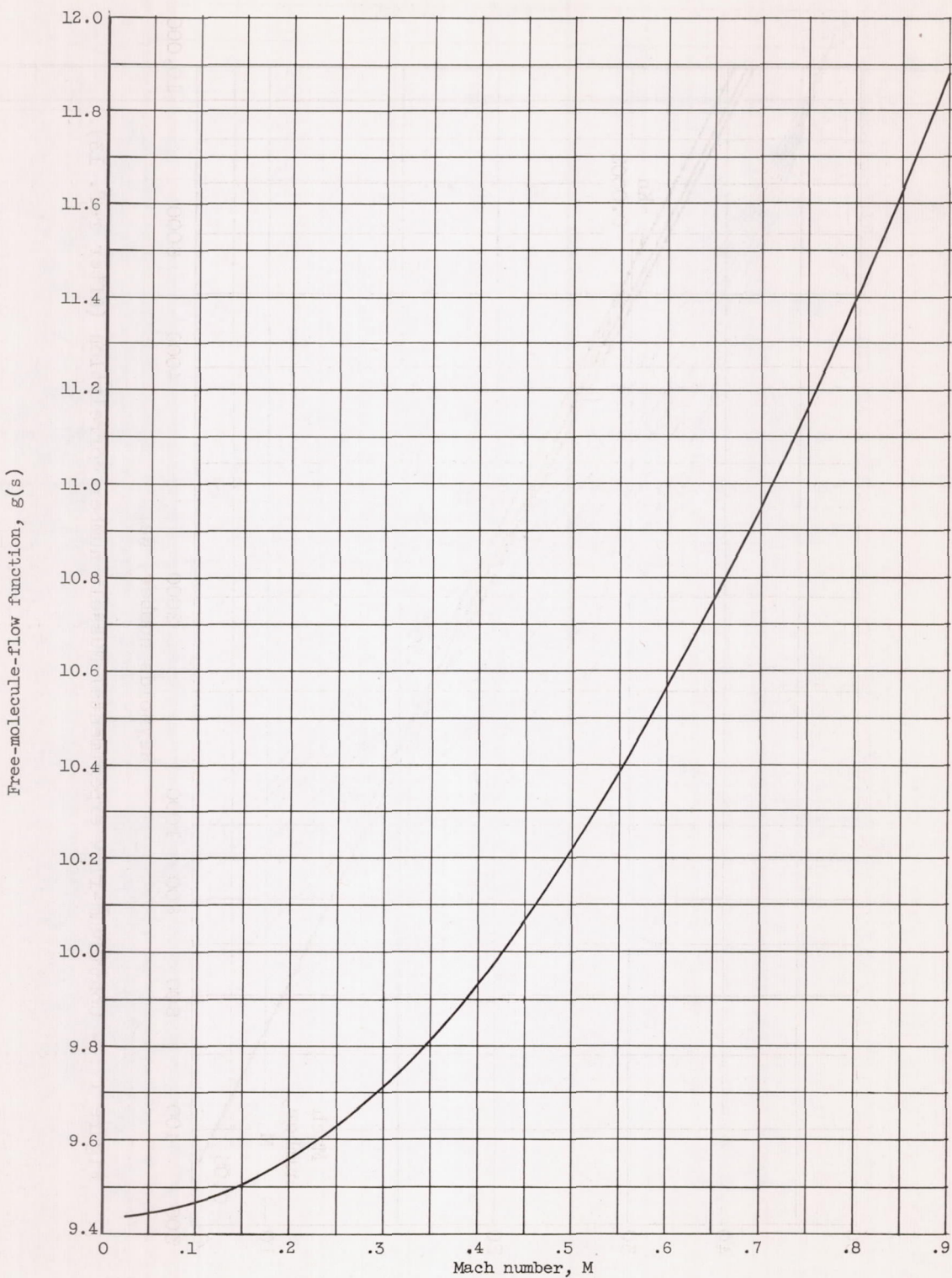


Figure 18. - Free-molecule-flow function $g(s)$ as function of Mach number.

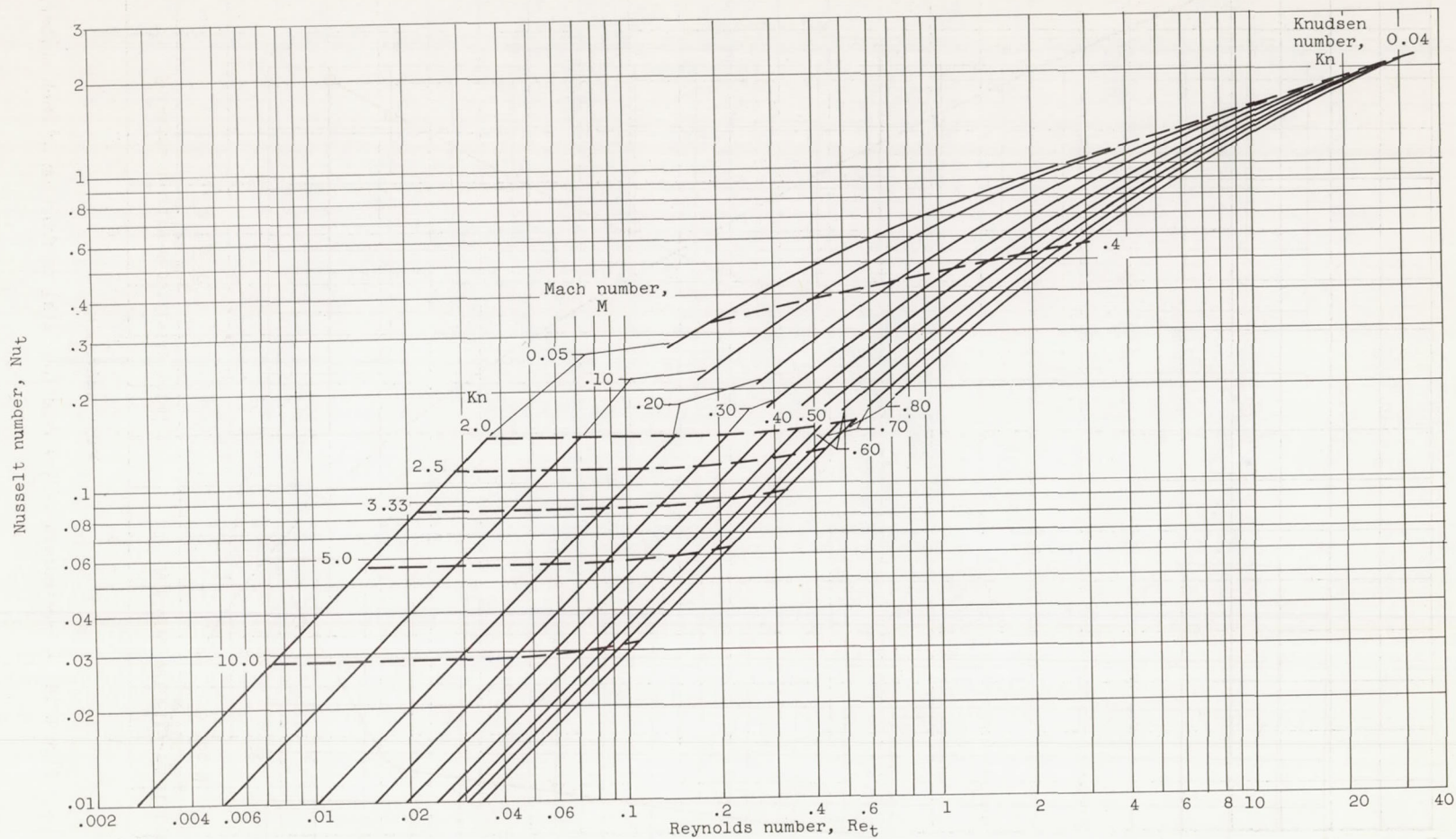
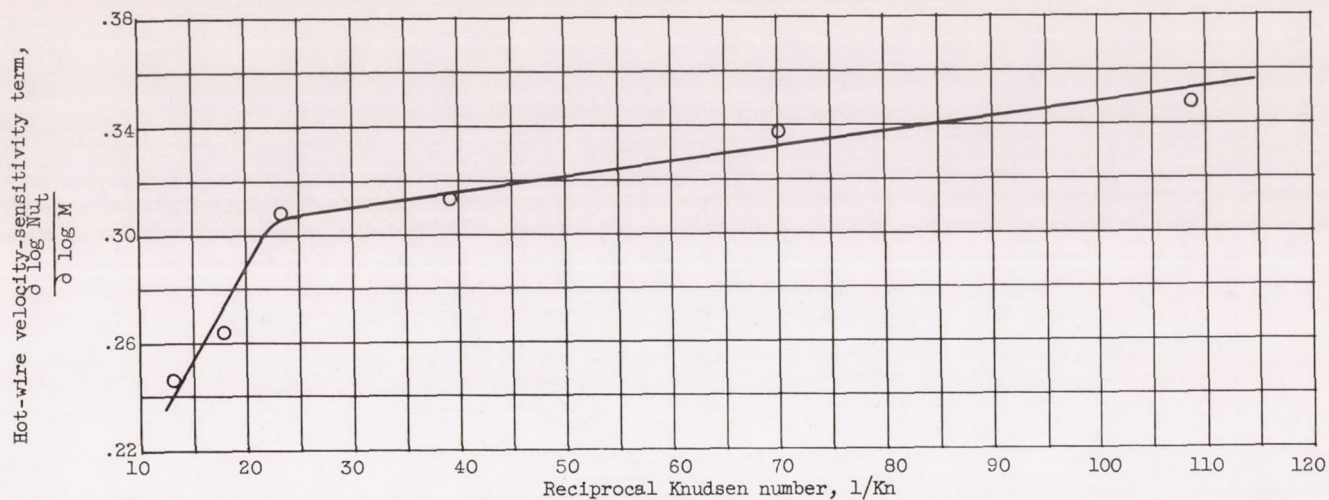
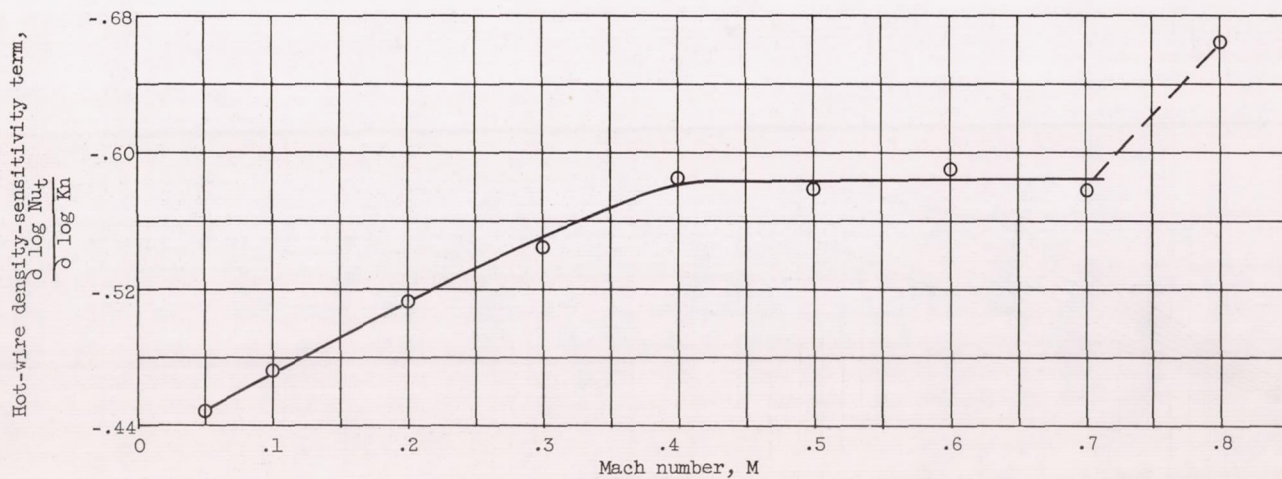


Figure 19. - Comparison of approximate slip-flow theory with free-molecule-flow prediction.



(a) Velocity sensitivity: $0.05 < M < 0.40$.



(b) Density sensitivity: $0.009 < Kn < 0.077$.

Figure 20. - Hot-wire sensitivity terms. Restrictions: $T_t = 80^\circ \text{F}$; $T_w - T_e > 200^\circ \text{F}$.

Содержание: 1. Введение. 2. Описание. 3. Заключение.

Введение. В настоящее время наблюдается тенденция к...

Описание. Данное устройство предназначено для...

Заключение. В результате проведенных исследований...

Итого

Всего страниц 100. Из них с иллюстрациями 20.

Содержание: 1. Введение. 2. Описание. 3. Заключение.

Выводы. Данное устройство имеет ряд преимуществ...

Содержание: 1. Введение. 2. Описание. 3. Заключение.

Введение. В настоящее время наблюдается тенденция к...

Описание. Данное устройство предназначено для...

Заключение. В результате проведенных исследований...

Итого

Всего страниц 100. Из них с иллюстрациями 20.

Содержание: 1. Введение. 2. Описание. 3. Заключение.

Выводы. Данное устройство имеет ряд преимуществ...